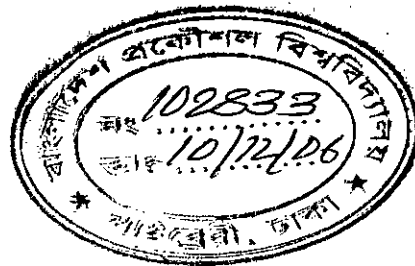


Nonlinear Analysis of a Superelastic Shape Memory Alloy Cantilever Beam of Variable Cross-Section

by

Md. Arefin Kowser

A Thesis submitted for partial fulfillment of the requirements for the degree of
MASTER OF SCIENCE IN MECHANICAL ENGINEERING



DEPARTMENT OF MECHANICAL ENGINEERING
BANGLADESH UNIVERSITY OF ENGINEERING AND TECHNOLOGY

Dhaka-1000 , Bangladesh

July 2006.



#102833#

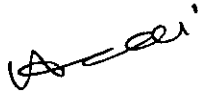
The thesis titled “ **Nonlinear Analysis of a Superelastic Shape Memory Alloy Cantilever Beam of Variable Cross-Section**”, Submitted by Md. Arefin Kowser, Student No: 040410029P, Session: April 2004 has been accepted as satisfactory in partial fulfillment of the requirements for the degree of MASTER OF SCIENCE IN MECHANICAL ENGINEERING on 01 July 2006.

BOARD OF EXAMINERS



Dr. M. Ashiqur Rahman
Associate Professor
Department of Mechanical Engineering
BUET, Dhaka-1000.

Chairman



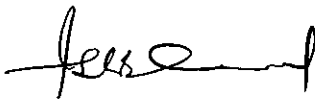
Dr. Md. Afsar Ali
Assistant Professor
Department of Mechanical Engineering
BUET, Dhaka-1000.

Member



Dr. Md. Maksud Helali
Professor and Head
Department of Mechanical Engineering
BUET, Dhaka-1000.

Member
(Ex- officio)

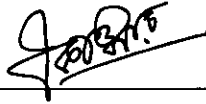


Dr. Ishtiaque Ahmed
Professor
Department of Civil Engineering
BUET, Dhaka-1000.

Member
(External)

CANDIDATE'S DECLARATION

It is hereby declared that this thesis or any part of it has not been submitted elsewhere for the award of any degree or diploma.



Md. Arefin Kowser

CONTENTS

		Page no.
Title page.....		i
Board of Examiners.....		ii
Candidate's Declaration		iii
Contents.....		iv
List of Tables.....		vi
List of Figures.....		vi
Nomenclature		x
Acknowledgement		xi
Abstract.....		xii
Chapter- 1	Introduction	1
1.1	Introduction to SMART/FUNCTIONAL materials.....	1
1.2	Shape memory alloy (SMA).....	3
1.3	Motivation for the present study.....	6
1.4	Objectives.....	7
Chapter – 2	Literature Review	9
Chapter - 3	Mathematical Analysis	13
3.1	General.....	13
3.2	Governing differential equations for the beam.....	13
3.3	Large deflection analysis of the beam.....	14
3.4	Analysis of the inelastic deformation of the beam (Timoshenko's method).....	17
Chapter – 4	Inelastic Deformations of Cantilever Stainless Steel Beams of Variable Cross-Section- Experiment and Nonlinear Analysis	19
4.1	General	19
4.2	Experiment.....	19
4.3	Accuracy and reliability of the analysis.....	21
4.4	Results and discussions.....	21
Chapter – 5	Nonlinear Analysis of a superelastic Shape Memory Alloy Cantilever Beam of Variable Cross-Section	28
5.1	General.....	28
5.2	Results and discussions.....	28

Chapter – 6	Conclusions and recommendations	35
6.1	Conclusions on stainless steel beam.....	35
6.2	Conclusions on shape memory alloy beam.....	36
6.3	Recommendations for future work.....	38
References.....		39
APPENDIX –A		92
A.1	Numerical analysis.....	92
APPENDIX- B	Programming features	94
B.1	Input of the program.....	94
B.2	Output of the program.....	94
B.3	Table of input-output variables.....	94
APPENDIX- C	Programme code	95

List of Tables

Table		Page
Table 4.1	Design parameters of stainless steel cantilever beams.....	44
Table 4.2	Comparison of experimental results by Bele'ndez et al. with the numerical results generated by the present study.....	44
Table 4.3	End-shortening results of stainless steel cantilever beam of variable cross- section.....	45
Table 5.1	Design parameters of SMA cantilever beams of variable cross-section ($b_0=100\text{mm}$, $h=50\text{ mm}$).....	45

List of Figures

Figure		Page
Figure 1.1	Idealized stress-strain diagram of the superelastic SMA.....	46
Figure 1.2	Experimental stress-strain curves for superelastic SMA, experiment done on a 2mm diameter rod.....	47
Figure 3.1	Shape of the beam of variable cross-section	48
Figure 3.2	Deflection of beam under load P and corresponding end-shortening.....	49
Figure 3.3	Generalized σ - ε diagram for beam	50
Figure 3.4	Parameters of beam.....	51
Figure 3.5	Flow Chart of Beam analysis (Timoshenko's method).....	52
Figure 4.1	Experimental setup.....	53
Figure 4.2	Experimental apparatus with tip load on beam.....	54
Figure 4.3(a)	Experimental stress-strain curve of stainless steel of specimen thickness 1mm.....	55
Figure 4.3(b)	Experimental true stress-strain curve of stainless steel of specimen thickness 1mm.....	56
Figure 4.4(a)	Experimental stress-strain curve stainless steel of specimen thickness 2mm.....	57
Figure 4.4(b)	Experimental true stress-strain curve of stainless steel of thickness 2mm.....	58
Figure 4.5	Different segments of cantilever beam.....	59
Figure 4.6(a)	Moment-strain curve for stainless steel beam of thickness 1mm.	60
Figure 4.6(b)	Moment-strain curve for stainless steel beam of thickness 2mm.	61
Figure 4.7	Effective modulus - strain curve of stainless steel beam.....	62
Figure 4.8	Load-deflection curve of stainless steel cantilever beam (Case 1: $L = 150\text{mm}$, $b_0 = 46\text{mm}$, $h = 1\text{mm}$, $\sigma_d = 198.74\text{MPa}$ at design load P_1 , Experimental. $\delta_h=4.53\text{mm}$ at P_2).....	63

Figure 4.9(a)	Stress distribution along the horizontal distance from the fixed end of the stainless steel beam by linear analysis (Case 1: $L = 150\text{mm}$, $b_0 = 46\text{mm}$, $h = 1\text{mm}$, $\sigma_d = 198.74\text{MPa}$ at design load P_1).....	64
Figure 4.9(b)	Stress distribution along the horizontal distance from the fixed end of the stainless steel beam by nonlinear analysis (Case 1: $L=150\text{mm}$, $b_0 = 46\text{mm}$, $h = 1\text{mm}$, $\sigma_d = 198.74\text{MPa}$ at design load P_1).....	65
Figure 4.10	Load-deflection curve of stainless steel cantilever beam (Case 2: $L = 200\text{mm}$, $b_0 = 61\text{mm}$, $h = 1\text{mm}$, $\sigma_d = 199.82\text{MPa}$ at design load P_1 , Experimental $\delta_h = 9.73\text{mm}$ at P_2).....	66
Figure 4.11(a)	Stress distribution along the horizontal distance from the fixed end of the stainless steel beam by linear analysis (Case 2: $L = 200\text{mm}$, $b_0 = 61\text{mm}$, $h = 1\text{mm}$, $\sigma_d = 199.82\text{MPa}$ at design load P_1).....	67
Figure 4.11(b)	Stress distribution along the horizontal distance from the fixed end of the stainless steel beam by nonlinear analysis (Case 2: $L = 200\text{mm}$, $b_0 = 61\text{mm}$, $h = 1\text{mm}$, $\sigma_d = 199.82\text{MPa}$ at design load P_1).....	68
Figure 4.12	Load-deflection curve of stainless steel cantilever beam (Case 3: $L = 150\text{mm}$, $b_0 = 18\text{mm}$, $h = 2\text{mm}$, $\sigma_d = 250.95\text{MPa}$, Experimental $\delta_h = 6.88\text{mm}$ at P_2).....	69
Figure 4.13(a)	Stress distribution along the horizontal distance from the fixed end of the stainless steel beam by linear analysis (Case 3: $L = 150\text{mm}$, $b_0 = 18\text{mm}$, $h = 2\text{mm}$, $\sigma_d = 250.95\text{MPa}$ at design load P_1).....	70
Figure 4.13(b)	Stress distribution along the horizontal distance from the fixed end of the stainless steel beam by nonlinear analysis (Case 3: $L = 150\text{mm}$, $b_0 = 18\text{mm}$, $h = 2\text{mm}$, $\sigma_d = 250.95\text{MPa}$ at design load P_1).....	71
Figure 4.14	Load-deflection curve of stainless steel cantilever beam (Case 4: $L = 200\text{mm}$, $b_0 = 24.1\text{mm}$, $h = 2\text{mm}$, $\sigma_d = 249.91\text{MPa}$ at design load P_1 , Experimental $\delta_h = 12\text{mm}$ at P_2).....	72
Figure 4.15(a)	Stress distribution along the horizontal distance from the fixed end of the stainless steel beam by linear analysis (Case4: $L = 200\text{mm}$, $b_0 = 24.1\text{mm}$, $h = 2\text{mm}$, $\sigma_d = 249.91\text{MPa}$ at design load P_1).....	73

Figure 4.15(b)	Stress distribution along the horizontal distance from the fixed end of the stainless steel beam by nonlinear analysis (Case 4: $L = 200\text{mm}$, $b_0 = 24.1\text{mm}$, $h = 2\text{mm}$, $\sigma_d = 249.91\text{MPa}$ at design load P_d).....	74
Figure 5.1	Moment-total strain curve of SMA cantilever beam.....	75
Figure 5.2	Modulus of elasticity-total strain curve of SMA cantilever beam	76
Figure 5.3	Load-deflection curve of SMA cantilever beam (Cases 1,2: $L = 500\text{mm}$, $b_0 = 100\text{mm}$, $h = 50\text{mm}$, Maximum design strain = 9.52% by linear theory without end-shortening).....	77
Figure 5.4(a)	Stress distribution along the horizontal distance from the fixed end of the SMA beam by linear analysis (Case 1: $L = 500\text{mm}$, $b_0 = 100\text{mm}$, $h = 50\text{mm}$, Maximum design strain = 9.52% by linear theory without end-shortening).....	78
Figure 5.4(b)	Stress distribution along the horizontal distance from the fixed end of the SMA beam by nonlinear analysis (Case 1: $L = 500\text{mm}$, $b_0 = 100\text{mm}$, $h = 50\text{mm}$, Maximum design strain = 9.52% by linear theory without end-shortening).....	79
Figure 5.5(a)	Stress distribution along the horizontal distance from the fixed end of the SMA beam by linear analysis (Case 2: $L = 500\text{mm}$, $b_0 = 100\text{mm}$, $h = 50\text{mm}$, Maximum design strain = 7.31% by linear theory without end-shortening).....	80
Figure 5.5(b)	Stress distribution along the horizontal distance from the fixed end of the SMA beam by nonlinear analysis (Case 2: $L = 500\text{mm}$, $b_0 = 100\text{mm}$, $h = 50\text{mm}$, Maximum design strain = 7.31% by linear theory without end-shortening).....	81
Figure 5.6	Load-deflection curve of SMA cantilever beam (Cases 3,4: $L = 400\text{mm}$, $b_0 = 100\text{mm}$, $h = 50\text{mm}$, Maximum design strain = 11.62% by linear theory without end-shortening).....	82
Figure 5.7(a)	Stress distribution along the horizontal distance from the fixed end of the SMA beam by linear analysis (Case 3: $L = 400\text{mm}$, $b_0 = 100\text{mm}$, $h = 50\text{mm}$, Maximum design strain = 11.62% by linear theory without end-shortening).....	83
Figure 5.7(b)	Stress distribution along the horizontal distance from the fixed end of the SMA beam by nonlinear analysis (Case 3: $L = 400\text{mm}$, $b_0 = 100\text{mm}$, $h = 50\text{mm}$, Maximum design strain = 11.62% by linear theory without end-shortening).....	84

Figure 5.8(a)	Stress distribution along the horizontal distance from the fixed end of the SMA beam by linear analysis (Case 4: $L = 400\text{mm}$, $b_0 = 100\text{mm}$, $h = 50\text{mm}$, Maximum design strain = 3.22% by linear theory without end-shortening).....	85
Figure 5.8(b)	Stress distribution along the horizontal distance from the fixed end of the SMA beam by nonlinear analysis (Case 4: $L = 400\text{mm}$, $b_0 = 100\text{mm}$, $h = 50\text{mm}$, Maximum design strain = 3.22% by linear theory without end-shortening).....	86
Figure 5.9	Load-deflection curve of SMA cantilever beam (Cases 5,6: $L = 300\text{mm}$, $b_0 = 100\text{mm}$, $h = 50\text{mm}$, Maximum design strain = 15.20% by linear theory without end-shortening).....	87
Figure 5.10(a)	Stress distribution along the horizontal distance from the fixed end of the SMA beam by linear analysis (Case 5: $L = 300\text{mm}$, $b_0 = 100\text{mm}$, $h = 50\text{mm}$, Maximum design strain = 15.20% by linear theory without end-shortening).....	88
Figure 5.10(b)	Stress distribution along the horizontal distance from the fixed end of the SMA beam by nonlinear analysis (Case 5: $L = 300\text{mm}$, $b_0 = 100\text{mm}$, $h = 50\text{mm}$, Maximum design strain = 15.20% by linear theory without end-shortening).....	89
Figure 5.11(a)	Stress distribution along the horizontal distance from the fixed end of the SMA beam by linear analysis (Case 6: $L = 300\text{mm}$, $b_0 = 100\text{mm}$, $h = 50\text{mm}$, Maximum design strain = 1.78% by linear theory without end-shortening).....	90
Figure 5.11(b)	Stress distribution along the horizontal distance from the fixed end of the SMA beam by nonlinear analysis (Case 6: $L = 300\text{mm}$, $b_0 = 100\text{mm}$, $h = 50\text{mm}$, Maximum design strain = 1.78% by linear theory without end-shortening).....	91

Nomenclature

A_f	Austenite finish temperature	A_s	Austenite start temperature
b	Width of the beam at any point on its span	b_0	Width of the beam at fixed end
E	Young's modulus of elasticity for the beam material	E''	Effective modulus of elasticity variable along the span
e	Engineering strain	H	Segment length
h	Height of the beam	h_1	Distance from the neutral axis to the lower surface of beam
h_2	Distance from the neutral axis to the upper surface of beam	I	Moment of inertia
L	Length of the beam	M, M_b	Bending moment
M_f	Martensite finish temperature	M_s	Martensite start temperature
MT	Martensitic transformation	P	Tip load on beam
P_d	Design load	SE	Superelasticity
$SIMT$	Stress induced martensitic transformation	SMA	Shape memory alloy
SME	Shape memory effect	x	Horizontal distance from fixed end
y, δ	Elastic curve's deflection	δ_s	End-shortening
δ_0	Change in length before and after loading	Δ	$ \epsilon_1 + \epsilon_2 = h/\rho$
ϵ	Strain	ϵ_t	Elongation in the extreme fiber in the convex side
ϵ_2	Elongation in the extreme fiber in the concave side	ρ	Radius of curvature
σ	Stress	σ_0	Engineering (nominal) stress
σ_d	Design stress		

Acknowledgements

The author would like to express his deep gratitude and indebtedness to his supervisor Dr. M. Ashiqur Rahman, Associate Professor, Department of Mechanical Engineering, Bangladesh University of Engineering and Technology (BUET), for his continuous inspirations, great interest, constructive criticism, super guidance, remarkable advice and invaluable supports during this research. The author would also like to thank him for his careful reading and correction of this thesis.

The author also wants to express his gratitude to Assistant Professor Dr. Md. Afsar Ali, Department of Mechanical Engineering, BUET, for his cooperation and help to continue this research work.

The author feels grateful to all of his colleagues, especially to Mr. Md. Anowar Hossain, and Nayeem Md. Lutful Huq, Lecturers, Department of Mechanical Engineering, DUET, Gazipur, for their invaluable supports throughout this research work.

Very special thanks are due for all the teachers of the Department of Mechanical Engineering, BUET for their help to the author during the whole period of his M. Sc. Engineering course.

The author is also indebted to all staffs of the strength of materials lab, applied mechanics lab, sheet metal lab, mechatronics and control laboratory of Department of Mechanical Engineering, BUET, for their cordial help and assistance.

Finally, the author expresses his gratefulness to DUET authority for allowing him to complete this research program granting him necessary permissions.

ABSTRACT

Cantilever beams, made of shape memory alloy (SMA), undergo much larger deflection in comparison to those made of other materials. Again, cantilever beams with reducing cross-section along the span show larger deflections compared to those of constant cross-section beams. Furthermore, the degree of variability/complexity will further increase if the material or physical nonlinearity is involved, typically for an SMA beam. That takes such a study in the domain of geometric nonlinearity together with material nonlinearity. Problems of physical and geometric nonlinearities are always challenges for the engineers. Analysis was conducted for such a cantilever beam with reducing cross-sectional area, made of SMA with highly nonlinear stress-strain curves. Initially, experiments were conducted for stainless steel cantilever beams theoretically of uniform strength, with nonlinear stress-strain curves. In addition to the experiment, a computer code in 'C++' has been developed using the Runge-Kutta technique for the purpose of simulation. Effective modulus-curvature relations obtained from the nonlinear stress-strain relations for different sections of the beam that are used for the analysis. Nonlinear analysis shows the stresses are not that high as predicted by ideal theories. Moreover, the tensile and compressive stresses are slightly different in magnitude and both decrease along the span. Experimental load-deflection curves are found to be initially linear but, nonlinear and convex upward at a high load. Comparison of the numerical results with the available experimental results and theory shows excellent agreement verifying the soundness of the entire numerical simulation scheme. Next the same computer code has been used for the purpose of simulation for SMA beam but with SMA's stress-strain data. Moment-curvature and effective modulus-curvature relations are obtained from the highly nonlinear stress-strain relations for different sections of the beam. For rigorous analysis, the true stress-strain curves in tension as well as in compression have been used for the study. It is seen that nonlinear stress-strain curve governs the response of the beam. Moreover, load-deflection curves are initially linear but, nonlinear and convex upward at a high load. It is found that more material can be removed from an SMA beam of uniform strength, originally designed without considering geometric nonlinearity and the effect of end-shortening.

Furthermore, the compressive stress is significantly higher than the tensile stress because of asymmetry in stress-strain relations. If 'end-shortening' is considered, stress falls along the span. Interestingly, for different cases considered, it is found that the beam material may remain in the parent austenite phase, mixed phase or in the stress induced martensitic phase.

1.1 Introduction to Smart/Functional materials

Smart materials are the new emerging materials system that combines contemporary materials science with information science. The smart system is composed of sensing, processing, actuating, providing feedback, self-diagnosing, and self-recovering sub systems. The system uses the functional properties of advanced materials to achieve high performances with capabilities of recognition, discrimination, and adjustment in response to a change of its environment. Each component of this system must have functionality, and the entire system is integrated to perform a self-controlled smart action, similar to a living creature that can think, judge, and act. A smart system can be considered as a design philosophy that emphasized predictivity, adaptivity, and repetition (Zhong, Wang and Kang (1998)).

A smart system or smart structure is defined to be a nonbiological physical structure with (i) a definite purpose, (ii) means and imperative to achieve that purpose, and (iii) a biological pattern of functioning.

Four of the most widely used smart materials nowadays are: (i) piezoelectric Pb (Zr, Ti)O₃ (PZT) (ii) magnetostrictive (Tb, Dy) Fe₂ (iii) electrostrictive Pb (Mg Nb)O₃ and (iv) shape memory alloy NiTi. These materials can be taken as typical examples to briefly illustrate the structural characters of the smart materials. Pb(Zr, Ti)O₃ is a ferroelectric ceramics which is bcc at a mediate temperature range and becomes ferroelectric on cooling through the Curie temperature (T_c). At room temperature (RT), it is poised on a rhombohedral-tetragonal phase boundary that enhances the piezoelectric coefficients. Terfeno, (Tb, Dy)Fe₂, experiences a rhombohedral-tetragonal transition at RT, which enhances its magneto-striction coefficient. Pb(Mg, Nb)O₃ and NiTi are cubic at high temperatures and, on annealing, transform to a partially ordered state. On further cooling, Pb(Mg, Nb)O₃ passes through a diffuse phase transformation at RT, forming a mixture of ordered and disordered phase domains that exhibits large dielectric and

electrostrictive coefficients under certain conditions. Just below RT, it transforms to a ferroelectric rhombohedral phase. The partially ordered shape memory alloy NiTi undergoes an austenitic (bcc) to martensitic (monoclinic) phase change just above RT. It is easily deformed in the martensitic state but recovers its original shape when reheated to austenite. The structural and phase transformation similarities of these four actuator materials are remarkable and could be a key in developing new smart materials.

Science and technology in the twenty-first century will rely heavily on the development of new materials that are expected to respond to the environmental changes and manifest their own functions according to optimum conditions. The development of smart materials will undoubtedly be an essential task in many fields of science and technology such as information science, energy, transportation, safety engineering, and military technologies. Materials development in the future, therefore, should be directed toward creation of hyperfunctional materials that surpass even biological organs in some aspects. The current materials research is to develop various pathways that will lead modern technology toward the smart system.

Functional materials (commercially termed as smart materials) are distinctly different from structural materials, and their physical and chemical properties are sensitive to a change in the environment such as temperature, pressure, electric field, magnetic field, optical wavelength, adsorbed gas molecules, and pH. Functional materials utilize their native properties and functions to achieve intelligent action. Functional materials cover a broader range of materials than smart materials. Any materials with functionality are attributed to functional materials, such as ferroelectric BaTiO_3 , the magnetic field sensor of $\text{La}_{1-x}\text{Ca}_x\text{MnO}_3$, surface acoustic wave sensor of LiNbO_3 , liquid petroleum gas sensor of Pd-doped SnO_2 , semiconductor light detectors (CdS, CdTe), high-temperature piezoelectric Ta_2O_5 , fast-ion conductor $\text{Y}_2(\text{Sn}_y\text{Ti}_{1-y})_2\text{O}_7$ (pyrochlore structure), electric-voltage-induced reversible coloring of WO_3 , and high-temperature superconductors, etc.



1.2 Shape memory alloy (SMA)

Shape memory alloys (SMAs) alter in response to changes in temperature. At a low temperature, the material is in its martensitic state. When heated, it will regain its original or memory shape. Most other materials undergo drastic material property changes upon heating; materials may become brittle or stiff and can thus be prone to breaking. Shape-Memory alloys can tolerate strain 3 to 25 times higher than piezoelectrics can.

Some Shape-Memory alloys:

- (i) nickel-titanium (Nitinol)
- (ii) gold-cadmium
- (iii) brass
- (iv) ferromagnetic (a thin film, low bandwidth alloy)

SMAs are thermoresponsive smart materials that change shape in response to heat or cold. They are most commonly Nitinol, or nickel and titanium combined. Less popular but still possessing the shape memory effect are gold cadmium, silver cadmium, copper-aluminum-nickel, copper tin, copper zinc, and copper zinc aluminum. They are useful in couplers, thermostats, automobile, plane and helicopter parts.

SMAs are metals that, after being strained at a certain temperature, revert back to their original shape by shape memory effect (changing temperature) or by superelasticity (withdrawing the load). A change in their crystal structure above their transformation temperature causes them to return to their original shape. SMA's enable large forces (generated when encountering any resistance during their transformation) and large movements actuation, as they can recover large strains.

In actual practice, the SMA, that inherently possesses a highly nonlinear stress-strain (σ - ϵ) behavior or characteristic, is frequently stressed beyond the proportional limit.

Shape memory alloys are called functional materials because of their two unique capabilities, namely, the shape memory effect (SME) and superelasticity (SE). Both SME and SE mainly depend on the solid-solid, diffusion-less phase transformation process known as martensitic transformation (MT) from a crystallographically more ordered parent phase (austenite) to a crystallographically less ordered product phase (martensite).

The phase transformation (from austenite to martensite or vice versa) is typically marked by four transition temperatures, namely martensite finish (M_f), martensite start (M_s), austenite finish (A_f), and austenite start (A_s). For the SMA used in this study, $M_f < M_s < A_s < A_f$. For $T > A_f$, the SMA exists in the parent austenite phase. Under mechanical loading stress induced martensitic transformation (SIMT) starts when a critical stress is exceeded. When SIMT is over the SMA exists in the martensite phase. This SIM phase is, however, unstable in the absence of stress at this temperature. Consequently, during unloading the initiation of reverse phase transformation is marked by another critical stress. When this reverse SIMT is complete the SMA returns to its parent austenite phase. The complete loading-unloading cycle shows a typical hysteresis loop (Figure 1.1) known as pseudo-elasticity. It can be noted that the SIMT and the reverse SIMT are marked by a reduction of the material stiffness (Figure 1.1).

At this point, it is interesting to know that the local strain is remarkably different from the total strain during this forward and reverse SIMT (Rahman and Khan (2006); Rahman et al. (2002); Rahman and Tani (2005b)). In their first study, Rahman et al. (2002) dealt with the local strain-overall strain relationship of the superelastic shape memory alloy (SMA) rods for consecutive tensile loading-unloading cycles. The local strains were measured by an extensometer and also by the strain gages. On the other hand, the total strains of the specimens were measured from displacements of the loading machine's fixture. Test results show that during the stress induced martensite transformation (SIMT), the local strains of the mid portion is significantly different from that of the overall strains of the specimen. This phenomenon is so distinct that it appears the start and finish points of the forward SIMT, as well as the reverse SIMT, can be identified by simply plotting midpoint local strain against over all strain of the

specimens. This unique local deformation pattern is explained elaborately in references (Rahman and Khan (2006); Rahman et al. (2002); Rahman and Tani (2005b)) in terms of the critical stress barrier. The critical stress necessary to initiate SIMT is found to be higher for the mid portion of the specimen than for any other portion. It was pointed out that local stress concentration is mainly responsible for the above-mentioned unique phenomena that are independent of the specimen size and gage length. The local strain, however, should be measured by the highly sensitive strain gages to observe the above-mentioned phenomena (Rahman and Khan (2006); Rahman et al. (2002); Rahman and Tani (2005b)).

That this excellent functional material can exhibit peculiar mechanical behavior under different loading conditions can be further verified from the literature; a few of those studies are listed in the references by Funakubo et al. (1987); Gadaj et al., (1999, 2002); Gong et al. (2000); Hutchinson (2000); Leo et al. (1993); Pieczyska et al. (2002, 2004); Shae et al. (1995); Tobushi et al. (1999); Sun et al. (2000). For example, recently Rahman and Khan (2006) demonstrated that during stress relaxation tests the so-called 'inertia driven SIMT' occurs as local strain increases significantly at constant overall deformation. That study dealt with the mechanical behavior of the superelastic SMA rods in terms of local deformations and time via tensile loading-unloading cycles for both ends fixed constraints. The so-called stress-relaxation tests have been performed to demonstrate and investigate the local strains-total strains relationships with time particularly during the forward SIMT. A 5000N capacity tensile testing machine (Tinius Olsen 1000) was used to conduct the test. The machine is actuated by an electric motor. For measuring the local strain, a mechanical extensometer was used in the experiment. It can measure up to 5% of strain with a constant of 0.005mm over a 50mm gauge length.

The specimens used in the experiment were superelastic SMA rods (Ti 49.3 at %, Ni 50.2 at %, V 0.5 at%), and Mild steel (MS) strips. The length and diameter of the SMA (NiTi) specimen was 445 mm and 2 mm respectively. SMA's transformation temperatures are -59°C , -34°C , -27°C and -3°C for M_f , M_s , A_s and A_f , respectively (Rahman and Khan (2006)).

It was demonstrated that some remarkable phenomena occur pertaining to SIMT that are absent in the traditional materials like mild steel. For example, at the stopped loading condition the two ends (fixed end and moving end of the tensile testing machine) were in fixed positions. So that there was no axial overall deformation of the specimen but some notable increase in the axial local deformation was shown by the extensometer placed at the middle position of the SMA specimen. It should be noted that this peculiar behavior termed as 'inertia driven SIMT' occurs when the loading was stopped at mixed phase condition (Rahman and Khan (2006)).

In terms of tension-compression asymmetry of the SMA's σ - ϵ curves, interested readers may refer to Rahman (2001); Raniecki and Lexcelent (1998). In all of these studies, it was demonstrated through rigorous proofs that SMA behaves asymmetrically under tension and compression particularly for large strains.

1.3 Motivation for the present study

Studies of modern adaptive structural elements are challenging as they often involve nonlinear (both geometric and material) analysis. This is because such elements (for example, beam or, column specially in adaptive structures) often undergo very large deflections during their applications. Again, cantilever beams are often made light by removing extra materials from it, mainly for economy and space constraints. Most common example is the classical leaf springs that are designed for uniform strength. Moreover, slots/openings are also made by removing materials from it by Rahman et al. (2005; 2006a). The present study concentrates on the response of such a cantilever beam made of SMA with variable cross-sectional area under a tip load. This study for the superelastic SMA beams would be especially important since SMA itself is one of the most widely used functional materials in many adaptive structures. Superelastic SMAs can recover extremely large strains when they are unloaded. They, however, possess a highly nonlinear stress-strain relations, with inherent asymmetry in tension and compression by Rahman (2001).

The present study is based on simultaneous use of the tension-compression curves of the SMA, as found by Rahman (2001) and reproduced in Figure 1.2. The composition of

superelastic SMA rods is as follows: Ti 49.3 at%, Ni 50.2 at%, V 0.5 at%. The diameter of the SMA rod is 2 mm and SMA's transformation temperatures are -59°C , -34°C , -27°C and -3°C for the martensite finish, martensite start, austenite start and austenite finish, respectively. Average measured Young's Modulus for the parent phase was 65 GPa by Rahman (2001).

In this study simulations would be conducted for a cantilever beam with varying cross-sectional area, made of superelastic shape memory alloy. The varying cross-section was due to reducing width with constant height along the span, in order to make the beam theoretically of uniform strength. This point was not considered in the previous studies by other researchers. Moreover, rigorous stress-strain curves for SMA obtained by uniaxial tension and compression tests have been used, without any idealization. Furthermore, since SMA beams can undergo very large deflections, this study also incorporates geometric nonlinearity in the analysis.

1.4 Objectives

In this thesis, response of SMA beam with reducing cross-section will be studied. A computer code based on C/C++ will be developed for the ease of analysis. The load-deformation curves of the SMA beams will be predicted by using the developed code exploiting the nonlinear as well as the classical linear theories of the beams. The available nonlinear stress-strain curves in tension-compression from Rahman (2001) will be used for calculating the moment-curvature and effective modulus-curvature relations for given cross-section of the beam. These will be used to find the deflection and stresses at different segments of the beam.

It is important to verify the soundness of any program by comparing its output with the available experimental results. But, specimens of SMA with variable cross-section are not available. However, those can be made according to the requirements of the design from high quality steel. Spring steel is available in coil form or, in the shape of thick bar. Since the beam specimen will be thinner than those bars, it would be difficult and costly to make thin specimens for the present study out of the available spring steel. On the other hand, specimens can be easily made from the available

stainless steel (SS) sheet. Stainless steel has quite high strength. The properties of SUS304 are also available; for example, yield strength of austenitic SUS304 is 30,000 psi ($\approx 207\text{MPa}$), and it can sustain an elongation of 50%. Of course, mild steel is cheaper than SUS304 but it is of lower yield strength and cannot prevent rust. Therefore, SS has been selected for the present study. At first, numerical results obtained for cantilever SS beams. Experiments of the cantilever beam made of SS have been performed to verify the program. Once the soundness of the code is verified for SS beam, it will be extended for the SMA beam. For a cantilever beam of uniform strength the cross-section is certainly rectangular. Beam height is constant but the width varies linearly with span, the maximum width being at the fixed end. Specimen sizes will be of different dimensions according to the requirement of the design.

Arrangements will be made to apply dead weight as point load at the tip. The load will be increased in steps up to the design value. Simultaneously, the tip deflections will be measured by the height gage.

Finally, integration technique will be used to completely simulate and analyze the nonlinear response of the superelastic SMA beam with variable cross-sectional area.

As already mentioned, once the soundness of the computer code/simulation scheme for a beam is verified by experimental results, it can be extended for simulating mechanical behavior of a beam made of any material. For more details in this regard, interested readers may refer to comprehensive studies carried out for SMA columns as well as for SUS304 columns by Rahman (2001) and Rahman et al. (2005a; 2006).

Therefore, the specific objectives of the present research work are as follows:

- (a) To develop a computer program for analyzing the response of a stainless steel cantilever beam of variable cross-section / uniform strength.
- (b) To conduct experiments of the cantilever beam made of stainless steel in order to verify the developed code.
- (c) To extend the computer code for the case of cantilever SMA beam taking into account its nonlinear material property and analyze the response/mechanical behavior of SMA beam under tip load by applying the extended computer code.

CHAPTER 2

LITERATURE REVIEW

In structural engineering, cantilever beams are often made light by removing extra materials from it, mainly for economy and space constraints (Rahman et al. 2005a, 2006a; Bratus and Posvyanskii 2000; Matulewicz and Szymczak 1985). The present study, thus, concentrates on the response of such a cantilever beam made of shape memory alloy (SMA) with variable cross-sectional area under a tip load.

A large number of studies are reported in the literature dealing with the large deflection analysis of cantilever beams made of conventional engineering materials, out of which only a few are discussed, followed by the discussions of SMA beams. For example, very recent study of Bele'ndez et al. (2005) can be discussed first. The authors carried out numerical simulation using Runge-Kutta-Felhberg method to find the tip deflection of a very slender beam under a combined load. The authors studied the large deflections of a uniform cantilever beam under the action of a combined load consisting of an external vertical concentrated load at the free end and a uniformly distributed load and compared the numerical results with the experimental ones. Young's modulus for the beam material was calculated by comparing the numerical results with the experimental ones. The present study takes into account the experimental results of Bele'ndez et al. (2005) to prove the soundness of the numerical results obtained from the developed numerical scheme.

Deflections of cantilever beam for different cross-sections are studied (Lo and Gupta, 1978; Baker 1993; Lee et al. 1993; Scott et al. 1955)

Lee (2002) dealt with large deflection of cantilever beams made of Ludwick type material under combined loading. Governing equation was derived from shearing force formulation, which has computational advantages over the bending moment formulation for large deflection member. It was pointed out that numerical solution is required to determine the large deflection because the governing equation is a complex non-linear differential equation. Numerical solution was obtained using Butcher's fifth order Runge-Kutta method.

Lewis and Monasa (1982) studied the large deflections of cantilever beams of non-linear materials of the Ludwick type subjected to an end moment.

Bratus and Posvyanskii (2000) dealt with the optimum shape of a bending beam. The problem of minimizing the elastic deflection of an elastic beam of variable cross-section and fixed volume in the case of free supported and rigidly clamped ends has been considered. In case of clamped ends, it has been proved that the optimum solutions must necessarily have points inside the solution range in which the distribution of the beam thickness degenerates to zero. Qualitative analytical and numerical solutions were given.

Matulewicz and Szymczak (1985) studied the optimum design of thin-walled I-beams undergoing torsion. The behaviour of the beam was described in accordance with the theory of thin-walled beams with nondeformable cross-section. The constraints on normal stress level, the magnitude of rotational displacement at a specified cross-section, variable along the beam axis, were discussed. An iterative method of solution, based upon the optimality condition, derived with the aid of Pontrygin's maximum principle, has also been developed.

Rahman et al. (2006a) carried out extensive numerical simulation for studying the response of a slender cantilever beam with an opening of different shapes (circle, ellipse and square slots). It was found that the elliptic holes develop the minimum stresses and deflections. However, in that study, no experimental results were available to verify the numerical results. Therefore, Rahman et al. (2005a) in their next study, performed tests to verify the soundness of the numerical results obtained considering varying cross-section because of a circular hole.

Studies on the bending of the SMA beams of constant cross-section are also reported in the literature. The investigations of the bending problems of pseudoelastic beam were initiated by Atanakov et al. (1989), where the explicit analytical moment curvature relation was derived for rectangular beams loaded by a single pulse moment.

Raniecki et al. (2000), studied the variation of stress and the phase content distribution in arbitrary symmetric cross-section of the beam for single bending cycle and derived the explicit analytical equations for the moment-curvature hysteresis loop.

By numerical simulation, Auricchio and Sacco (1997) demonstrated that for pure bending of a Nitinol superelastic SMA beam, with different properties in tension and compression, the axial strain has a non-monotonous response with the bending moment during loading and unloading. The complicated movement of the neutral axis of the cross-section of the beam due to SIMT leads to such peculiar response.

More recent studies regarding the bending of pseudoelastic SMA beams are reported by Raniecki et al. (2001), Rejnar et al. (2002).

As far as the importance of numerical analysis is concerned, numerical and experimental studies were carried out for the superelastic shape memory alloy beams that can recover large deformations upon unloading. Extensive study on slender cantilever beams' behaviour was carried out considering constant cross-sectional area and it has been demonstrated that experimental results match with the predictions of large deflection theory incorporating the geometric nonlinearity (Rahman et al. (2003)).

SMA is widely used/proposed as an actuator for the hybrid composites mainly for the purpose of active control. Bending/buckling of SMA hybrid composites is also a popular topic (Turner 2005; Turner and Patel 2005; Thompson and Loughlan 2001; Tawfik et al. 2002). It is perhaps important to study the bending of the SMA column itself, before studying the bending/buckling of SMA hybrid composites. This study, therefore concentrates on the study of bending of SMA beams with reducing cross-sections, which was not considered in the previous studies by other researchers.

Moreover, rigorous stress-strain curves for SMA obtained by uniaxial tension and compression tests have been used, without any idealization. Furthermore, since SMA beams can undergo very large deflections, this study also incorporates geometric nonlinearity in the analysis.

The phenomena of buckling of pseudoelastic SMA columns and shafts have also been extensively demonstrated by Rahman et al. (2001, 2005b, 2006b). Furthermore, Rahman et al. (2006c) also studied the buckling of the stainless steel columns. Experiments were conducted and later numerical simulation was carried out in order to analyze the observed buckling and postbuckling behavior for the columns. Precise and quantitative analyses of the results verify the fact that the material's σ - ϵ properties, both in tension and compression, attribute to column's buckling behavior. Obviously, elastic instability analysis (based on Hooke's law) is not sufficient for the SMA beams that has highly nonlinear σ - ϵ relations (Figure 1.2). Moreover, for a high intensity load rigorous σ - ϵ curves in tension and compression should be used for analysis, as pointed by Rahman (2001). Consequently, it was concluded that the best results from numerical simulation would be possible, particularly for the short SMA columns, if both the tensile and compressive σ - ϵ curves can be considered simultaneously (Rahman et al. 2005, 6).

Therefore, the present study is based on simultaneous use of the tension-compression curves of the SMA beams. Following Rahman (2005b, 2006c), very recently Hossain (2006) investigated the buckling of short SMA columns and compared the results with those from Timoshenko's method (1981).

For study of tension-compression asymmetry of the SMA's σ - ϵ curves, interested readers may refer to Orgeas and Favier (1995), Rahman and Khan (2006), Rahman and Tani (2006). In all of these studies, it was demonstrated through rigorous proofs that SMA behaves asymmetrically under tension and compression particularly for large strains.

3.1 General

In this chapter governing differential equations and the additional equations necessary to obtain the effective modulus at different positions of the beam are discussed.

3.2 Governing differential equations for the beam

The basic equations for the analysis of beam can be derived by considering the beam subjected to a tip load P . The Euler-Bernoulli's governing equations are:

$$EI \frac{d^2 y}{dx^2} - PL + Px = 0 \dots\dots\dots(3.1)$$

$$EI \frac{\frac{d^2 y}{dx^2}}{\left[1 + \left(\frac{dy}{dx}\right)^2\right]^{\frac{3}{2}}} - PL + Px = 0 \dots\dots\dots(3.2)$$

Equations (3.1) and (3.2) are linear and nonlinear Bernoulli-Euler's equation, respectively.

Boundary Conditions:

$$y = 0 \quad \text{at } x = 0$$

$$\frac{dy}{dx} = 0 \quad \text{at } x = 0$$

Though the boundary conditions remain the same, the governing equation itself has become much more complicated than that obtained from the linear theory. Therefore, numerical techniques should be used to get the deflection. As, both the boundary values are given at the initial point, the solution has been obtained through initial value integration by Runge-Kutta Method. The design is based on the inelastic properties of structural materials. The shearing effects have been neglected because it is a slender beam.

The load versus deflection curve is obtained by solving the second order governing equation (3.2) for different modulus of elasticity (E , E''). The deflections are determined with the help of Runge-Kutta method (APPENDIX-A). Knowing the bending moment (M_b) from the equilibrium condition at different grid points, E'' at those grid points can be calculated as depicted in flow chart (Figure 3.5). Next, using these E'' at different grid points in the governing equation 3.2, P - δ curve is plotted. From stress-strain relations (Figures 1.2, 4.3(b), 4.4(b)), stresses are found from corresponding different strains and stress versus horizontal distance curves are plotted..

3.3 Large deflection analysis of the beam of uniform strength

A cantilever beam with linearly varying cross-sectional area (Figure 3.1) was simulated. The varying cross-section was due to reducing width with constant height along the span in order to make the beam theoretically of uniform strength, assuming the maximum stress remains within the proportional limit.

Since the beams are slender for the present case, only pure bending is taken into account ignoring the effect of shearing stresses. When bending is large with respect to the span of the beam the governing equation of the elastic curve for a cantilever beam with a point load P (Figures 3.1, 3.2), in terms of large deflection formulation is given in equation (3.2).

Equation (3.2) neglects the effect of end-shortening of the tip (δ_h). If this end shortening is considered, only the second term of equation (3.2), is to be changed as $P(L-\delta_h)$. The above equation is highly nonlinear (geometrically) and has been solved numerically in the present study by Runge-Kutta method.

For calculating this end shortening δ_h , let us consider a cantilever beam having length L acted upon by a load P . On the elastic curve, an infinitesimal segment length ds is given by

$$ds = \sqrt{dx^2 + dy^2}$$

Therefore, the total length of the elastic curve is given by

$$s = \int_0^{X_H} \sqrt{dx^2 + dy^2}$$

$$= \int_0^{X_H} \sqrt{1 + \left(\frac{dy}{dx}\right)^2} dx \dots\dots\dots(3.3)$$

where, $X_H = L - \delta_h$

With the assumption of inextensible elastic curve, δ_h is calculated numerically by trial. At first the elastic curve is evaluated from the solutions equation (3.2) without considering δ_h . Next, assuming the value of $X_H = L - \delta_h$, in such a way that the value of integration of equation (3.3) becomes $s \approx L$, it can be said that end shortening is $\delta_h = L - X_H$. In this thesis δ_h was calculated with the following convergence criteria, $L \geq s \geq 0.998L$. Then putting the value of δ_h in the equation (3.2) of the elastic curve, deflections at corresponding loads can be found. Alternately, at first a small value of δ_h is assumed and equation (3.2) is solved. Once the elastic curve is known, equation (3.3) is integrated numerically by Simpson's 3/8th rule to check whether the assumed value of δ_h is accurate or, needs to be improved by the next step. Therefore, in order to take into account the end shortening, equations (3.2) and (3.3) have to be solved simultaneously.

Next, the design parameters based on classical linear theory for the beams of uniform strength are described. From the definition it follows that,

$$\frac{M}{Z} = \frac{6PL}{b_0 h^2} = \frac{6P(L-x)}{bh^2}$$

in which b_0 is the width of the beam at the built-in end. Then,

$$b = \frac{b_0(L-x)}{L}$$

Since the section modulus (Z) and moment of inertia of a beam of triangular shape changes with x in the same proportion as the bending moment, the maximum stress and the curvature remain constant along the beam (Figures 3.1, 3.2). Therefore, the deflection of the beam at the end, without considering the end shortening, is,

$$\delta = \int_0^L \frac{12.P(L-x).x}{E.bh^3} dx = \frac{12.PL}{E.b_0h^3} \int_0^L x dx = \frac{1}{2} \frac{PL^3}{EI_0} \dots (3.4)$$

where, $I_0 = \frac{b_0h^3}{12}$ represents the moment of inertia of the cross section at the built-in end.

It can be noted that the solutions from equations (3.3) and (3.4) are likely to vary significantly at a high load and that is one of the important points of discussion for the present study. Moreover, though solution from equation (3.4) is exact and readily available; a lot of numerical analysis is involved to get the solutions from the highly nonlinear equations (3.2) and (3.3). In particular, the end shortening calculations takes considerable time during numerical simulations.

More importantly, since for the present study the stress exceeds far beyond the proportional limit and also cross-section varies along the span, the stiffness (EI) also becomes variable at the grid points. The following section describes in detail the strategy to tackle the material nonlinearity for pure bending of such a beam.

3.4 Analysis of the inelastic deformation of the beam [Timoshenko's method (1981)]

The theory is based upon the assumption that cross-section of the beam remains plane during bending and hence longitudinal strains are proportional to their distance from the neutral surface. σ - ε diagram of Figure 3.3 will be referred to during the deviation.

Let us begin with a beam of rectangular cross section (Figure 3.4) at the fixed end and assume that the radius of curvature of the neutral surface produced by the bending moment M is equal to ρ . In such a case the unit elongation of a fiber at distance y from the neutral surface is

$$\varepsilon = \frac{y}{\rho} \dots\dots\dots(3.5)$$

Denoting by h_1 and h_2 the distance from the neutral axis to the lower and upper surfaces of the beam, respectively, we find that the elongations in the extreme fibers are

$$\varepsilon_1 = \frac{h_1}{\rho} \quad \varepsilon_2 = -\frac{h_2}{\rho} \dots\dots\dots(3.6)$$

It is seen that the elongation or contraction of any fiber is readily obtained provided we know the position of the neutral axis and the radius of curvature ρ . These two quantities can be found from the following two equations of static equilibrium.

$$\int \sigma dA = b \int_{-h_2}^{h_1} \sigma dy = 0 \dots\dots\dots(3.7)$$

$$\int \sigma y dA = b \int_{-h_2}^{h_1} \sigma y dy = M_b \dots\dots\dots(3.8)$$

Equation (3.7) is now used for determining the position of the neutral axis. From equation (3.5) we have

$$y = \rho \varepsilon \quad dy = \rho d\varepsilon \dots\dots\dots(3.9)$$

Substituting into equation (3.7) we obtain

$$\int_{-h_2}^{h_1} \sigma dy = \rho \int_{\varepsilon_2}^{\varepsilon_1} \sigma d\varepsilon = 0$$

Hence the position of the neutral axis is such that the integral vanishes. The integral can be represented by the area under stress-strain diagram (Figure 3.3) from ε_2 to ε_1 . Now we define Δ as the sum of the absolute values of the maximum elongation and maximum contraction, which is

$$\Delta = \varepsilon_1 - \varepsilon_2 = \left| \frac{h_1}{\rho} \right| + \left| \frac{h_2}{\rho} \right| = \frac{h}{\rho}$$

In calculating the radius of curvature ρ we use equation (3.8) in the following form

$$b\rho^2 \int_{\epsilon_2}^{\epsilon_1} \sigma \epsilon d\epsilon = M_b$$

Next, by observing that $\rho = \frac{h}{\Delta}$ and $\frac{E''I}{\rho} = M_b$, we get, $E'' = \frac{12}{\Delta^3} \int_{\epsilon_2}^{\epsilon_1} \sigma \epsilon d\epsilon$

The integral in this expression represents the moment of the area under $\sigma-\epsilon$ diagram from ϵ_2 to ϵ_1 with respect to the vertical axis as shown in Figure 3.3. Of course, for numerical simulation we used Figures 4.3(b), 4.4(b) for stainless steel beam and Figure 1.2 for SMA beam in place of the fictitious Figure 3.3.

True strain in tension (ϵ_t) and true strain in compression (ϵ_c) are given by the following equations. Where h_0 is original length, h is changed length, δ_0 is difference between original and changed lengths and e is engineering strain.

$$\epsilon_t = \int d\epsilon_t = \int_{h_0}^h \frac{dh}{h} = \ln \frac{h}{h_0} = \ln \frac{h_0 + \delta_0}{h_0} = \ln(1 + e) \dots (3.10)$$

$$\epsilon_c = \ln \frac{h_0}{h} = \ln \frac{h_0}{h_0 - \delta} = -\ln \frac{h_0 - \delta_0}{h_0} = -\ln(1 - e) \dots (3.11)$$

True stresses are obtained from condition of incompressibility. The true stress in tension $(\sigma_{true})_{tension}$ and true strain in compression $(\sigma_{true})_{compression}$ are given by following equations.

$$(\sigma_{true})_{tension} = \frac{F}{A} = \frac{F}{A_0} (e^{\epsilon_t})$$

$$\text{or, } (\sigma_{true})_{tension} = \sigma_0 (1 + e) \dots \dots \dots (3.12)$$

$$\text{or, } (\sigma_{true})_{compression} = \sigma_0 (1 - e) \dots \dots \dots (3.13)$$

Where A_0 is original cross-section, A is changed cross-section and σ_0 is engineering (nominal) stress.

Once the $M-\Delta$ and $E''-\Delta$ curves are known for different sections of the beam, the stresses can be easily calculated at those sections using equilibrium approach. At first, governing equation (3.2) has to be solved replacing the stiffness parameter EI by its appropriate values at different grid points.

INELASTIC DEFORMATIONS OF CANTILEVER STAINLESS STEEL BEAMS OF VARIABLE CROSS-SECTION- EXPERIMENT AND NONLINEAR ANALYSIS

4.1 General

Since the stainless steel is one of the most widely used structural materials, elastic-plastic study of stainless steel beam, originally designed for uniform strength, is essential. Such study could not be found in the available literatures. Therefore, the present thesis concentrates on inelastic deformation of a stainless steel beam with varying cross-section.

Obviously, elastic bending analysis (based on Hooke's law) is not sufficient for the stainless steel beams that has highly nonlinear σ - ε relations. For simplicity of analysis, sometimes stress-strain curves are assumed to follow certain material type as already discussed. But as pointed by Rahman et al. (2006c), for a stainless steel column under a high intensity load, rigorous σ - ε curves in tension and compression must be used for numerical analysis. Therefore, stress-strain curves for stainless steel, obtained by uniaxial tension tests, have been used for simulation purpose without any idealization (Figures 4.3, 4.4). Furthermore, since stainless steel beams are assumed to undergo very large deflections, this study also incorporates geometric nonlinearity in the analysis.

4.2 Experiment

Thin stainless steel (SS) sheet with relatively moderate/low yield strength is perfectly suited for the present study that concerns inelastic deformations of the beams. Therefore, specimens of the beams of different dimensions were produced from two commercially available SS sheets. Tensile test specimens were taken from the same sheets.

Figures. 3.1 to 4.4 and Table 4.1 are presented to clearly explain different important physical and geometrical parameters of the beam of variable cross-section studied in this thesis. The geometrical parameters shown are different dimensions and end shortening

of the beam (Figures 3.1, 3.2). Figures 4.1 and 4.2 show the experimental setup. Nominal stress-strain curve is obtained by experiment and then converted to true stress-strain curves (Figures 4.3(a) to 4.4(b)).

Tensile test results of the four specimens of thickness 1mm, obtained by taking the load cell reading of the universal testing machine and the corresponding reading of strain by a mechanical extensometer, show that the stress-strain curves for the specimens remain linear initially but nonlinear at a high stress (Figure 4.3(a)). These linear and nonlinear stress-strain relations are the main criteria of selection of the beam material for this study for performing experiment of the cantilever beams that must undergo large deflections, as far geometric nonlinearity and material nonlinearity are concerned. Similar stress-strain relations were obtained for other four specimens of thickness 2 mm under similar test conditions (Figure 4.4(a)). From those eight stress-strain curves apparently the best two representative curves (one of thickness 1mm and another of thickness 2mm) are selected for analysis. Next, the true stress-strain relation is taken for stainless steel from experimental stress-strain relation (Figures 4.3(b), 4.4(b)). By using true stress-strain relation, moment-curvature and modulus of elasticity-curvature relation are obtained. Those values are essentially used for the purpose of simulation of beam's response under a tip load. It is important to note that conversion of nominal (engineering) σ - ϵ curves separately into true tensile σ - ϵ curve and true compressive σ - ϵ curve, will automatically induce tension-compression asymmetry for the beams as will be evident in the results and discussion chapter of the thesis.

A sufficiently rigid structure made of wood, as shown in Figures 4.1, 4.2, was constructed for conducting the experiment, in order to trace the beam's load-deflection relation. Dead weight was applied at the tip and the corresponding deflection was measured by the height gage (one small division of its dial can read 0.01mm). To eliminate eye estimation errors, a simple circuit (with a DC source and light emitting diode) was wired between the specimen and height gage pointer. Therefore, whenever the height gage touched the beam, it was indicated by a flash. The whole process of experiment is shown in Figures 4.1, 4.2. For each of the four cases described (Table 4.1), three specimens were tested and the average results of tip deflections and end-shortening are presented for analysis. The end-shortening of the tip was measured by a digital vernier scale and these values are presented in Table 4.3.

4.3 Accuracy and reliability of the analysis

A numerical technique, integrated in a computer program written in C++ (APPENDIX-C), has been employed here to solve the problem of deflections and stresses of stainless steel and superelastic SMA beams at tip load and using different moduli of elasticity for variable cross-section. Before presenting the analysis of the results, it is necessary to give an idea about the accuracy of the numerical technique and the reliability of the program used. Here, ten segments are taken along the beam span, and 4th order Runge-Kutta method (APPENDIX-A) is used for analysis of the beam. So that the accuracy of 4th order remains uniform.

4.4 Results and discussion

Soundness of the present numerical scheme can be proved by comparing the results, taking into account only geometric nonlinearity, for a highly flexible cantilever beam of constant cross-section under a combined load as treated by Bele'ndez et al. (2005). Table 4.2 shows the comparison of experimental tip deflections with those obtained using present numerical analyses. The Young's modulus for a particular load was not explicitly given by Bele'ndez et al. (2005). It was stated to be within 180-210GPa. We used its value as 200GPa. As may be seen from table 4.2 that the numerical nonlinear solution matches within an error of only 3.5% at the highest experimental load found by Bele'ndez et al. (2005). A better match would be possible with the known correct value E . For example, $E=194.5\text{GPa}$ was found to give least error as shown by Bele'ndez et al. (2005). Therefore, our numerical predictions would match even better with the experimental results with $E=194.5\text{GPa}$. Anyway, it is now proven that the present numerical scheme as used here is capable of predicting the elastic curve with reasonable accuracy by large deflection theory taking into account the associated end-shortening even under a combined load.

Again as cross-section varies linearly with the span, $M-\Delta$ relation is calculated for the different segments as shown in Figures. 4.5, 4.6(a), (b). Figures. 4.6(a) and 4.6(b) present the comparison of bending moment with total strain for different segments

obtained from experimental σ - ε diagram (Figures 4.3(b), 4.4(b)). Since nonlinear σ - ε relation is used, the M - Δ relation also becomes nonlinear.

From Figure 4.7, it is found that the modulus of elasticity is almost constant for very low strain ($\Delta = 0.202\%$ for 1mm and $\Delta = 0.102\%$ for 2mm) with a value of 181GPa and 223GPa for specimen thickness of 1mm and 2mm, respectively. These values are actually the Young's modulus of elasticity of the material, which satisfies Hooke's law for proportional limit. In the nonlinear range of σ - ε curves, the slope significantly decreases with strain and hence the modulus of elasticity, E , is termed as effective modulus of elasticity, E'' .

From Figure 4.7, it is seen that E'' remains the same for all the segments though M varies for different segments (as shown in Figures 4.6(a), (b)) along the span. This is because of the fact that b varies along the length, but h remains the same.

All the results (Figures 4.8-4.15) presented in this thesis are based on the M - Δ and E'' - Δ relations of Figures 4.6(a), (b) and Figure 4.7, respectively.

The concept of so-called uniform strength ideal beam has been applied in the following steps. With the aid of Figures 4.6(a), (b) we can select a value of maximum design moment (M) that will occur at the fixed end. Assuming linear stress-strain relation and ignoring end-shortening, corresponding design load P_1 is known from the equilibrium condition and consequently, strains (Δ), are known from Figures 4.6(a), (b). In this way, corresponding to the design load P_1 , for 1mm thick beam a uniform design stress was set approximately at 200MPa while for 2mm thick beam the uniform design stress was set approximately at 250MPa. Figures 4.3 and 4.4 show that these stress values are in the vicinity of the proportional limits. However, since dead weight was used for loading, the closely possible actual values of the uniform design stresses are as shown in Table 4.1. Moreover, analysis is also carried out for the same beam but at a higher load, P_2 (Tables 1, 3), in order to take the analysis distinctly in the regime of high geometric and material nonlinearities. The deflections and stresses corresponding to P_1 and P_2 are presented in Figures 4.8-4.15.

The results for the four designed beams are presented in the following way. At first, the complete load-deflection curves (both from experiment and simulation) are discussed for a particular beam. Next, the comprehensive stress analyses (by linear and

nonlinear theories and with and without end-shortening) are presented for the same beam.

Before discussing in detail the numerical results, it is important to give an idea of accuracy of those results with the aid of Figure 4.8 for case 1. For this purpose, at first, results predicted from the linear theory and elastic material can be compared with the exact formula ($PL^3/2EI$) given by equation (3.4), considering the case of a beam of variable cross-section without end shortening. Therefore, for the dimensions of case 1 as shown in Table 4.1, for the load of 14.529N, the analytical tip deflection is 35.33mm. From the data of Figure 4.8, for linear theory, the computer code gives a close value of 35.34mm. Thus, predictions of all other solutions for the beams at different cases (according to linear/nonlinear theory with and without end-shortening), using the same code, can also be considered as highly accurate. It is because the numerical scheme is based on initial value integration technique and easily yields much more accurate and reliable results than those from other numerical techniques like finite difference or finite element.

Figure 4.8 shows that at a low load of 5.004N the value of tip deflection obtained by experiment is 3.6mm. Corresponding solutions by ideal case is 3.13mm and the tip deflections for the case of linear and nonlinear analysis together with end-shortening are 2.66mm and 2.74mm, respectively.

At design load ($P_1=10.158N$) the tip deflection obtained by experiment is 22.8mm. Corresponding solutions by ideal case is 24.55mm and by linear and nonlinear theories without end-shortening are 23.04mm and 25.8mm, respectively. But the tip deflections for the case of linear and nonlinear analysis together with end-shortening are 20.6mm and 21.97mm, respectively.

Finally, the tip deflection at a load of 14.529N, as predicted by the nonlinear solution taking into account the end-shortening is only 1.37% more than that from experiment and the linear solution together with end-shortening is 8.80% less than that from experiment. However, the tip deflection obtained by experiment is 7.51% less than that from linear solution and 26.7% less than that from nonlinear solution if the effect of end shortening is ignored.

As seen from Figure 4.8, the ideal solutions for linearly elastic beam ($E=181GPa$), that can also be obtained using equation 3, are superimposed with the

more comprehensive and realistic numerical results including that from experiment. As seen, if the load is not that high, all the solutions merge together, simply verifying the soundness of the numerical scheme. At higher loads, however, the solutions diverge because of the fact that the effect of material and geometrical nonlinearities and also end shortening become important (Figure 4.8).

It should be mentioned here that the terms 'nonlinear' in the captions of Figures 4.8-4.15 refer to the geometrical nonlinearity. Although, except the ideal case as shown in Figure 4.8 and Figure 4.12 all the solutions (either linear or, nonlinear) take into account the material nonlinearity. Among the numerical results of tip deflections and stresses obtained, apparently the best predicted results are that takes into account both types of nonlinearities together with end shortening from practical point of view (Figure 4.8). It should be mentioned here that the importance of geometric and material nonlinearities can be clearly realized if a comparison is made with ideal case. Therefore, a few comparisons are given in this regard.

It has already been mentioned that for ideal case, that is for linear theory, elastic material and ignoring the effect of end-shortening, a beam with linearly reducing cross-section has its tip deflection given by equation (3.4) and more importantly, it should develop equal stress all along its span. In order to visualize the real situations, however, Figures 4.9(a) and 4.9(b) show the actual stress distributions for variable cross-section (case 1) along the beam-span for the geometrically linear and nonlinear cases, respectively. If end-shortening is ignored, both geometrically linear and nonlinear cases predict constant stresses (either tensile or compressive) along beam span. On the other hand, stress decreases along the span of the beam because of end-shortening together with material nonlinearity.

The stress according to ideal case, for case 1 (Mc/I) at the design load ($P_1=10.158\text{N}$) is 198.74MPa , but at a higher load ($P_2=14.529\text{N}$) for the same beam geometry is 284MPa . Now let us examine their real values at the fixed end according to nonlinear analyses from Figures 4.9.

For the design load, P_1 , the linear theory together with end-shortening predicts 191.42MPa tensile stress and 192.09MPa compressive stress (Figure 4.9(a)). The nonlinear theory with end-shortening, on the other hand, predicts 191.14MPa tensile stress and 191.69MPa compressive stress (Figure 4.9(b)). These stresses are

significantly lower than their design values of 198.74MPa (both in tension and compression).

Again, as seen in Figure 4.9(b), for a higher load P_2 , the nonlinear theory with end-shortening, predicts 244.14MPa tensile stress and 244.09MPa compressive stress (Figure 4.9(b)) that are drastically less than their values of 284MPa (same in tension and compression) according to ideal beam formula (Mc/I).

Moreover, an ideal beam of uniform strength should retain uniform stress along its span. But it is very clear that the stresses do not remain constant but decreases along the span. For instance, Figure 4.9(b) shows that if end-shortening is taken into account, at P_2 , the tensile and compressive stresses are 234.77MPa and 235.04MPa, respectively, at the grid point just before the tip. These values are notably less than their corresponding values at the fixed end. At this point, it can be said that slightly more material can be removed, in particular near the beam tips, to make the beam of uniform strength more economical. Similar pattern of stress distribution can be seen for other three cases 2-4, as shown in Figures 4.11, 4.13 and 4.15.

Those results can be physically interpreted as below. First of all, in the inelastic deformation region, stress increases quite insignificantly with strain (Figures 4.3, 4.4). Thus the effect of considering material nonlinearity results in reduction of stress in comparison to ideal linear flexural stress ($=Mc/I$). The asymmetry in tension-compression is because of conversion of the nominal stress-strain curves into their true stress-strain values.

Secondly, the effect of end-shortening is to reduce the bending moment and corresponding stresses at the fixed end. Further, end-shortening causes a continuous reduction of stress along the span.

Finally, the effect of geometric nonlinearity is an additional (though slight) reduction of stress in comparison to the linear theory (linear theory is consistently conservative).

Figure 4.10 shows that the load-deflection curves for case 2 is similar to those in Figure 4.8. From Figure 4.10, at the load of 14.529N, the tip deflection by nonlinear solution with end-shortening is 57.8mm and by linear solution with end-shortening is 54.91mm. The experimental value at the same load is 61.6mm.

Figures 4.11(a), (b) show the stress distribution along the span of the beam for case 2 at a design load of $P_1=10.158\text{N}$ and a higher load of $P_2=14.529\text{N}$. Since the beam parameters are same except the load, the corresponding point on the equilibrium configuration path can be located in Figure 4.10 corresponding to P_1 and P_2 . For the higher load, P_2 , the compressive and tensile stresses at the fixed end by nonlinear theories together with end-shortening are 244.10MPa and 243.71MPa , respectively. The stresses decrease along the span. The stress values at the grid point just before the tip are 225.57MPa (tensile) and 226.42MPa (compressive). It can be noted that the stresses are 285.82MPa according to ideal beam theory and should remain constant along the span.

As far as prediction of tip deflections and end-shortening are concerned, Case 3 shows the best match between prediction and real values found by experiment as shown in Figure 4.12 and Table 4.3. The shape of the equilibrium configuration path even in the highly nonlinear range is quite accurately predicted by the nonlinear theory with end-shortening (Figure 4.12). In Figure 4.12, the tip deflection at design load ($P_1=20.076\text{N}$) obtained by experiment is 15.0mm . Corresponding ideal solution (by equation (3) with $E=223\text{GPa}$) is 12.66mm and by linear theory, solution obtained by computer code is 12.67mm . The numerical results at the same design load by linear and nonlinear analysis together with end-shortening are 12.85mm and 13.43mm , respectively. At the higher load of 34.51N tip deflection, as predicted by the nonlinear solution taking into account the end-shortening, is only 1.74% more than that from experiment. Similarly, for the same load the linear solution together with end-shortening is 8.69% less than that from experiment.

Figures 4.13(a), (b) show the stress distribution along the beam span for case 3 at two different loads, at the design value $P_1=20.076\text{N}$ and the higher load $P_2=34.51\text{N}$. The effect of high load on the beam's response is very clear. By formula of ideal beam (Mc/I) stresses should be 250.95MPa at ($P_1=20.076\text{N}$) and 431.375MPa at a high load ($P_2=34.51\text{N}$). The stress pattern as shown in Figures 4.13 is similar to those of cases 1,2 (Figures 4.9, 4.11). At P_2 , the compressive and tensile stresses at the fixed end by nonlinear theories together with end shortening are 335.77MPa and 340.84MPa , respectively. It shows that the stress decreases along the span. Stress pattern is similar at the design load $P_1=20.076\text{N}$.

In Figure 4.14 the tip deflection for case 4 is shown up to a high load of 34.51N load. The design load is $P_f=20.076\text{N}$. At the highest load, the tip deflection for nonlinear solution with end-shortening is 5.98% more than that from experiment. In case of linear solution with end-shortening, the tip deflection is 10.34% less than that from experiment. Of course, the tip deflection is found to be unrealistically high if end-shortening is ignored, though those results are not shown here explicitly.

Stress distributions along the span are shown in Figures 4.15(a), (b) for case 4. The compressive and tensile stresses at the fixed end by nonlinear theories together with end shortening are 334.72MPa and 337.61MPa, respectively (Figure 4.15(b)). The tension compression asymmetry is also a bit prominent for this high load. Though the stresses are quite high, both tensile and compressive stresses fall along the span. As usually, the linear theory (ignoring the geometric nonlinearity) predicts slightly conservative values of the stresses (Figure 4.15 (a)). The ideal beam theory will predict a high stress of 429.59MPa at 34.51N.

Modern structures demand light structures made of the structural materials like steel. It in turn, necessitates comprehensive stress and deflection analysis of the beams/columns that are made light removing any extra, unnecessary material. An optimum design of a beam, for example would make sure that all the cross-sections of the beam utilizes the maximum available safe strength of the beam material. The present study therefore, shows that the actual stresses are significantly less than their values are according to ideal theory. Moreover, at the vicinity of tip, stress further decreases from the maximum value at the fixed end.

Correct prediction of end-shortening is important. Effect of end-shortening on the stress analysis has already been discussed. But, end-shortening effect is found to be also important for calculating tip deflections at high load. Therefore, before concluding, a further comparison between the experiment and numerical analysis can be made with reference to end-shortening as presented in Table 4.3. Normally the nonlinear theory predicts slightly more end-shortening than that predicted by linear theory. Consequently, the experimental results match more closely with those of nonlinear theory. The best match is seen for case 3 for end-shortening as well, as it was for the case of tip-deflections (Figure 4.12).

CHAPTER 5

NONLINEAR ANALYSIS OF A SUPERELASTIC SHAPE MEMORY ALLOY CANTILEVER BEAM OF VARIABLE CROSS-SECTION

5.1 General

It has been shown, in the previous chapter, that the soundness of the present numerical scheme by comparing the results, taking into account only geometric nonlinearity, for a highly flexible cantilever beam of constant cross-section under a combined load as treated by Beléndez et al. (2005). Also very good match has been found for experiment and numerical analysis for an stainless steel beam of uniform strength. Now, response of an SMA beam (theoretically of uniform strength) under a tip load will be studied.

5.2 Results and discussions

Figure 4.5 shows 10 different segments of the beam that are taken for the analysis and Figure 5.1 presents the comparison of bending moment for different segments obtained from experimental σ - ε diagram (Figure 1.2). As cross-section varies linearly with the span, M - Δ relation is calculated for the different segments as shown in Figure 5.1. In this figure, increase in bending moment is linear in the proportional limit up to a strain of 1%. But, in the nonlinear range of σ - ε curve, it increases nonlinearly with strain.

From Figure 5.2, it is found that E'' is almost constant for very low strain ($\Delta = 1\%$) with a value of 65GPa; of course, E'' decreases significantly for larger value of Δ . From Figure 5.2, it is seen that E'' remains the same for all the segments though M varies for different segments (as shown in Figure 5.1) along the length. This is because of the fact that b varies along the length, but h remains the same.

All other results (Figures 5.3-5.11) presented in this thesis are based on the M - Δ and E'' - Δ relations of Figures 5.1, 5.2, respectively.

With the aid of Figure 5.1 we can select a value of maximum design strain (Δ) that will occur at the fixed end. Corresponding M and consequently, load ($P=M/L$) are known from Figures 5.1. Table 5.1 presents the dimensions and maximum design strains of the beams of variable cross-section analyzed in this study (cases 1-6). The beams are designed in such a way that at the applied load it can be either in austenite phase (case 6), mixed phase (cases 2, 4), or in the SIM phase (cases 1, 3, 5). The deflections and stresses corresponding to cases 1-6 are presented in Figures 5.3-5.11.

The results for the six designed beams are presented in the following way. At first, the complete load-deflection curves are discussed for a particular beam. Next, the comprehensive stress analyses (by linear and nonlinear theories and with and without end-shortening) are presented for the same beam.

In general, equilibrium configuration paths (Figures 5.3, 5.6, 5.9) are initially linear but convex upward at the higher loads, because of material nonlinearity. The nonlinear solutions with end-shortening gives the most realistic results from practical point of view. In comparison, the linear solutions with end-shortening predict slightly lower tip deflections. But the deflections are too large if the end-shortening is not taken into account.

On the other hand, comprehensive stress analysis results are presented in Figures 5.4, 5.5, 5.7, 5.8, 5.10, 5.11. Generally, tension-compression asymmetry is prominent for all the cases considered, the higher the design strains, the more prominent is the asymmetry. Another distinguishing feature is the fall of stress along the beam span, the highest stress being at the fixed end; in contrast, a classical leaf spring under ideal conditions should develop uniform stresses all along its span. Moreover, nonlinear solutions with end-shortening predict the stresses that are significantly smaller than those predicted by neglecting the effect of end-shortening. Linear solutions slightly over predict the stresses in comparison to the nonlinear solutions. Regarding the presentation style of the stresses, we prefer to use x on the abscissa for Figures 5.4, 5.5, 5.7, 5.8, 5.10, 5.11. x has been defined in Figure 1 as the horizontal distance of a point on the elastic curve, measured from the fixed end. For clarity, $x=X_H$ corresponds to the projection of the deflected elastic curve's tip on x axis. The advantage of stress versus x curve is that, one can get an idea of end-shortening directly.

Now we shall discuss results cases 1-6 more specifically, giving emphasis on cases 1 and 5. But, before discussing in detail the numerical results, it is important to give an idea of accuracy of those results with the aid of Figure 5.3. For this purpose, at first, results predicted from the linear theory can be compared with the exact formula ($PL^3/2EI$) given by equation (3.4), considering the case of a beam of variable cross-section without end-shortening. Therefore, for the dimensions of case 1 as shown in Figure 3.1, at a load of 80 kN, the analytical tip deflection ($E=65\text{GPa}$) is 73.85mm. From the data of Figure 5.3, for linear theory, with only 10 segments, the computer code gives a close value of 73.13mm. Thus, predictions of all other solutions for the beams at different cases (according to linear/nonlinear theory with and without end-shortening), using the same code, can also be considered as sufficiently accurate. Of course, higher accuracy is possible by using more number of segments. But it is avoided for the sake of simplicity in calculations; other wise constructions of Figures 5.1,5.2 would be more tedious.

As seen from Figure 5.3, the ideal solutions for linearly elastic beam, that can also be obtained using equation 3, are superimposed with the more comprehensive and realistic results. As seen, if the load is not that high, all the solutions merge together, simply verifying the soundness of the numerical scheme. At higher loads, however, the solutions diverge because of the fact that the effect of material and geometrical nonlinearities and also end-shortening become important (Figure 5.3).

It should be mentioned here that the terms 'nonlinear' in the captions of Figures 5.3-5.11 refer to the geometrical nonlinearity. Although, except the ideal case as shown in Figure 5.3, all the solutions (either linear or, nonlinear) take into account the material nonlinearity. Among the numerical results of tip deflections and stresses obtained, apparently the best results are that takes into account both types of nonlinearities together with end-shortening from practical point of view.

Figure 5.3 shows that the tip deflection at the design load of 80kN for case 1, as predicted by the nonlinear solution taking into account the end-shortening is 10.82% more than that from linear solution with end-shortening. However, the tip deflection is 36.59% less than that from linear solution and 126.5 % less than that from nonlinear solution if the effect of end-shortening is ignored.

It has already been mentioned that for ideal case, that is for linear theory, elastic material and ignoring the effect of end-shortening, a beam with linearly reducing cross-section has its tip deflection given by equation (3) and more importantly, it should develop equal stress all along its span. In order to visualize the real situations, however, Figures 5.4(a) and (b) show the stress distributions for variable cross-section (case 1) along the beam-span for the geometrically linear and nonlinear cases, respectively. First of all it is clear that the tensile and compressive stresses are highly asymmetric (Figures 5.4). Moreover, if end-shortening is ignored, both geometrically linear and nonlinear cases predict same solutions of stresses (either tensile or, compressive) for the cantilever beams. On the other hand, stress decreases along the span of the beam mainly because of end-shortening. It is found that compressive stress falls more significantly than the tensile stress because of asymmetry in the stress-strain relation.

In case of linear analysis (Figure 5.4(a)), when material nonlinearity and end-shortening are considered, the stresses do not remain constant but decreases along the span. At fixed-end the tensile and compressive stresses without end-shortening are found to be 601.2 MPa and 947.9MPa, respectively. But, with end-shortening the tensile and compressive stresses are 558.91MPa and 854.64MPa, respectively. With end-shortening, at immediate precedent of the last point (at $x=425.34\text{mm}$) the tensile and compressive stresses are 539.72MPa and 655.2MPa, respectively. Therefore, tensile stress and compressive stress are 10.23% and 30.84% less, respectively, than the corresponding stresses found without end-shortening.

Again by nonlinear analysis considering end-shortening, tensile and compressive stresses at the fixed end are, respectively, 557.12MPa and 847.69MPa as shown in Figure 5.4(b). At the immediate precedent of the last point (at $x=422.19\text{mm}$) these tensile and compressive stresses are 543.26MPa and 705.18MPa, respectively.

Figures 5.5(a), (b) show that for case 2, the stress distribution along the span of the beam at a load of 75kN. Since the beam parameters are same as those of case 1 except the load, the corresponding point (on the equilibrium configuration path) can be located in Figure 5.3. The stress pattern as shown in Figures 5.5 is similar to but of lower magnitude than that of case 1 (Figures 5.4). The compressive and tensile stresses at the fixed end by nonlinear theories together with end-shortening are 778.19MPa and 549.21MPa, respectively. As discussed, if end-shortening is ignored, the tensile and

compressive stresses are still asymmetric but remains constant along the span. The effect of end-shortening is, therefore, mainly a reduction of the stress values calculated either by linear or, nonlinear theory.

For case 3 Figure 5.6 shows at the design load 110kN, the tip deflection predicted by nonlinear solution with end-shortening is 19.32% more than that found by linear solution with end-shortening.

Figures 5.7(a), (b) show the stress distribution along the span of the beam for case 3 at a load of 110 kN. The compressive and tensile stresses at the fixed end by nonlinear theories together with end-shortening are 978.55MPa and 661.48MPa, respectively. Because of a higher load than those for cases 1,2, the tension-compression asymmetry of the stresses are quite prominent. Also stresses decrease quite significantly along the span.

Figures 5.8(a), (b) show the stress distribution along the beam span for case 4 at a load of 75kN. The compressive and tensile stresses at the fixed end by nonlinear theories together with end-shortening are 584.04MPa and 534.31MPa, respectively. The fall of stress along the span is less prominent in comparison to case 3.

Figure 5.9 shows that the load-deflection curves obtained for case 5. Since, the highest strains occur in the beams for this case, therefore, the tension-compression asymmetry and also the effect of end-shortening should also be the most prominent. Tip deflection is found to increase substantially with an insignificant increase of the loading parameter at the higher loads. Because of very large strains, the effective modulus is small enough, and it appears load-deflection curves would become almost flat if further increase is made at the highest load, as predicted by linear as well as nonlinear solutions with end-shortening. As can be seen, at a design load of 180kN, tip deflection for nonlinear solution with end-shortening is 12.37% more than that from linear solution with end-shortening. Of course, this tip deflection is found to be considerably less if end-shortening is ignored.

For case 5, the effect of high load on the beam's response is very clear in terms of stress analysis as shown in Figures 5.10. The maximum stresses at the fixed end, by nonlinear theory, without end-shortening are 1131.7MPa and 1389.2MPa in tension and compression, respectively. But with end-shortening the values are 995MPa and 1192.4MPa in tension and compression, respectively. The corresponding tensile and

compressive strains are 7.47% and 5.85%, respectively, their sum being 13.32%. Upon unloading, this SMA beam can fully recover its shape by virtue of superelasticity. It is interesting to note that the maximum design strains for this case, that is the summation of tensile and compressive strains (but, of course without considering geometric nonlinearity and end-shortening) was 15.2% as shown in Table 4.2.

Though the fixed end stresses are quite high, both the tensile and compressive stresses fall remarkably along the span and their values are 539.72MPa and 655.2MPa, respectively, at immediate precedent of the last point on span. It clearly indicates more material can be safely removed particularly, near the vicinity of the tip, to make the SMA beam lighter and more economic.

Figures 5.11(a) and (b) show the stress distribution for case 6 along the beam span at a load of 75kN. Since beam parameters are exactly the same as that of case 5 except the small magnitude of load; the corresponding point can be located on the load-deflection curve of Figure 5.9. Because of significantly lower load than the previous case, the effect of end-shortening is less prominent as can be seen in Figures 5.11. The material's tension compression asymmetry, however, can be clearly visualized. The compressive and tensile stresses at the fixed end by nonlinear theories together with end-shortening are 478.18MPa and 486.24MPa, respectively.

Modern adaptive structures demand light structures made of the functional materials. It in turn, necessitates comprehensive stress and deflection analysis of the beams/columns that are made light removing any extra, unnecessary material. An optimum design of a beam, for example, would make sure that all the cross-sections of the beam utilizes the maximum available safe strength of the beam material. The present study therefore, shows that more material can be removed from an SMA beam of reducing cross-sections.

With the background of the above detail discussions, a further analysis can be made as far as stress induced martensitic transformations (SIMT) is concerned for the SMA beams with reference to Figures 1.1,1.2,5.4,5.5,5.7,5.8,5.10,5.11. The highest stresses occur for case 5 at the fixed end. The compressive and tensile stresses at the fixed end by nonlinear theories together with end-shortening are 1192.33MPa and 994.96MPa, respectively. Presumably, the SMA should be in SIM phase at this load. For this case, the stresses that are at the tip, may also be in the SIM phase because of

high magnitude. On the other extreme end, for case 6, the minimum stresses are developed at the fixed end (the compressive and tensile stresses at the fixed end by nonlinear theories together with end-shortening are 478.18MPa and 486.24MPa, respectively). Obviously, the entire beam material is likely to be in the parent austenite phase at this load. For all other case1-4, the beam material will be in either of these two phases or, in the mixed phase (SIMT), at the design load. In all of these cases, the beams are likely to return the original straight shape upon unloading because of superelasticity. A future study should incorporate the unloading issue of these beams.

6.1 Conclusions on stainless steel beam analysis

The effects of three important factors, namely, the end-shortening, geometric nonlinearity and material nonlinearity (with associated asymmetric tension-compression relation) on the response of the beams (of reducing cross-sections along the span) have been comprehensively demonstrated by numerical analysis and experiment. Four beams are designed and made from stainless steel so that they can undergo large deflections with large inelastic/plastic strains. The choice of stainless steel is based on the fact that it possesses a highly nonlinear stress-strain curve, can undergo large plastic deformation before failure and also it is one of the most important structural materials.

Very good agreement has been proven between the numerical results generated by the present numerical scheme and experimental results obtained by another research group. Therefore, the numerical scheme adopted here can be reliably used for predicting nonlinear response of stainless steel beams of any cross-section.

The experimental as well as numerical results show that the load-deflection curves can be considered concave upward initially, but starts to deviate nonlinearly at the higher loads. Those experimental as well as numerical curves are found to be convex upward at higher loads. Case 3 shows excellent match between numerical analysis and experiment as far as tip deflection and end-shortening effects are concerned. Even at the highest load the tip deflection is very accurately predicted by the nonlinear theory with end-shortening. The corresponding stresses at fixed end are 340.84MPa and 335.77MPa in tension and compression, respectively. While at the grid point just before the tip, the corresponding tensile and compressive stresses are 329.86MPa and 330.76MPa, respectively. The effect of material nonlinearity and end shortening are found to be important in deciding the response of the beam. Because of the highly nonlinear stress-strain relation for the stainless steel beams originally designed for uniform strength, inclusions of material nonlinearity is found to be the most important factor in predicting the stresses. Moreover, it is seen that if end shortening is ignored, the stress distribution remains constant along the span. On the other hand, stress along the span of the beam

decreases because of end shortening. Tension-compression asymmetry imposed by true σ - ϵ curve is found to be important particularly at a high load. The numerical values stated above for case 3 typically verify the above mentioned facts. If geometric nonlinearity is ignored, the stresses are, however, slightly over predicted as shown by the conservative linear theory.

6.2 Conclusions on SMA beam analysis

The effects of three important factors, namely, the end-shortening, geometric nonlinearity and material nonlinearity (with associated tension-compression asymmetry) on the response of superelastic SMA beams of reducing cross-section have been demonstrated by numerical analysis. Three beams are designed by superelastic shape memory alloy in such a way that they all involve nonlinear stress-strain curves at the maximum design strains.

The effect of material nonlinearity and end-shortening are found to be important in deciding the response of the beam. The numerical results show that the load-deflection curves can be considered straight initially, but starts to deviate nonlinearly at the higher loads. Those curves are found to be convex upward at higher loads mainly because of the material nonlinearity. Moreover, end-shortening must be taken into account to correctly predict the tip deflections by nonlinear theory.

The linear theory is conservative in predicting stresses. Moreover, it is seen that if end-shortening is ignored, the stress distribution remains constant along the span, though the tensile and compressive stresses are still notably asymmetric/unequal. On the other hand, stresses along the span of the beam decrease because of end-shortening.

If end-shortening is ignored, a higher stress is predicted. Therefore, the nonlinear theory with end-shortening effect being taken into account, predicts 7-20% less tensile stress and 7-14 % less compressive stress than the stresses found by neglecting the effect of end-shortening at the fixed end at maximum design strain. Again, stresses fall significantly along the beam span, in particular for the beams designed for higher loads (cases 1,3,5).

If the load is small the beam material may exist in the parent phase. For higher loads, the beam material may be in the SIM phase or in the mixed phase. In all of these

cases, the beams are like to return the original straight shape upon unloading because of superelasticity. A future study should incorporate the unloading issue of these beams.

The main objective of using a beam with variable cross-section is to make the best use of material in terms of economy. It can be concluded from this study that more material can be removed from a beam with variable cross-section by taking into account the geometric nonlinearity, material nonlinearity and the effect of end-shortening. This is very important for superelastic SMA beams that are likely to fully recover the shapes upon unloading owing to superelasticity. A future study can incorporate the unloading issue of these beams. Of course, attention should be given to the point that deflection with increase if more material is removed.

It is important to test the beam's response by rigorous experiment. Unfortunately, SMA's are manufactured mostly in round wire form; it restricts us only with present numerical simulations. However, the accuracy of the numerical scheme has been verified by comparing results with some specific cases.

At first, the soundness of the numerical scheme has been comprehensively proven for the case of stainless steel beams of variable cross-sections. Using the same scheme, therefore, the results of SMA beam of variable cross-sections can also be considered as reliable.

6.3 Recommendations for future work

The following recommendations can be made for future works from experience gained while achieving the set objectives of this thesis:

- (1) The present analysis can be extended to other shapes such as width parabolically varying along the span.
- (2) Experimental studies can be carried out to verify the results obtained from numerical analysis for the SMA beam.
- (3) Finite element method or multisegment method of integration (Uddin, 1969) can be applied because of variable material property.

REFERENCES

- [1] Atanakov T., Achenbach M. (1989). "Moment curvature relations for a pseudoelastic beam". *Continuum Mechanics and Thermodynamics* 1, pp.73-80.
- [2] Auricchio, F. and Sacco, E. (1997). "A superelastic shape-memory-alloy beam model". *Journal of Intelligent Material Systems and Structures* 8, 489-13.
- [3] Baker, G. (1993). "Large deflection of non- prismatic cantilevers with a finite depth". *Comput.Struct.*46,pp.365-370.
- [4] Bele'ndez, T., Pe'ro-Polo, M., Neipp, C., Bele'ndez, A.(2005). "Numerical and experimental analysis of large deflections of cantilever beams under a combined load". *Physica scripta*, Vol. T118, pp.61-65.
- [5] Bratus, A. S. and Posvyanskii, V. P. (2000). "The optimum shape of a bending beam". *Journal of Applied Mathematics and Mechanics*, 64(6), pp.993-1004.
- [6] FunaKubo, H. ed. (1987). "Shape Memory Alloys". Gordon and Breach Science, New York. pp. 39-41.
- [7] Gadaj, S.P., Nowacki, W. K. and Tobushi H. (1999). "Temperature Evolution during Tensile Test of TiNi Shape Memory Alloy". *Arch. Mech.*, Vol.51, No.6, pp. 649-663.
- [8] Gadaj, S.P., Nowacki, W.K., Pieczyska, E.A. (2002). "Temperature evolution in deformed shape memory allow". *Infrared Physics & Tech*, 43 , pp.151-155.
- [9] Gong, J., Tobushi, H., Takata, K., Okumura, K.(2000). "Superelastic properties of TiNi shape memory alloy under various loading conditions". *Proceedings of the 11th ICAST (Nagoya).*]
- [10] Hossain, M. A. (2006). "Buckling of short column of superelastic shape memory alloy with tension-compression asymmetry". M. Sc. Engg. Thesis. Department of Mechanical Engineering, Bangladesh University of Engineering and Technology (BUET), Bangladesh.
- [11] Hutchinson, J. W. (2000) "Plasticity at the micron scale". *Int. J. Solids and structures*, Vol 37 , pp.255-238.

- [12] Khan R. M. (2003). "Investigation of local strain of the superelastic shape memory alloy rods for tensile loading-unloading cycles". M. Sc Engg. Thesis, Bangladesh University of Engineering & Technology, Dhaka.
- [13] Lee, B.K. Wilson, J.F. and Oh, S.L. (1993). "Elastica of cantilever beams with variable cross sections". *Int. J. Non Linear Mech.* 28, pp.579-589.
- [14] Lee, K. (2002). "Large deflection of cantilever beams of non-linear elastic material under a combined loading". *International Journal of Non-linear Mechanics*, 37(3), pp. 439-443.
- [15] Leo, P. H., Shield T. W. and Bruno, O.P. (1993). "Transient Heat transfer Effects on the Pseudoelastic Behavior of Shape Memory Wires". *Acta Metall. Mater.*, Vol.41, No.8, pp.2477-2485.
- [16] Lo, C.C. and Gupta, S.D. (1978). "Bending of a non linear rectangular beam in large deflection". *J. Appl. Mech.* 45, pp.213-215.
- [17] Lewis, G. and Monasa, F. (1982). "Large deflections of cantilever beams of non-linear materials of the Ludwick type to an end moment". *International Journal of Non-linear Mechanics*, 17(1), pp. 1-6.
- [18] Matulewicz, Z. and Szymczak, C. (1985). "The optimum design of thin-walled I beams undergoing torsion". *Thin-walled Structures*, 3(2), pp.135-144.
- [19] Orgeas, L. and Favier, D. (1995). "Non-symmetric tension-compression behaviour of NiTi alloy". *J. Phys. IV, Colloq. (France)*, vol. 5, no. c8, PT.2, 605-610.
- [20] Pieczyska, E.A., Gadaj, S.P., Nowacki W.K. (2002). "Thermoelastic and thermoplastic effects in steel, polyamide and shape memory alloys". *Proc. of SPIE's AeroSense*, Vol.4710, pp.479-487.
- [21] Pieczyska, E.A., Gadaj, S.P., Nowacki, W.K., Tobushi, H. (2004). "Transformation in TiNi Shape Memory Alloy". *Bul. of the Polish Academy of Sciences, Technical Sciences* (3), pp. 165-171.
- [22] Rahman M. A. (2001). "Behavior of the superelastic shape memory alloy columns under compression and torsion". Ph.D. Thesis, Tohoku University, Japan.

- [23] Rahman, M. A., Chowdhury, R. K., Ahsan, M. M. R. (2005). "Response of a Slender Cantilever Beam with a Circular Hole- Experiment and Large Deflection Analysis". JMED, Institution of Engineers, Bangladesh, 34, pp. 46-59.
- [24] Rahman M. A. and Khan R. M. (2006). "Unique local deformation of the superelastic shape memory alloy rods during relaxation tests for tensile loading-unloading cycles". International Journal of Structural Engineering & Mechanics, 22(5), pp 563-574..
- [25] Rahman M. A., Qiu. J., Tani. J. (2001). "Buckling and postbuckling characteristics of the superelastic SMA columns". International Journal of Solids and Structures 38, pp. 9253-9265.
- [26] Rahman M. A., Qiu. J., Tani. J. (2005a). "Buckling and postbuckling characteristics of the superelastic SMA columns-Numerical Simulation". Journal of Intelligent Material Systems and Structures,16(9), pp.691-702.
- [27] Rahman, M. A., Rahman, S., Hossain, A. H. M. Z., (2006a). "Large Deflection Analysis of Cantilever Beams with an Opening". International Journal of Applied Mechanics and Engineering, Poland (In Press).
- [28] Rahman M. A., Qiu. J., Tani. J. (2006b). "Buckling and postbuckling behavior of solid superelastic shape memory alloy shafts". International Journal of Structural Engineering & Mechanics (In Press).
- [29]Rahman, M. A., Rahman, S., Noman K.N. Ahsan, Islam, S. (2003). "Large Deflection Analysis of the Super elastic Shape Memory Alloy Beams". Proceeding of 5th International conference on Mechanical Engineering., pp. AM-54, BUET, Dhaka, Bangladesh.
- [30] Rahman M. A., Tani, J., Qiu, J. (2001). "Unique behaviors of the superelastic shape memory alloy under tensile and compressive loading". Proceedings of International Conference on Mechanical Engineering, Dhaka, Bangladesh. Vol-3, Sec-5, pp.185-187.
- [31] Rahman M. A., Tani , J., Qiu , J. (2002). "Direct method to estimate stress induced-martensitic transformation points by tensile test". Proceedings of BSME-ASME-International conference on Thermal Engineering, Dhaka, Bangladesh. pp. 761-765.

- [32] Rahman, M. A. and Tani, J. (2005b). "Local Deformation Characteristics of the Shape Memory Alloy Rods during Forward and Reverse Stress Induced Martensitic Transformations". JIMSS (In Press).
- [33] Rahman, M. A., Tani, J., Afsar, A. M. (2006c). "Postbuckling Behaviour of Stainless Steel (SUS304) Columns Under Loading-unloading Cycles". Journal of Constructional Steel Research 62, pp.812-819.
- [34] Raniecki, B. and Lexcellent, CH. (1998). "Thermodynamics of isotropic pseudoelasticity in shape memory alloys". European Journal of Mechanics, A/Solids, Vol. 17, no2, pp. 85-205.
- 7 [35] Raniecki, B., Rejnar, J., Lexcellent, CH. (2000). "Anatomization of hysteresis loop in pure bending of ideal pseudoelastic beams". International Journal of Mechanical Sciences. pp.1-30.
- [36] Raniecki, B., Rejzner, J., Lexcellent, C. (2001). "Anatomization of hysteresis loops in pure bending of ideal pseudoelastic SMA beams". International Journal of Mechanical Sciences 43, pp.1339-1368.
- [37] Rejnar, J., Lexcellent, C., Raniecki, B. (2002). "Pseudoelastic behaviour of shape memory alloy beams under pure bending; Experiment and modeling". International Journal of Mechanical Sciences 44. pp. 665-686.
- [38] Scott, E.J. Carver, D.R. and Kan, M. (1955), "On the linear differential equation for beam deflection". J. Appl. Mech. 22, pp. 245-248.
- [39] Shaw, J.A. and Kyriakides, S. (1995). "Thermomechanical Aspects of NiTi". J. Mech. Phys. Solids, Vol.43, No.8, pp.1243-1281.
- [40] Sun, Q.P., Li, Z.Q. and TSE, K.K. (2000). "On super elastic deformation of NiTi Shape memory Alloy Micro-tube and wires band nucleation and propagation". Proceedings of IUTAM Symposium on Smart Structures and Structronics systems, Magdeburg, Germany, Sept, 26-29.
- [41] Tawfik, M., Ro, J. J. and Mei, C. (2002). "Thermal Post-buckling and Aeroelastic Behavior of Shape Memory Alloy Reinforced Plates". Smart Materials and Structures, 11, pp. 297-307.

- [42] Thompson, S. P. and Loughlan, J. (2001). "Enhancing the Post-buckling Response of a Composite Panel Structure Utilizing Shape Memory Alloy Actuators – A Smart Structural Concept". *Composite Structures*, 51, pp. 21-36.
- [43] Tobushi H., Takata K., Shimeno Y., Nowacki, W.K. and Gadaj S.P. (1999). "Influence of strain rate on superelastic behavior of TiNi shape memory alloy", *Proc. Instn. Mech. Engrs.*, 213, part L, pp. 93-102.
- [44] Tobusi, H., Okumura, K., Endo, M., Takata K. (2000). "Stress-induced martensitic transformation behavior and lateral strain of TiNi shape memory alloy". *Proceedings of the 11th ICAST (Nagoya)*, pp. 367-374.
- [45] Timoshenko, S. and Gere, J. M. (1981) "Theory of elastic stability". McGraw-Hill Book Company, Inc.
- [46] Turner, T. L. (2005). "SMA Hybrid Composites for Dynamic Response Abatement Applications". *ASME Journal of Vibration and Acoustics*, 127(3), pp.273-279.
- [47] Turner, T. L. and Patel, H. D. (2005). "Input Files and Procedures for Analysis of SMA Hybrid Composite Beams in MSC.Nastran and ABAQUS". NASA/TM-2005-213517.
- [48] Uddin, Md. W. (1969). "Large deflection analysis of composite shells of revolution". Ph. D. thesis, Carleton University, Canada.
- [49] Zhong Lin Wang, Wang Zhong-Lin Wang, Z C Kang (1998). "Functional and Smart Materials: Structural Evolution and Structure Analysis". Springer.

Tables

Table 4.1. Design parameters of stainless steel cantilever beams

(a) Beam of variable cross-section ($h=1$ mm, $P_d = 10.158$ N, $\sigma_d \approx 200$ MPa)

Case 1: Width at fixed end: 46mm Length of beam : 150 mm $\sigma_d = 198.74$ MPa	Case 2: Width at fixed end: 61mm Length of beam : 200 mm $\sigma_d = 199.82$ MPa
---	---

(b) Beam of variable cross-section ($h=2$ mm, $P_d = 20.076$ N, $\sigma_d \approx 250$ MPa)

Case 3: Width at fixed end: 18mm Length of beam : 150 mm $\sigma_d = 250.95$ MPa	Case 4: Width at fixed end: 24.1mm Length of beam : 200 mm $\sigma_d = 249.91$ MPa
---	---

Table 4.2. Comparison of experimental results by Bele'ndez et al.(2005) with the numerical results generated by the present study

(Thickness, $h=0.0004$ m; length, $L=0.40$ m; uniform weight, $w=0.758$ N/m)

Tip load (N)	Tip deflections(mm)			Number of iterations required (present study)	
	Experiment by Bele'ndez et al.(2005)	Numerical solutions with δ_h (present study)		Linear	Nonlinear
		Linear	Nonlinear		
0	89±1	81.8	84.48	4	4 (first trial $\delta_h = 00$ mm)
0.098	149±1	132.5	142.65	4	6 (first trial $\delta_h = 00$ mm)
0.196	195±1	166.22	184.71	6	8 (first trial $\delta_h = 00$ mm)
0.294	227±1	188.38	210.96	6	12 (first trial $\delta_h = 00$ mm)
0.396	251±1	211.96	236.28	7	8 (first trial $\delta_h = 100$ mm)
0.490	268±1	229.67	254.57	7	8 (first trial $\delta_h = 117$ mm)
0.588	281±1	236.84	271.77	7	9 (first trial $\delta_h = 135$ mm)

Table 4.3. End-shortening results of cantilever beam of variable cross-section

Case No.	L/b_0	Load(N)	End-shortening, δ_h (mm)			No. of iterations	
			Linear	Nonlinear	Experimental	Linear	Nonlinear
1	3.26	14.529	4.1	4.1	4.53±0.005	4	4
2	3.28	14.529	8.3	11	9.73±0.005	4	5
3	8.33	34.51	5.4	6.6	6.88±0.005	5	7
4	8.3	34.51	10.4	10.6	12.0±0.005	6	6

Table 5.1. Design parameters of SMA cantilever beams of variable cross-section ($b_0=100\text{mm}$, $h=50\text{ mm}$)

No.of Case	Beam length L (m)	Maximum Design Strain (%)	Corresponding Moment, M (kN-m)	Corresponding load at tip, $P=M/L$ (kN)
1	0.50	9.52	40	80
2	0.50	7.31	37.5	75
3	0.40	11.62	44	110
4	0.40	3.22	30	75
5	0.30	15.2	54	180
6	0.30	1.78	22.5	75

Figures

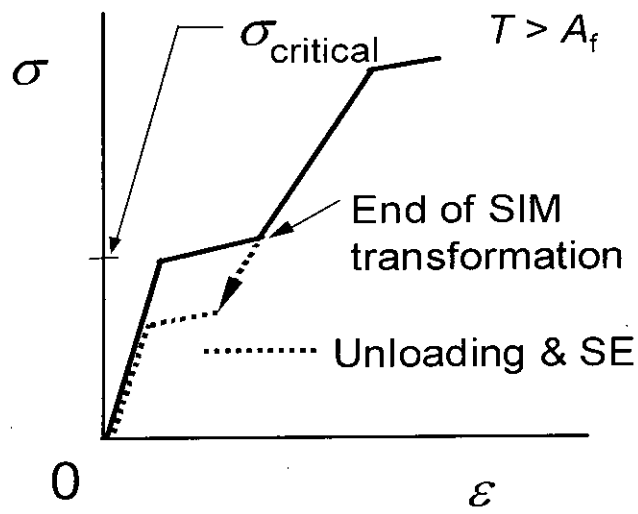


Figure 1.1: Idealized stress-strain diagram of the superelastic SMA.

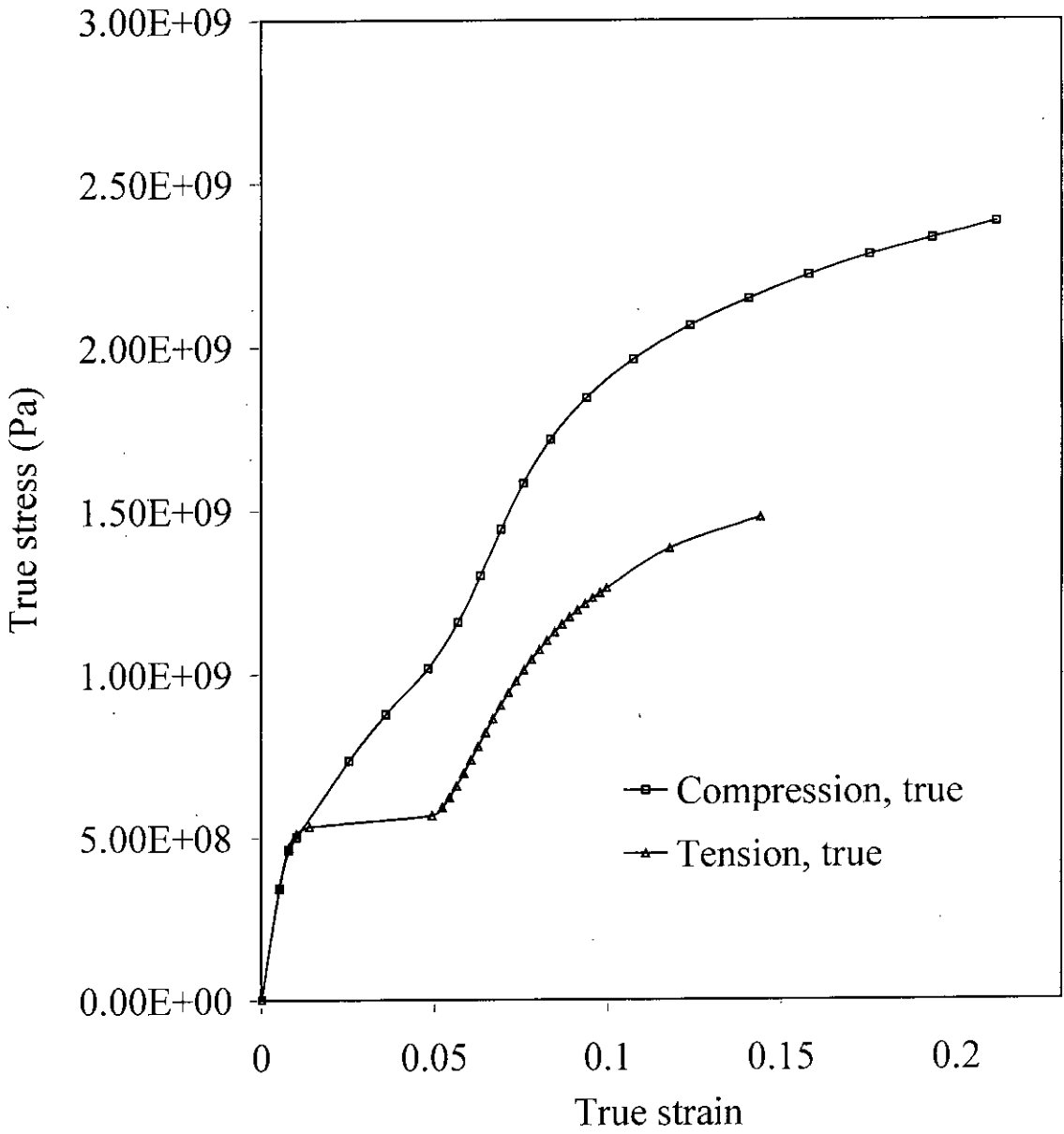


Figure 1.2: Experimental stress-strain curves for superelastic SMA, experiment done on a 2mm diameter rod after Rahman (2001).

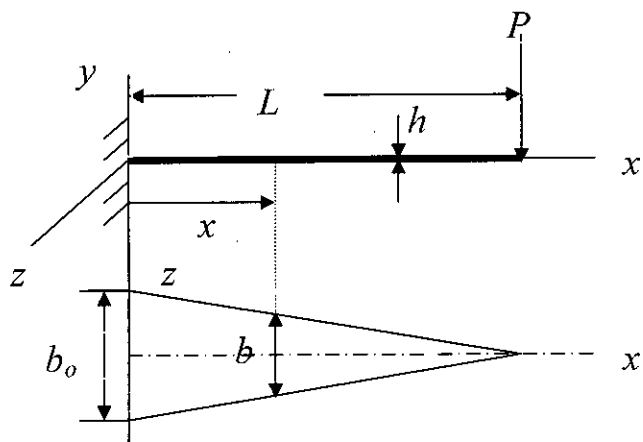


Figure 3.1: shape of the beam of variable cross-section.

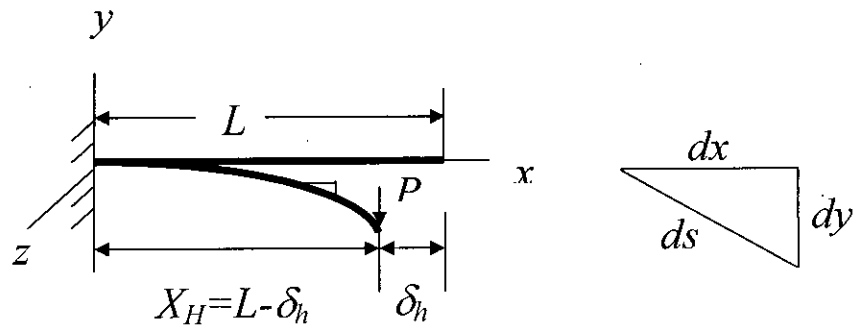
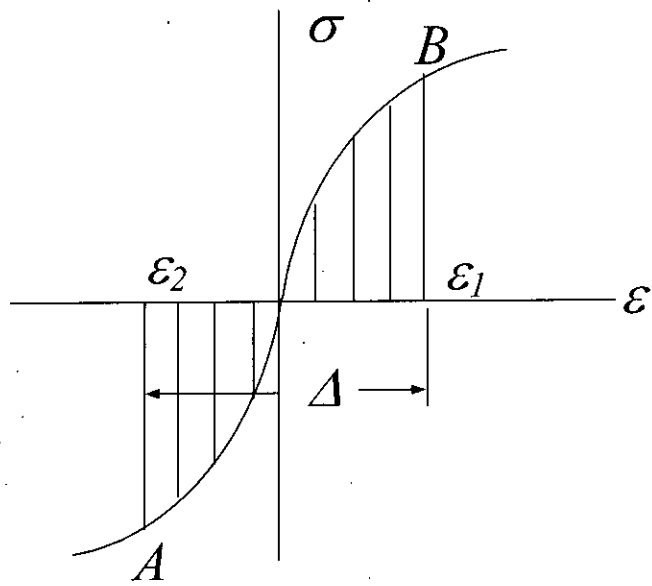


Figure 3.2: Deflection of beam under load P and corresponding end-shortening.



Figures 3.3: Generalized σ - ϵ diagram for beam.

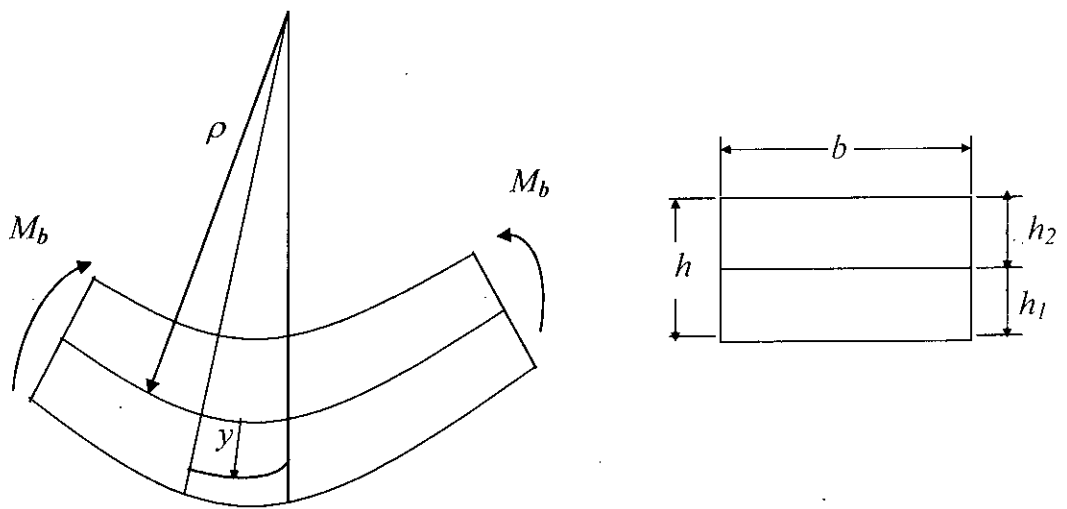


Figure 3.4: Parameters of beam.

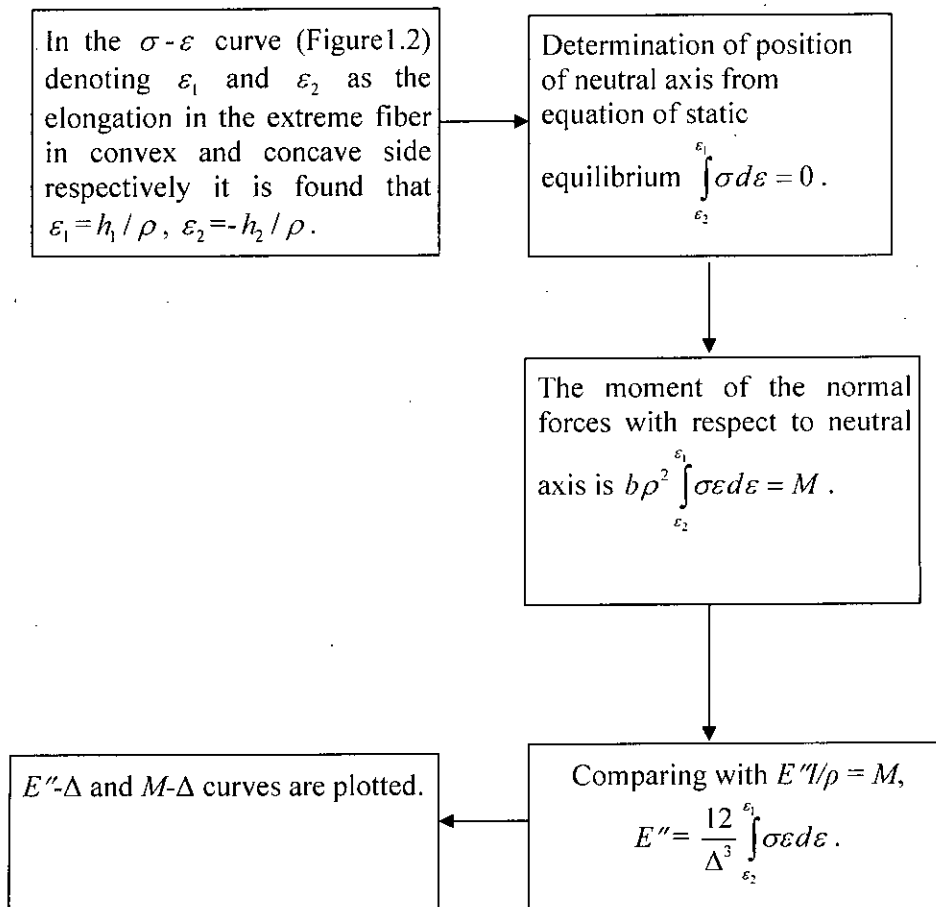


Figure 3.5: Flow Chart of Beam analysis (Timoshenko's method).

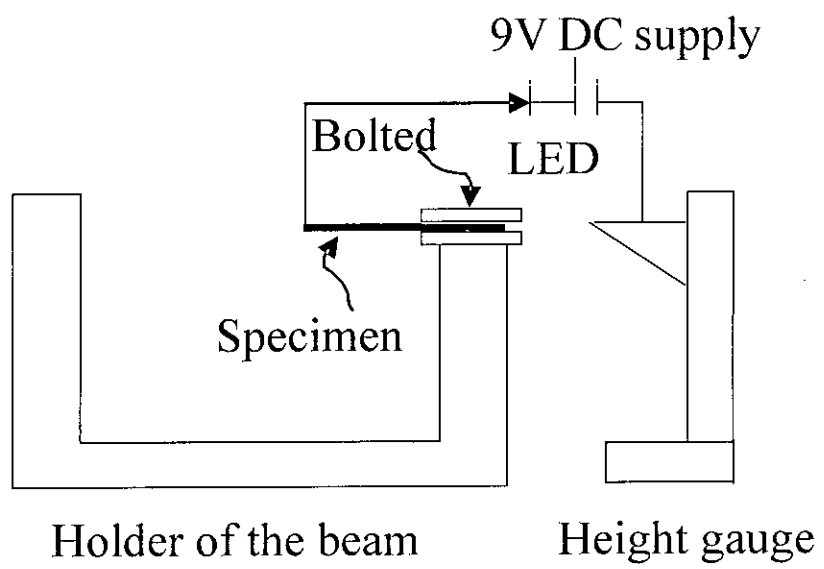


Figure 4.1: Experimental setup.

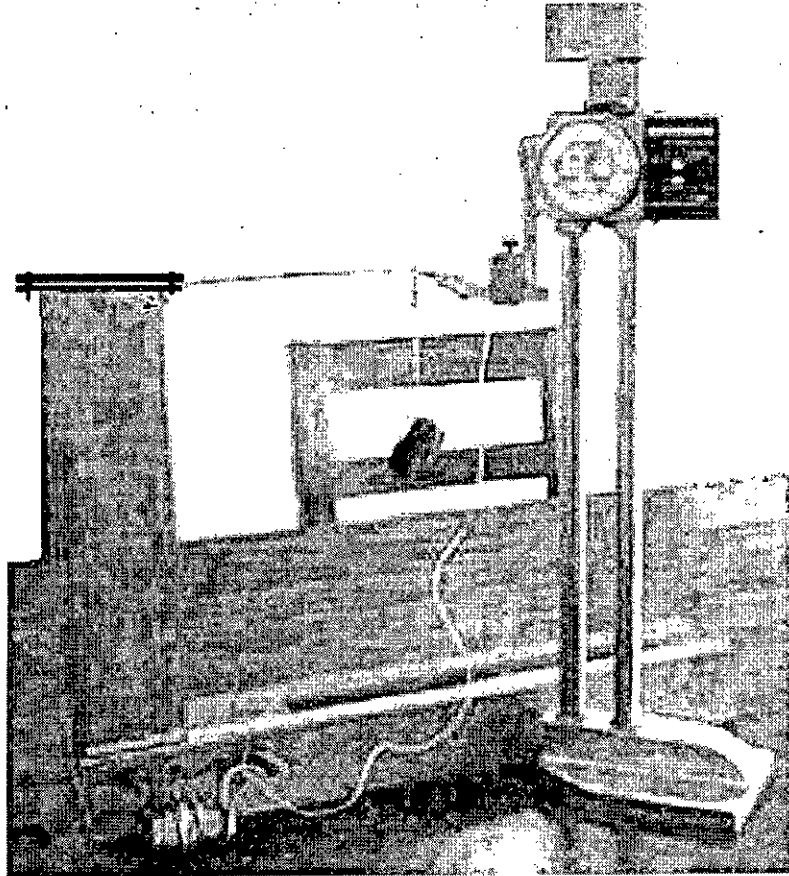


Figure 4.2: Experimental apparatus with tip load on beam.

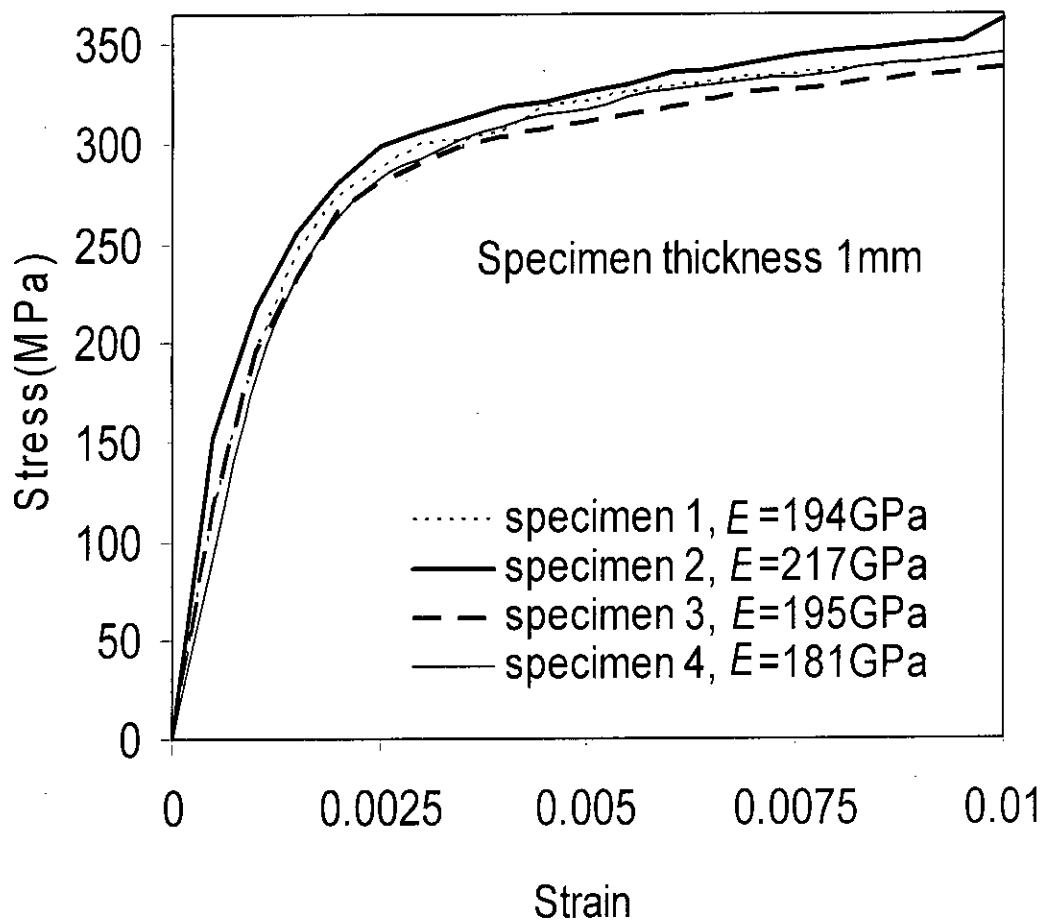


Figure 4.3(a): Experimental stress-strain curve of stainless steel specimen of thickness 1mm.

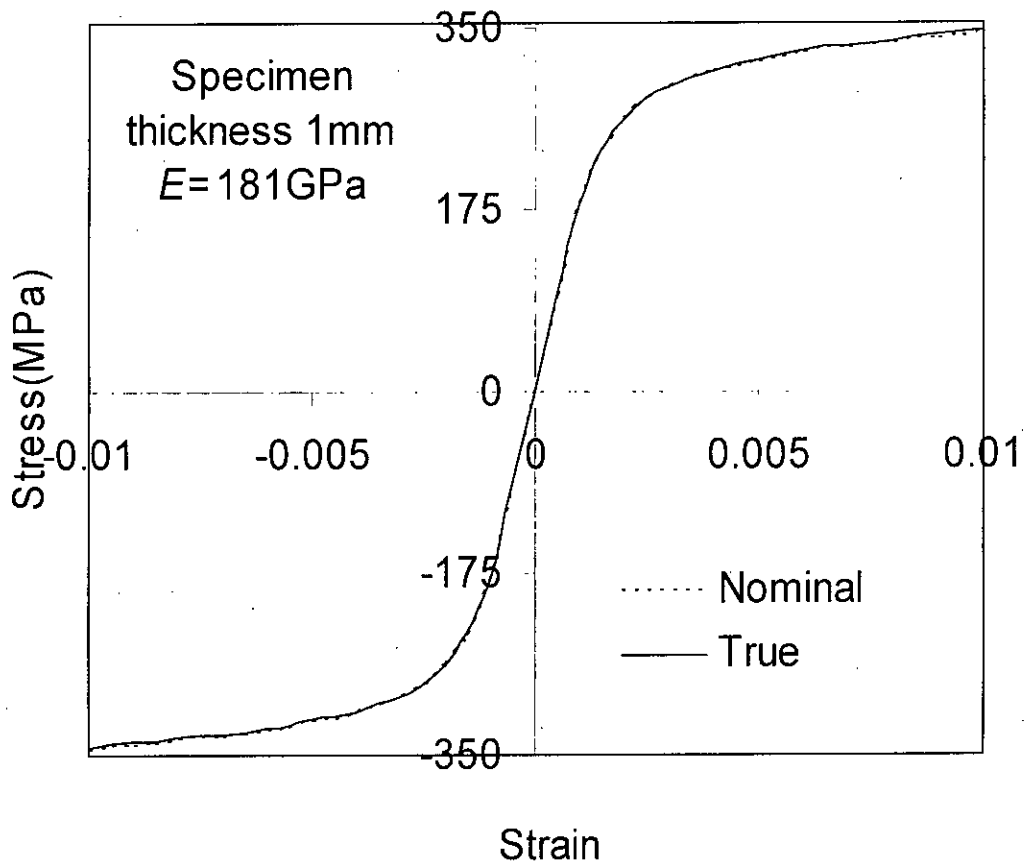


Figure 4.3(b): Experimental true stress-strain curve of stainless steel specimen of thickness 1mm.

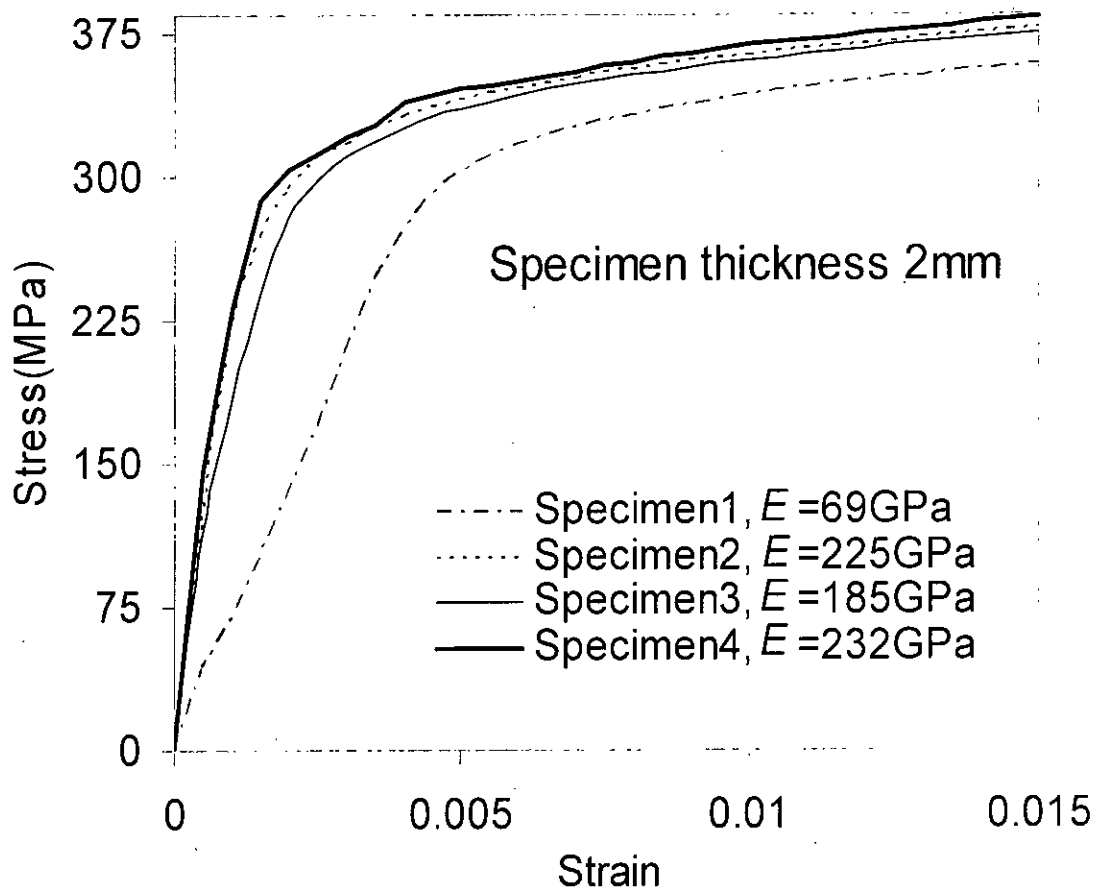


Figure 4.4(a): Experimental stress-strain curve of stainless steel specimen of thickness 2mm.

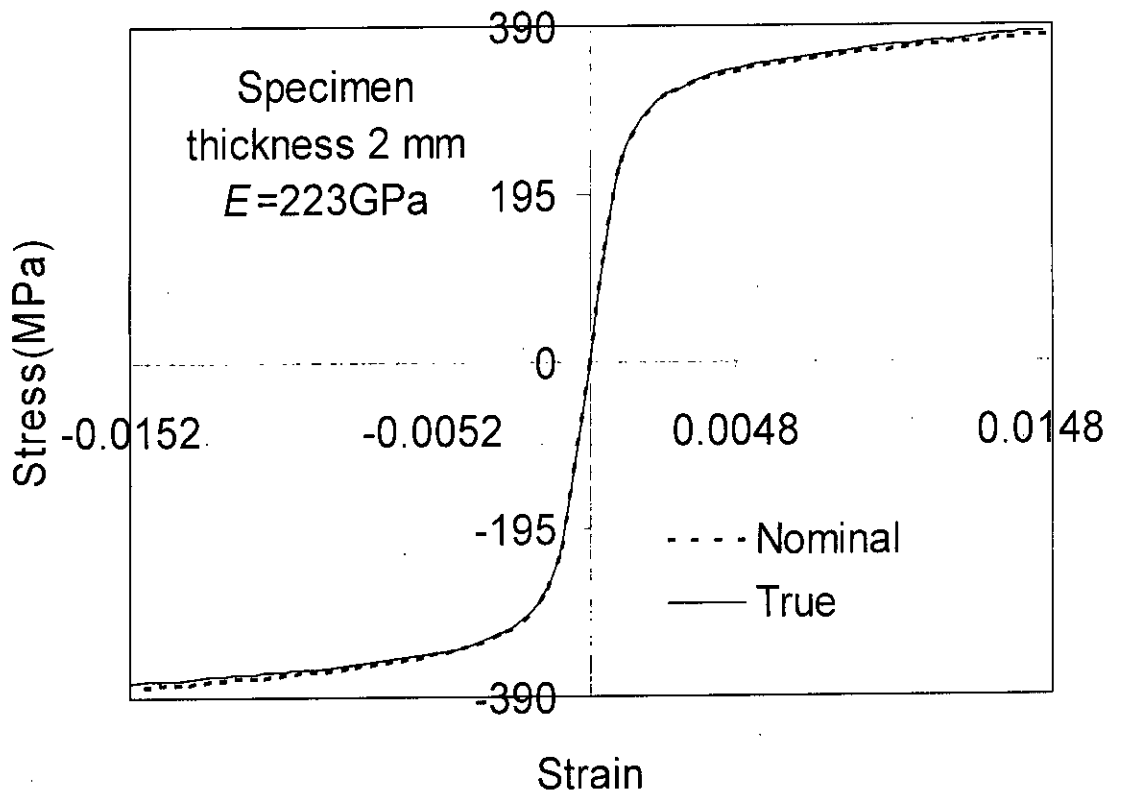


Figure 4.4(b): Experimental true stress-strain curve of stainless steel specimen of thickness 2mm.

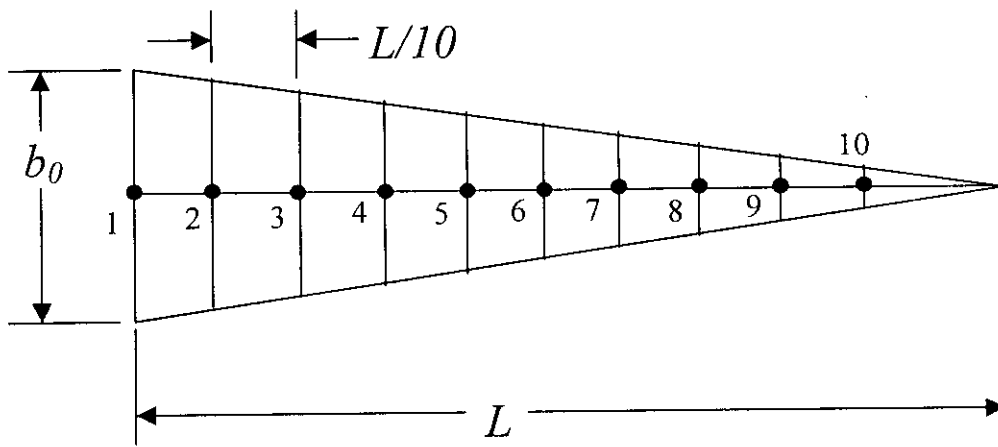


Figure 4.5: Different segments of cantilever beam.

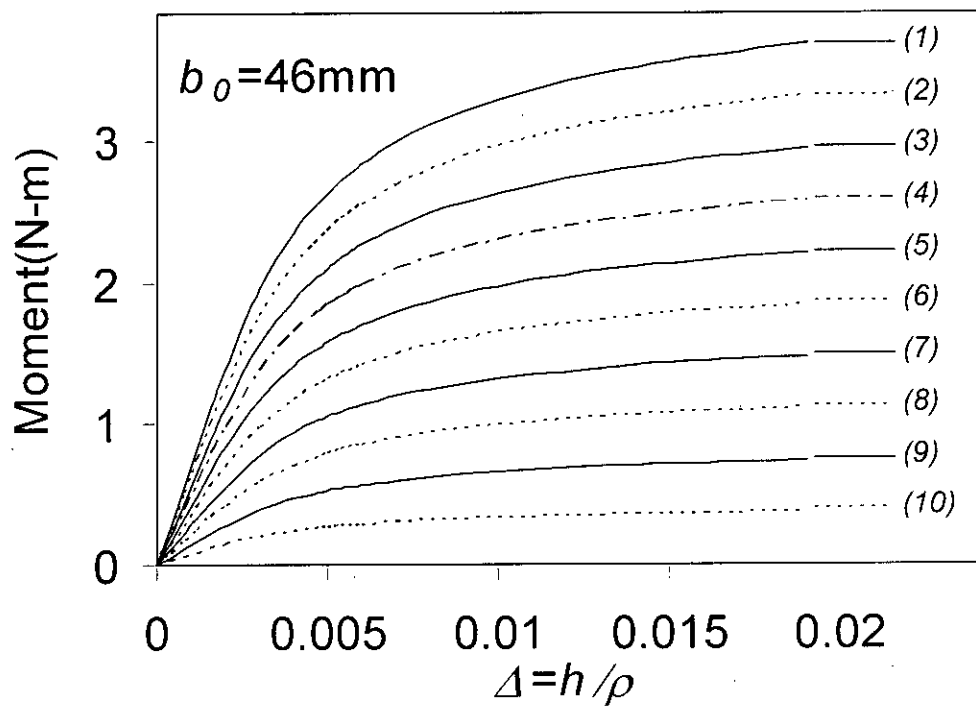


Figure 4.6(a): Moment- strain curve for the stainless steel beam of thickness 1 mm.

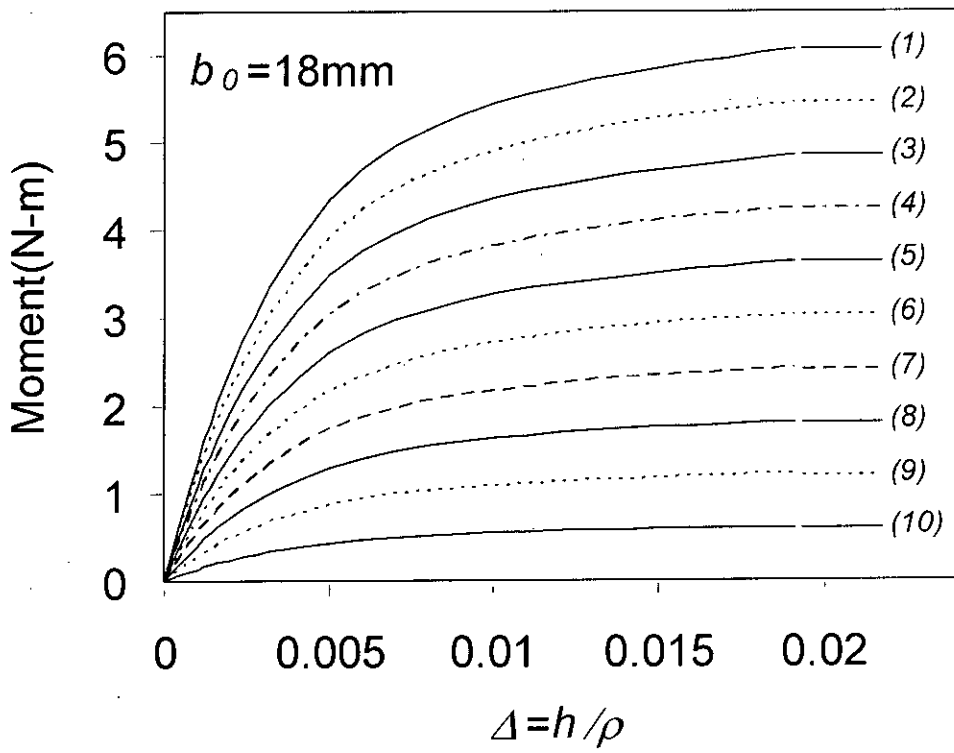


Figure 4.6(b): Moment- strain curve for the stainless steel beam of thickness 2mm.

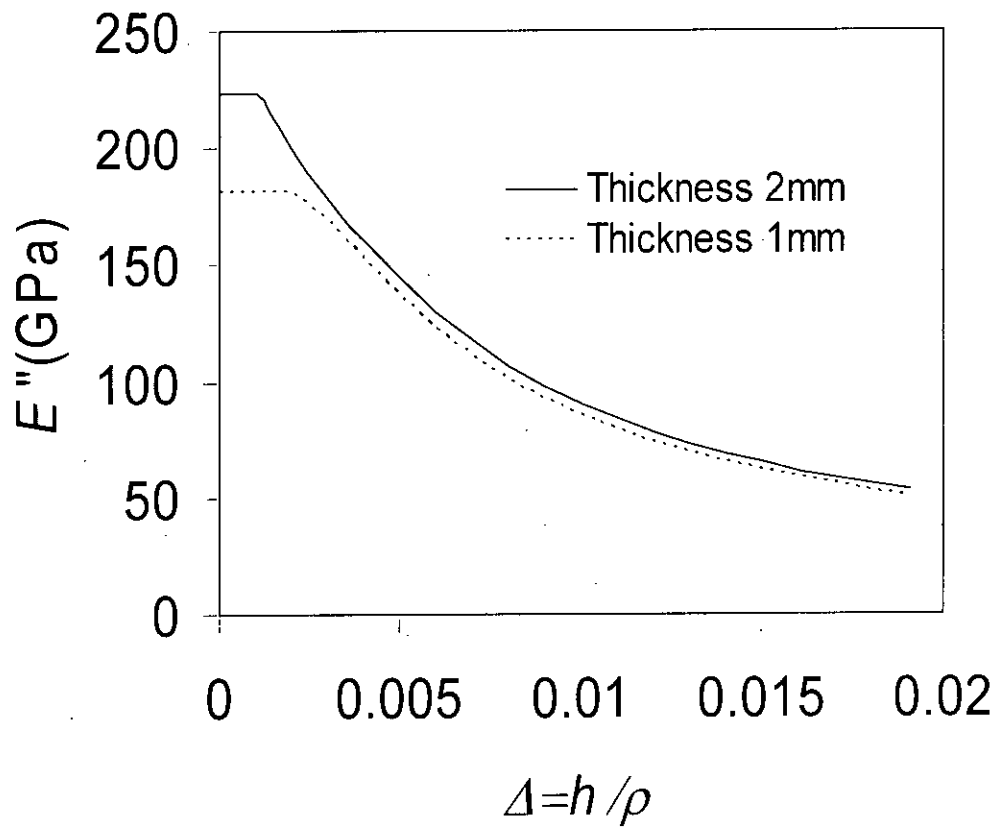


Figure 4.7: Effective modulus- strain curve of stainless steel beam.

102833

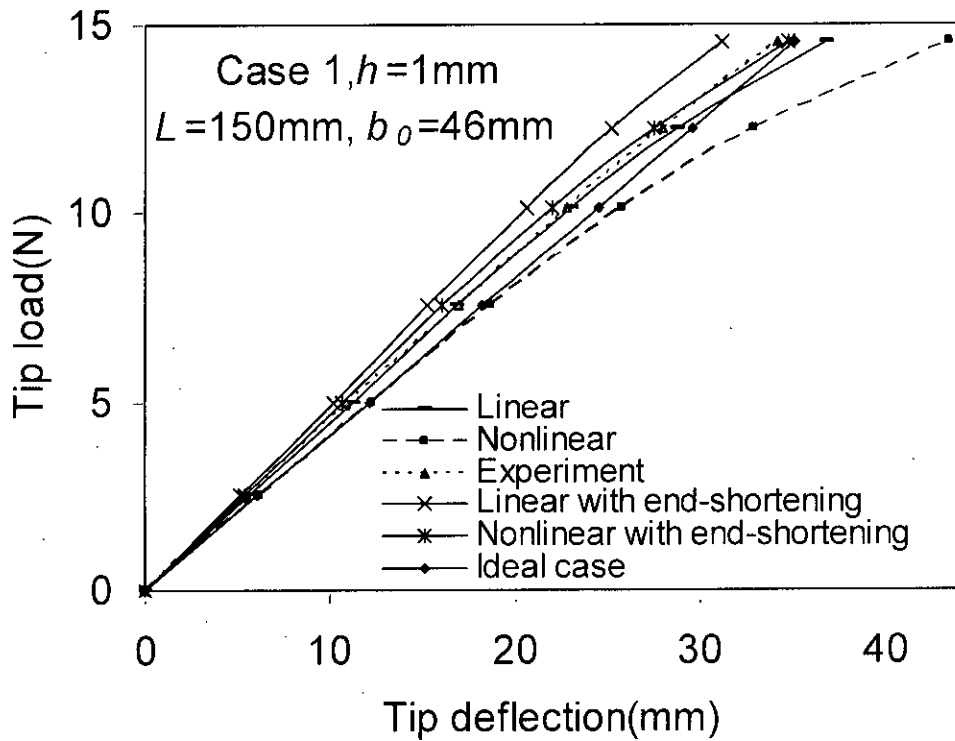


Figure 4.8: Load-deflection curve of stainless steel cantilever beam (Case 1: $L = 150\text{mm}$, $b_0 = 46\text{mm}$, $h = 1\text{mm}$, $\sigma_d = 198.74\text{MPa}$ at design load P_1 , Experimental $\delta_h = 4.53\text{mm}$ at P_2).

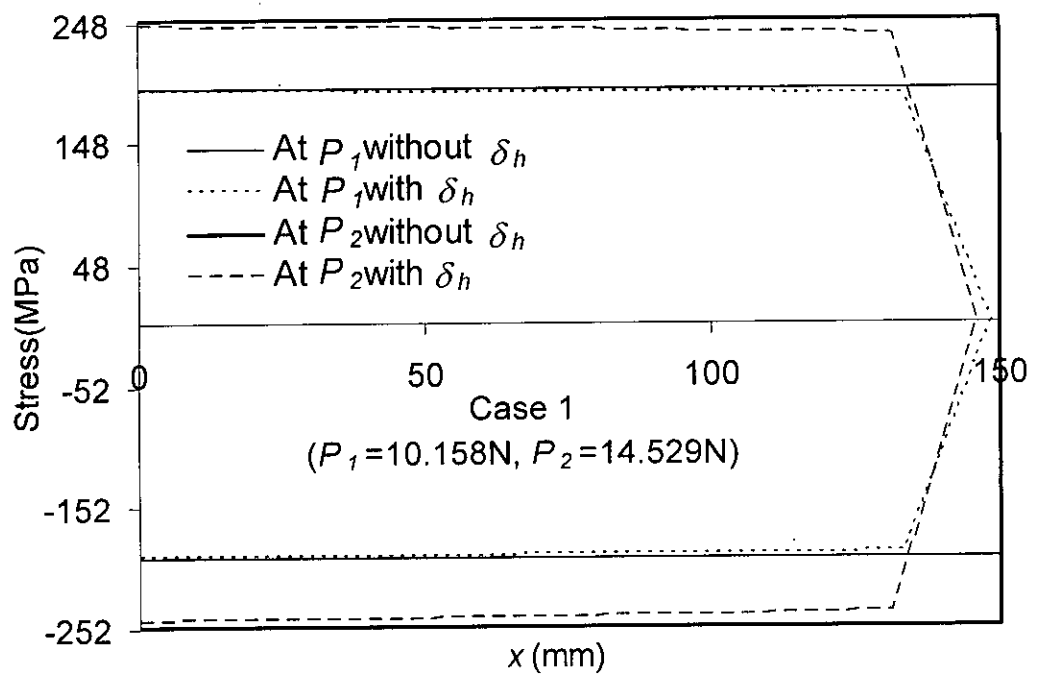


Figure 4.9(a): Stress distribution along the horizontal distance from the fixed end of the stainless steel beam by linear analysis (Case 1: $L = 150\text{mm}$, $b_0 = 46\text{mm}$, $h = 1\text{mm}$, $\sigma_d = 198.74\text{MPa}$ at design load P_I).

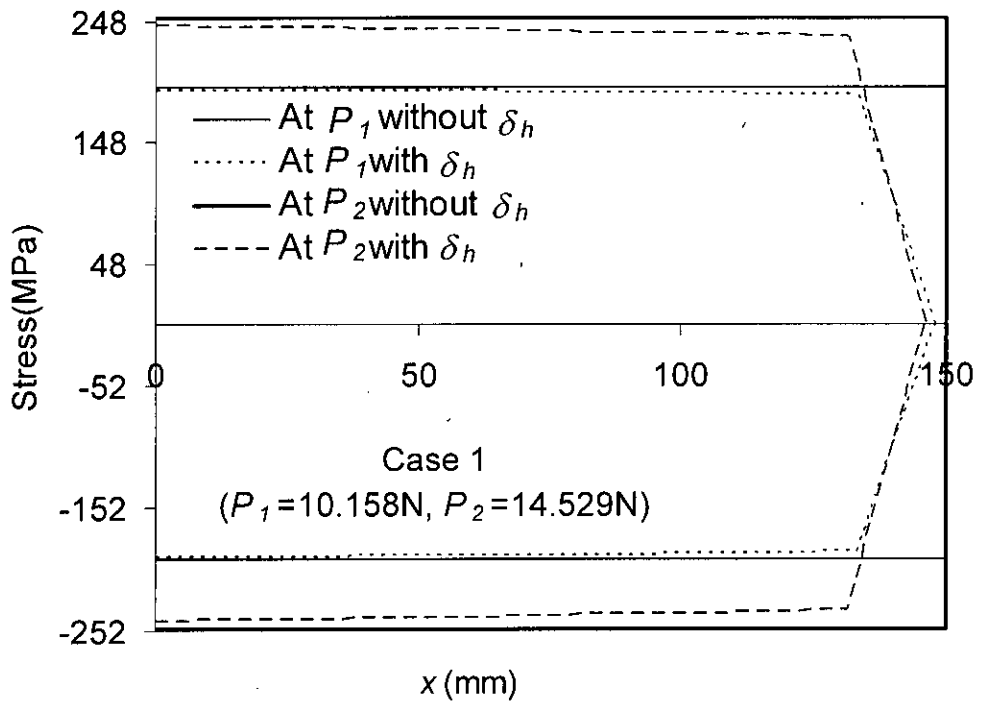


Figure 4.9(b): Stress distribution along the horizontal distance from the fixed end of the stainless steel beam by nonlinear analysis (Case 1: $L=150\text{mm}$, $b_0 = 46\text{mm}$, $h = 1\text{mm}$, $\sigma_d = 198.74\text{MPa}$ at design load P_1).

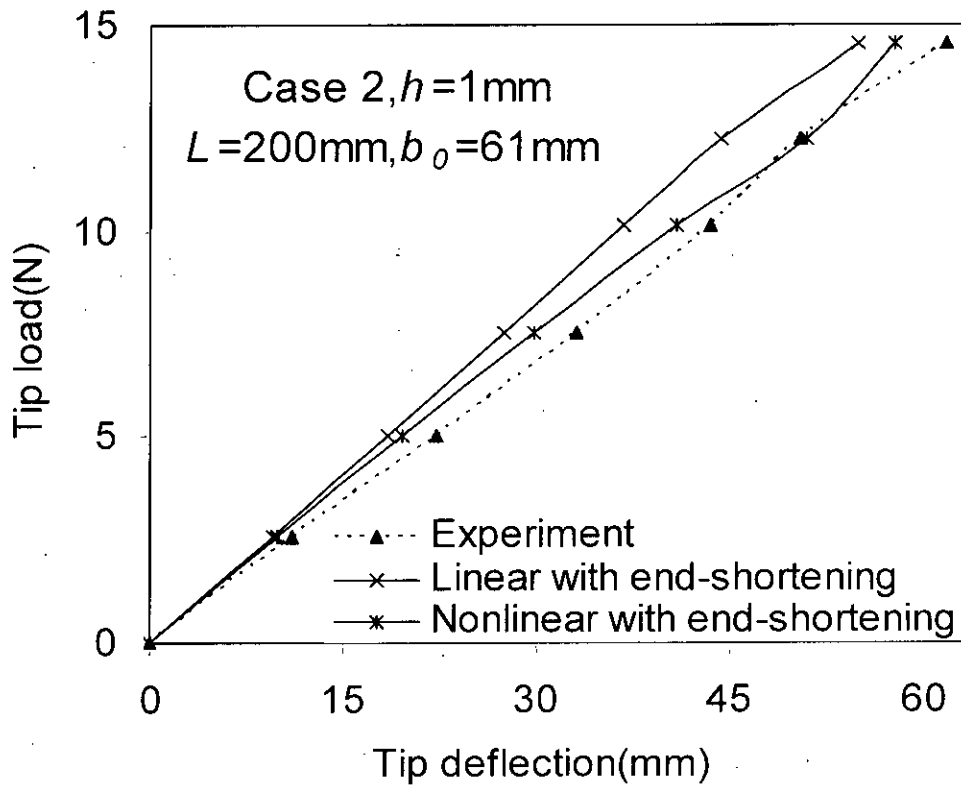


Figure 4.10: Load-deflection curve of stainless steel cantilever beam (Case 2: $L = 200\text{mm}$, $b_0 = 61\text{mm}$, $h = 1\text{mm}$, $\sigma_d = 199.82\text{MPa}$ at design load P_1 , Experimental $\delta_h = 9.73\text{mm}$ at P_2).

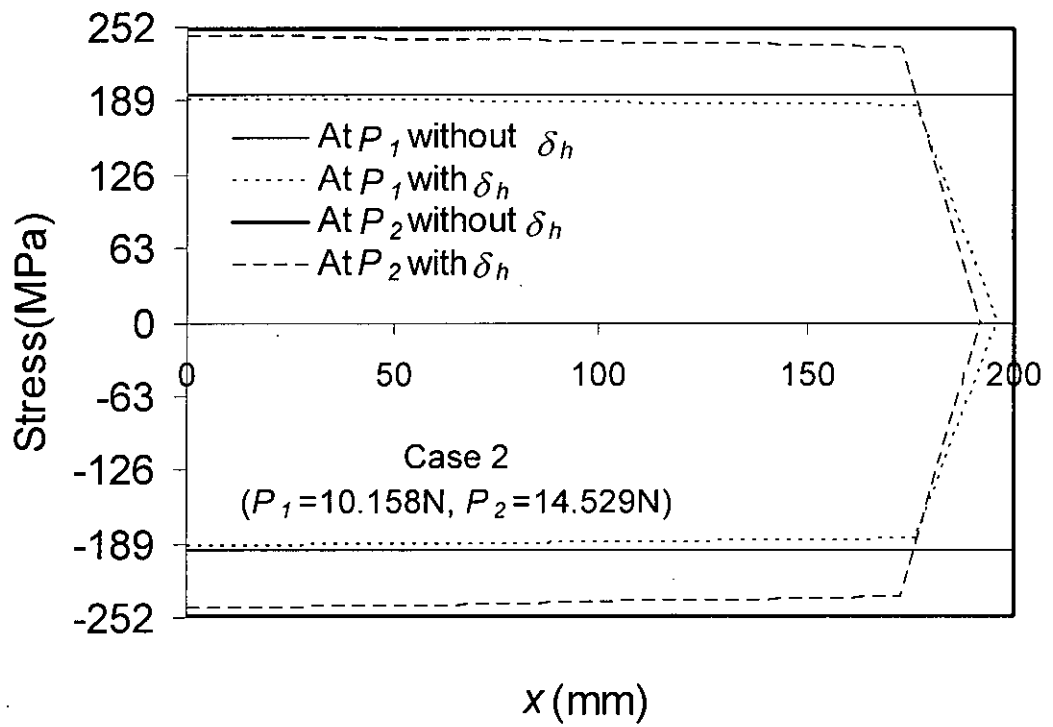


Figure 4.11(a): Stress distribution along the horizontal distance from the fixed end of the stainless steel beam by linear analysis (Case 2: $L = 200\text{mm}$, $b_0 = 61\text{mm}$, $h = 1\text{mm}$, $\sigma_d = 199.82\text{MPa}$ at design load P_1).

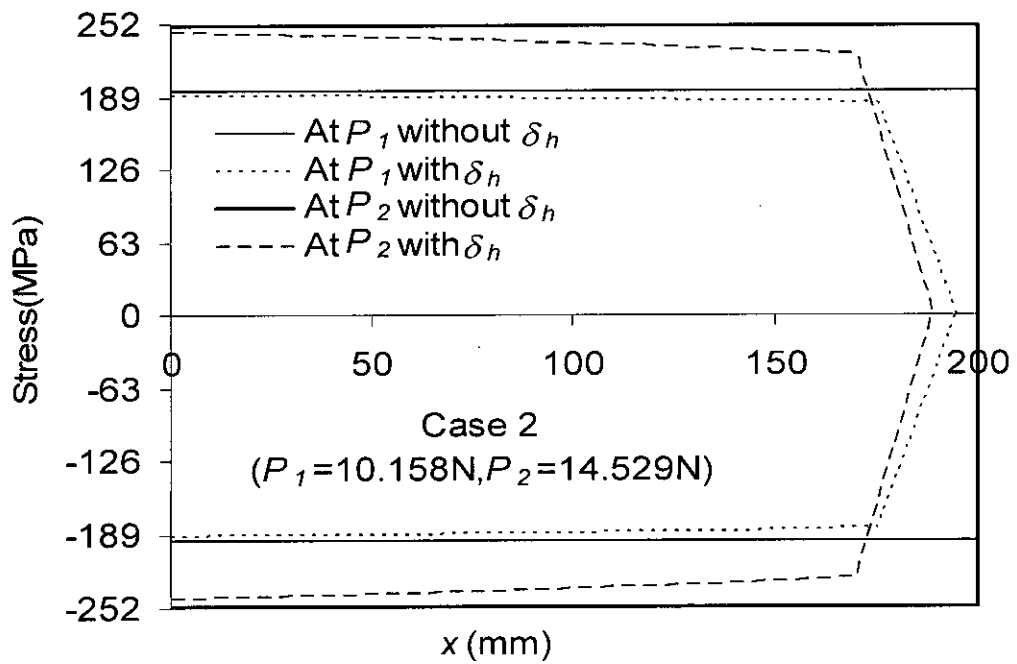


Figure 4.11(b): Stress distribution along the horizontal distance from the fixed end of the stainless steel beam by nonlinear analysis (Case 2: $L = 200\text{mm}$, $b_0 = 61\text{mm}$, $h = 1\text{mm}$, $\sigma_d = 199.82\text{MPa}$ at design load P_1).

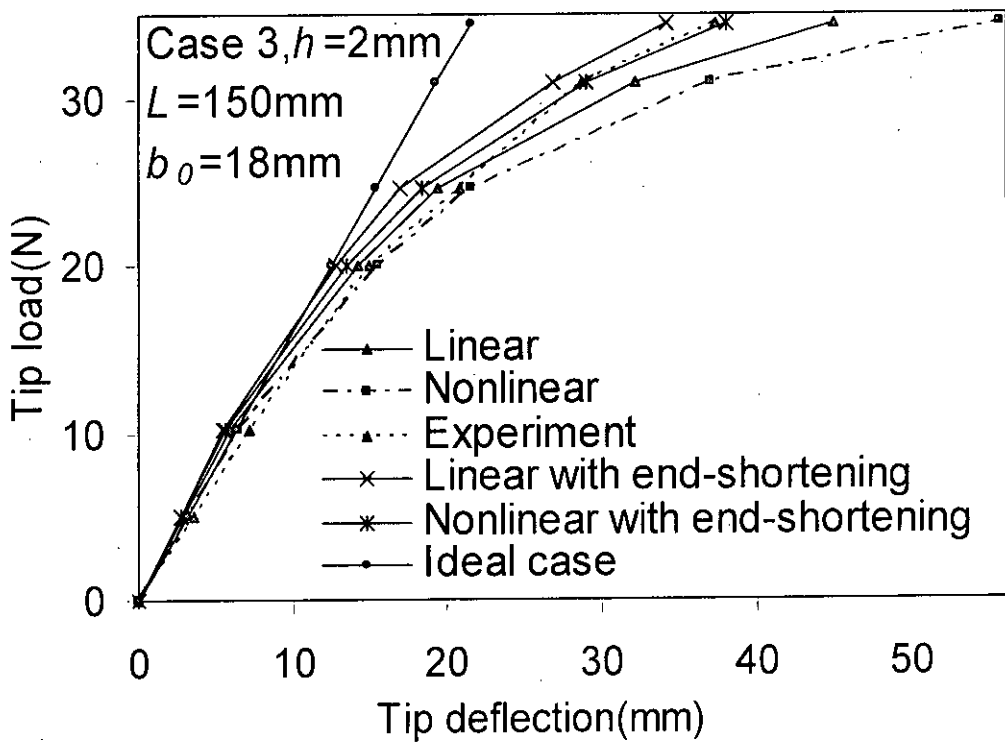


Figure 4.12: Load-deflection curve of stainless steel cantilever beam (Case 3: $L = 150\text{mm}$, $b_0 = 18\text{mm}$, $h = 2\text{mm}$, $\sigma_d = 250.95\text{MPa}$, Experimental $\delta_h = 6.88\text{mm}$ at P_2).

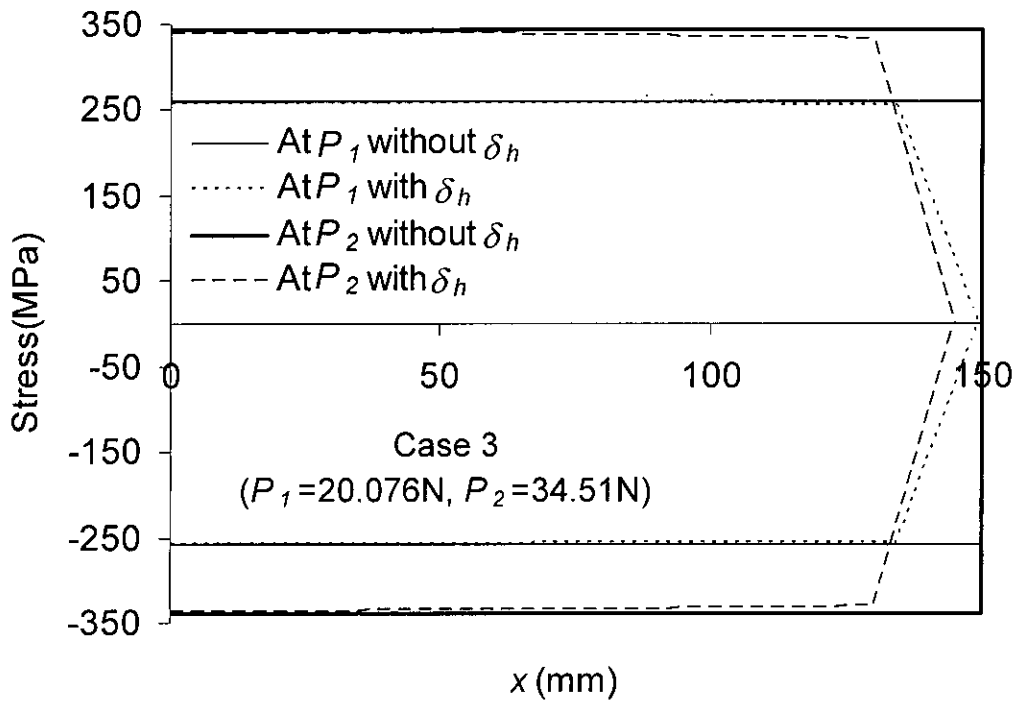


Figure 4.13(a): Stress distribution along the horizontal distance from the fixed end of the stainless steel beam by linear analysis (Case 3: $L = 150\text{mm}$, $b_0 = 18\text{mm}$, $h = 2\text{mm}$, $\sigma_d = 250.95\text{MPa}$ at design load P_1).

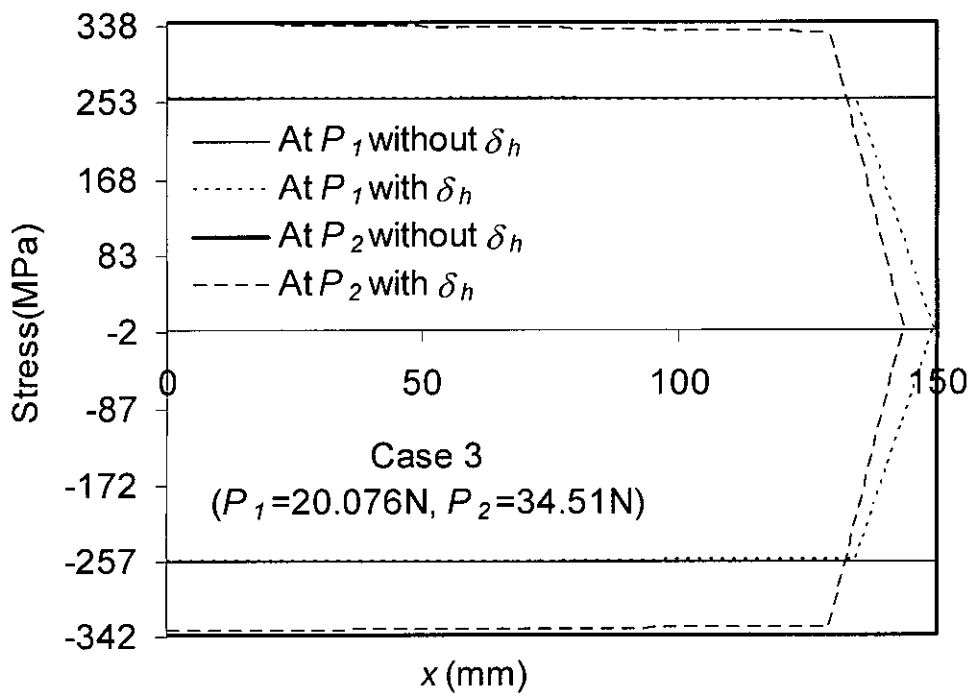


Figure 4.13(b): Stress distribution along the horizontal distance from the fixed end of the stainless steel beam by nonlinear analysis (Case 3: $L = 150\text{mm}$, $b_0 = 18\text{mm}$, $h = 2\text{mm}$, $\sigma_d = 250.95\text{MPa}$ at design load P_1).

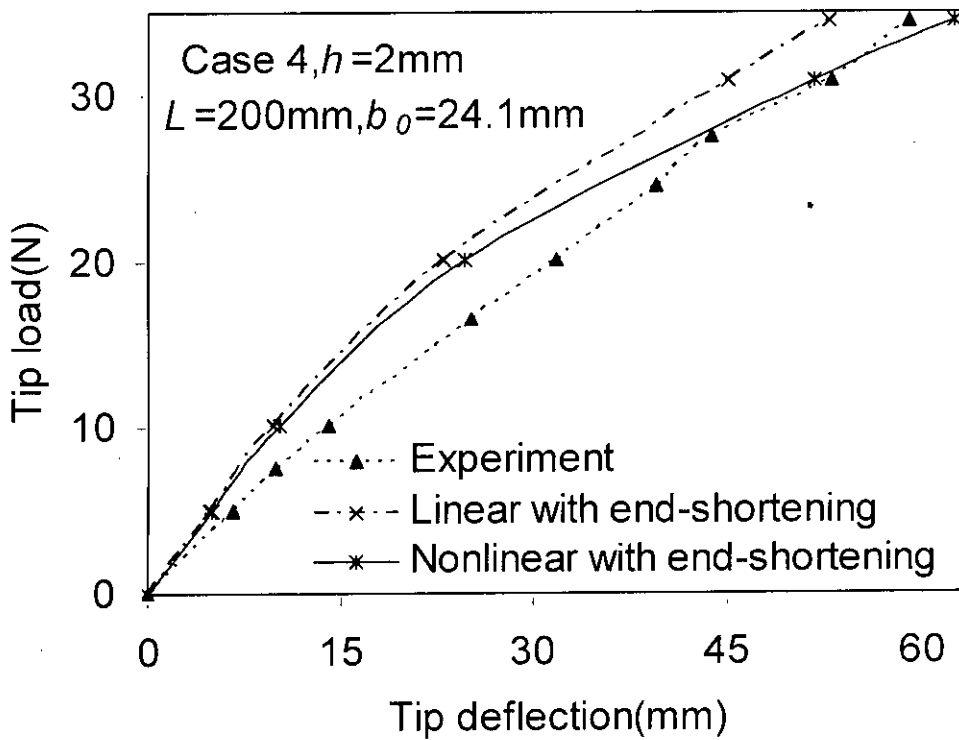


Figure 4.14: Load-deflection curve of stainless steel cantilever beam (Case 4: $L = 200\text{mm}$, $b_0 = 24.1\text{mm}$, $h = 2\text{mm}$, $\sigma_d = 249.91\text{MPa}$ at design load P_1 , Experimental $\delta_h = 12\text{mm}$ at P_2).

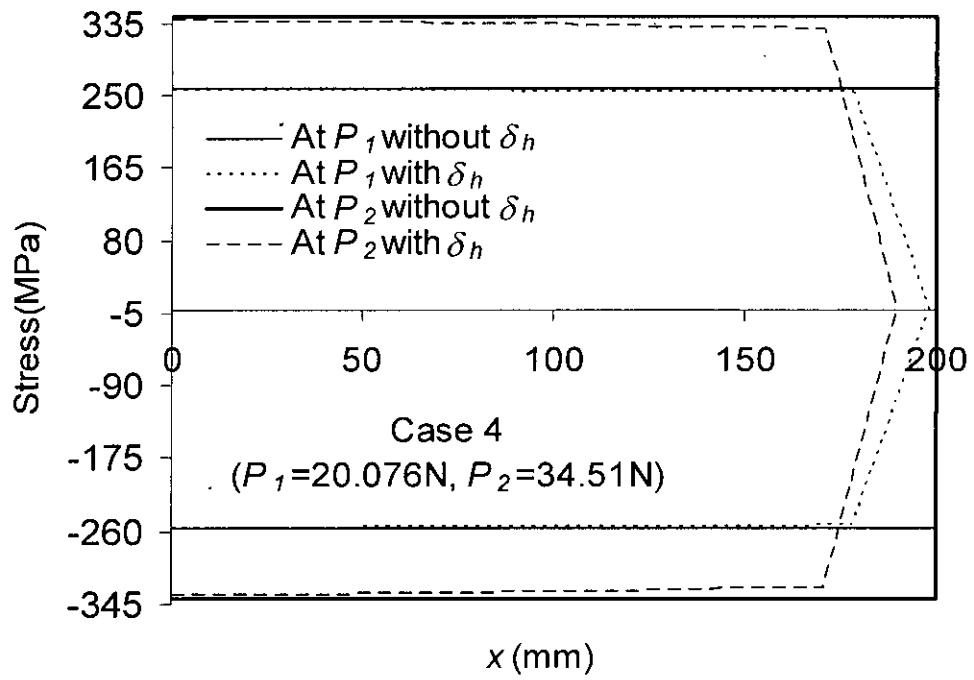


Figure 4.15(a): Stress distribution along the horizontal distance from the fixed end of the stainless steel beam by linear analysis (Case4: $L = 200\text{mm}$, $b_0 = 24.1\text{mm}$, $h = 2\text{mm}$, $\sigma_d = 249.91\text{MPa}$ at design load P_I).

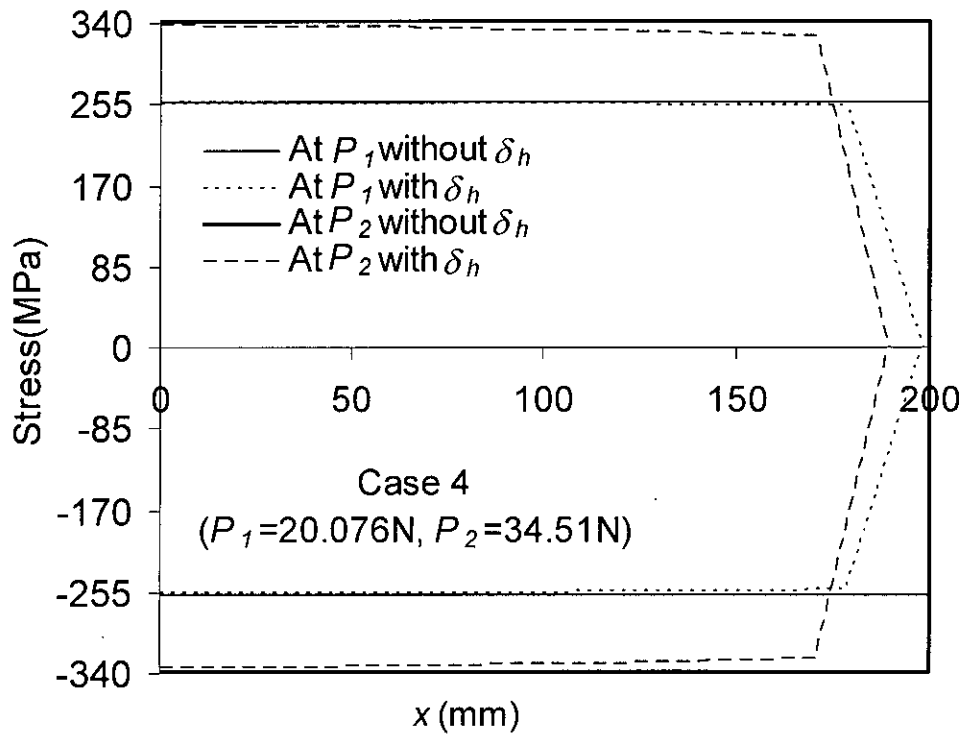


Figure 4.15(b): Stress distribution along the horizontal distance from the fixed end of the stainless steel beam by nonlinear analysis (Case 4: $L = 200\text{mm}$, $b_0 = 24.1\text{mm}$, $h = 2\text{mm}$, $\sigma_d = 249.91\text{MPa}$ at design load P_1).

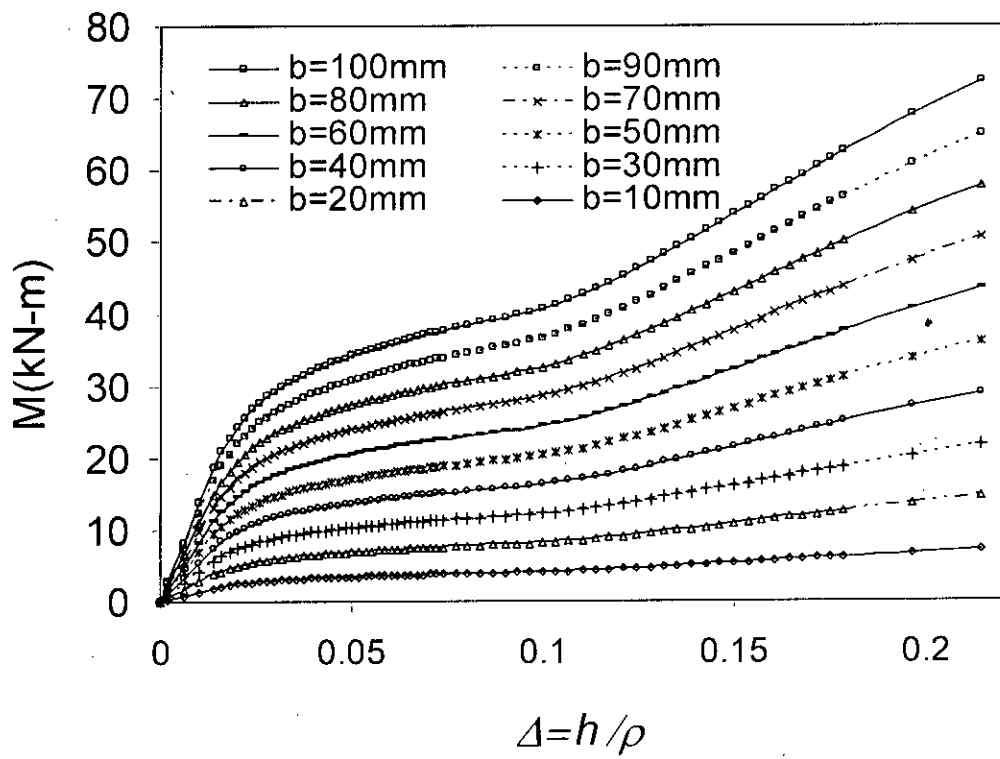


Figure 5.1: Moment- strain curve of SMA cantilever beam.

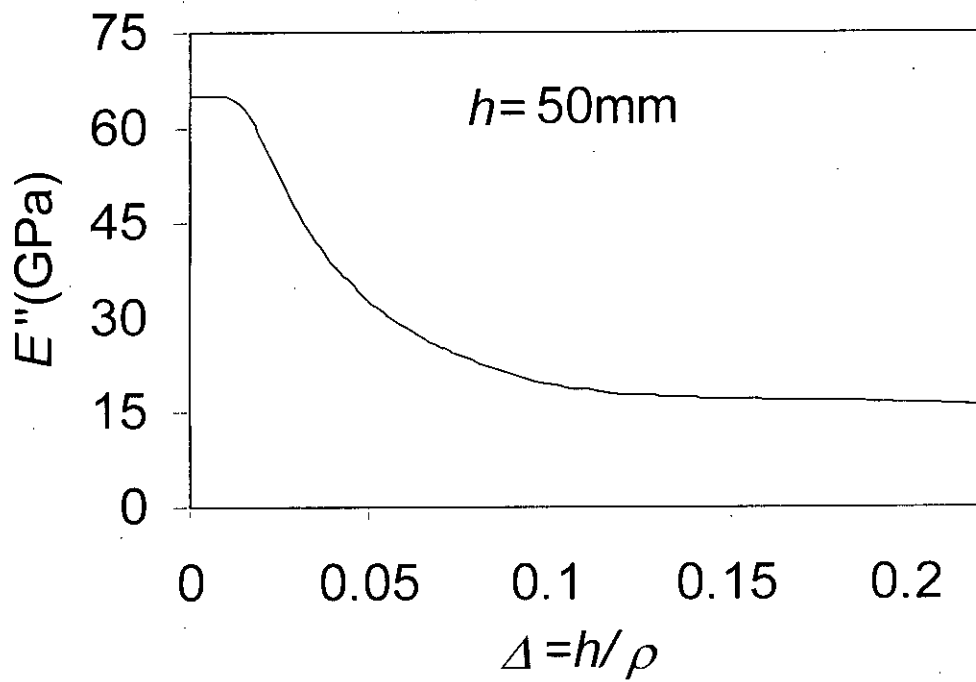


Figure 5.2: Effective modulus- strain curve of SMA cantilever beam.

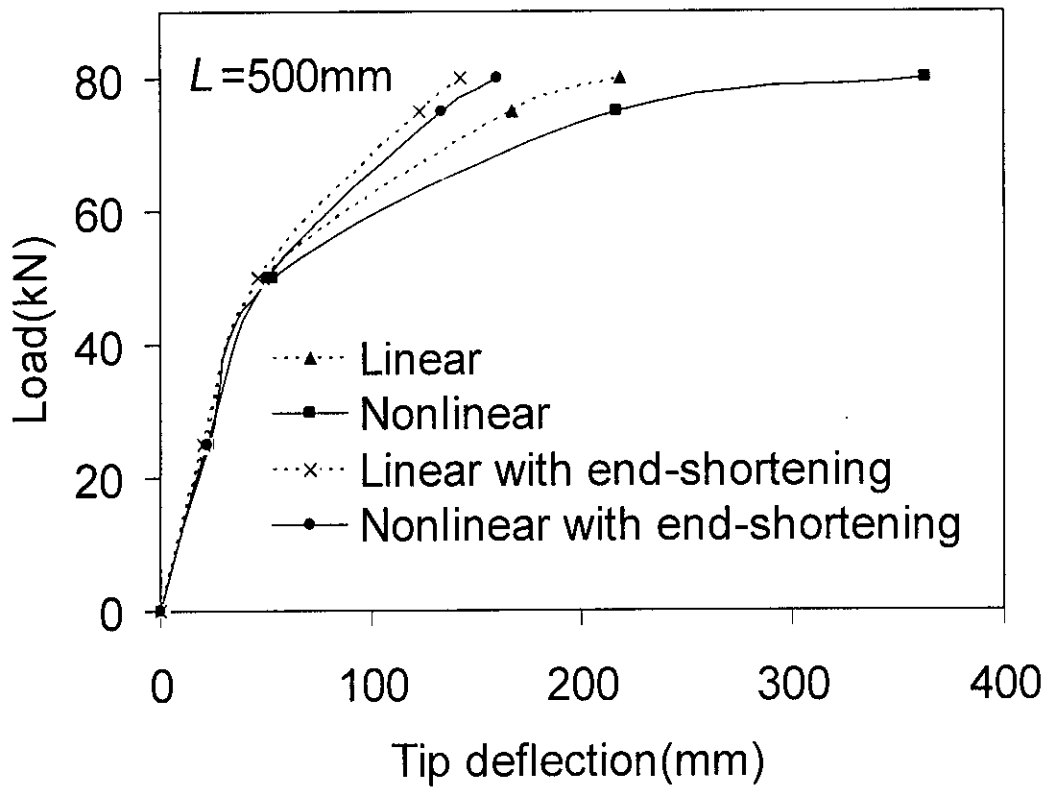


Figure 5.3: Load-deflection curve of SMA cantilever beam (Cases 1,2: $L = 500\text{mm}$, $b_0 = 100\text{mm}$, $h = 50\text{mm}$, Maximum design strain = 9.52% by linear theory without end-shortening).

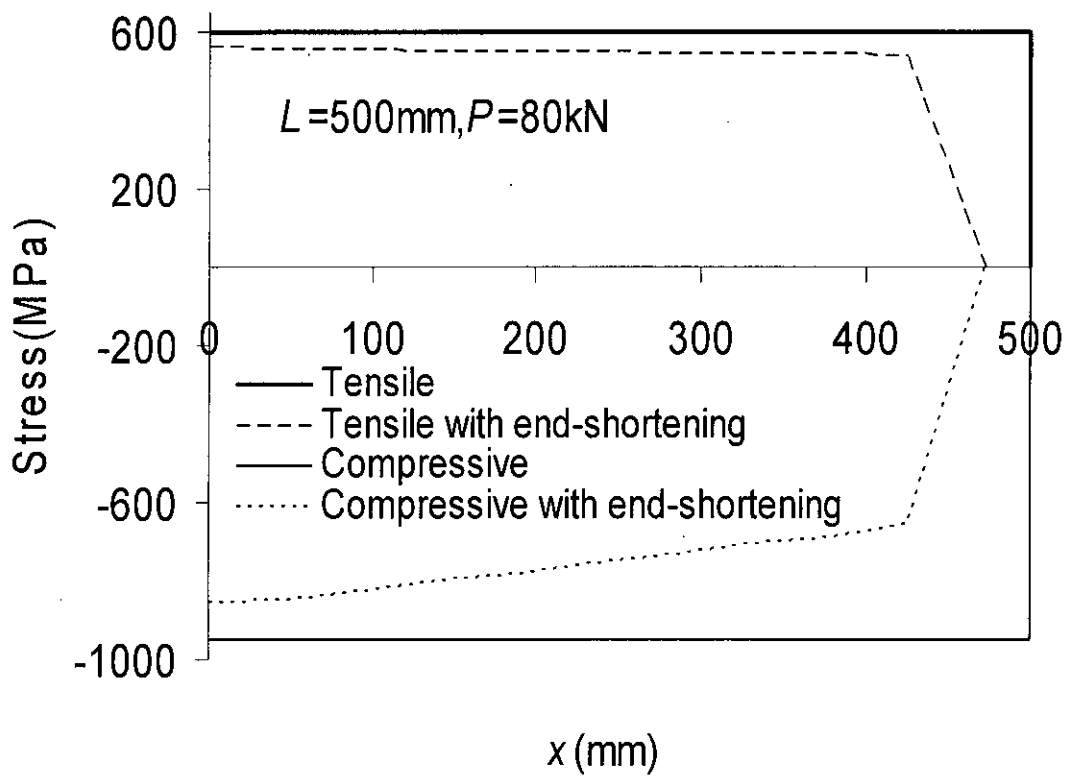


Figure 5.4(a): Stress distribution along the horizontal distance from the fixed end of the SMA beam by linear analysis (Case 1: $L = 500 \text{ mm}$, $b_0 = 100 \text{ mm}$, $h = 50 \text{ mm}$, Maximum design strain = 9.52% by linear theory without end-shortening)

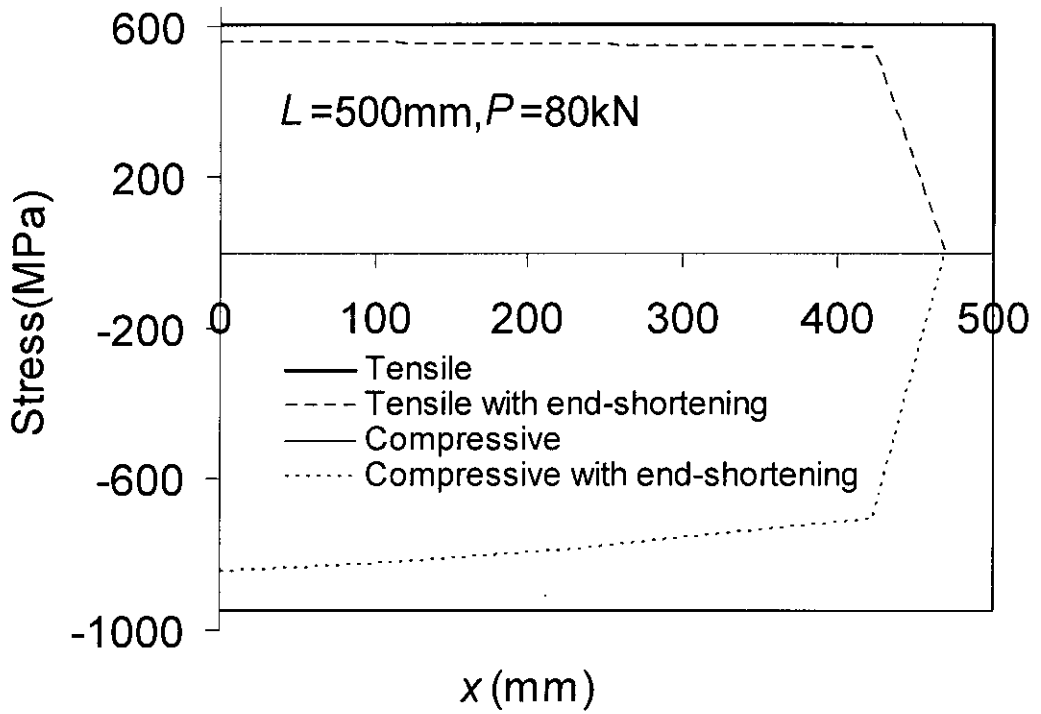


Figure 5.4(b): Stress distribution along the horizontal distance from the fixed end of the SMA beam by nonlinear analysis (Case 1: $L = 500\text{mm}$, $b_0 = 100\text{mm}$, $h = 50\text{mm}$, Maximum design strain = 9.52% by linear theory without end-shortening).

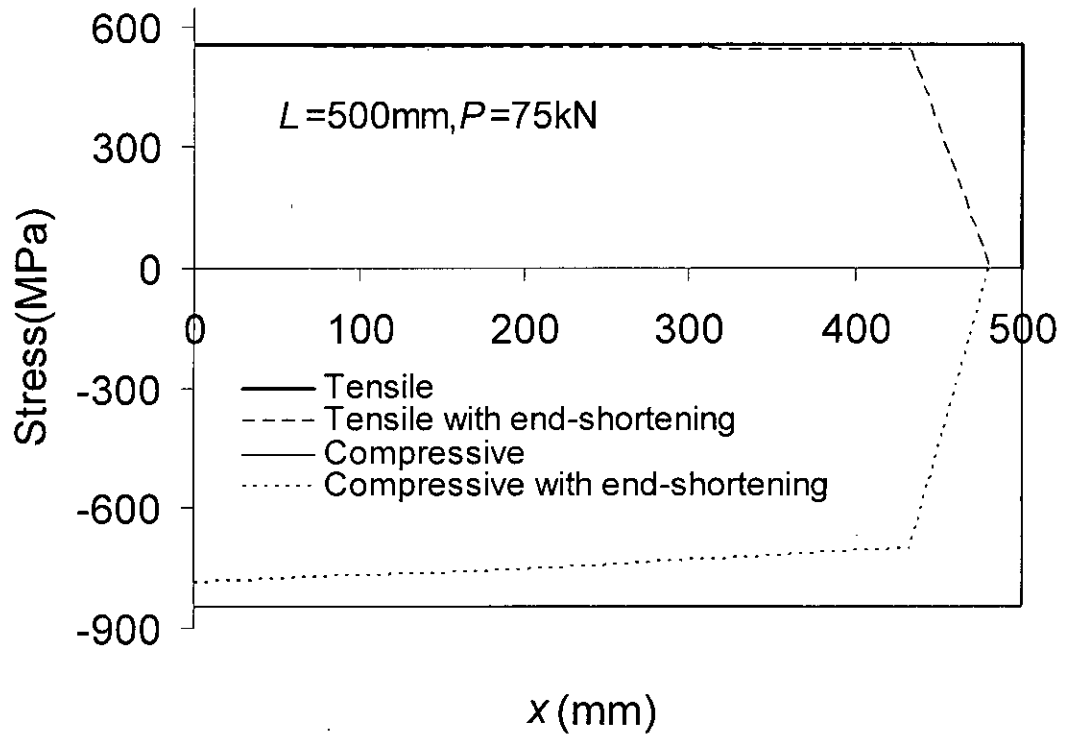


Figure 5.5(a): Stress distribution along the horizontal distance from the fixed end of the SMA beam by linear analysis (Case 2: $L = 500\text{mm}$, $b_0 = 100\text{mm}$, $h = 50\text{mm}$, Maximum design strain = 7.31% by linear theory without end-shortening).

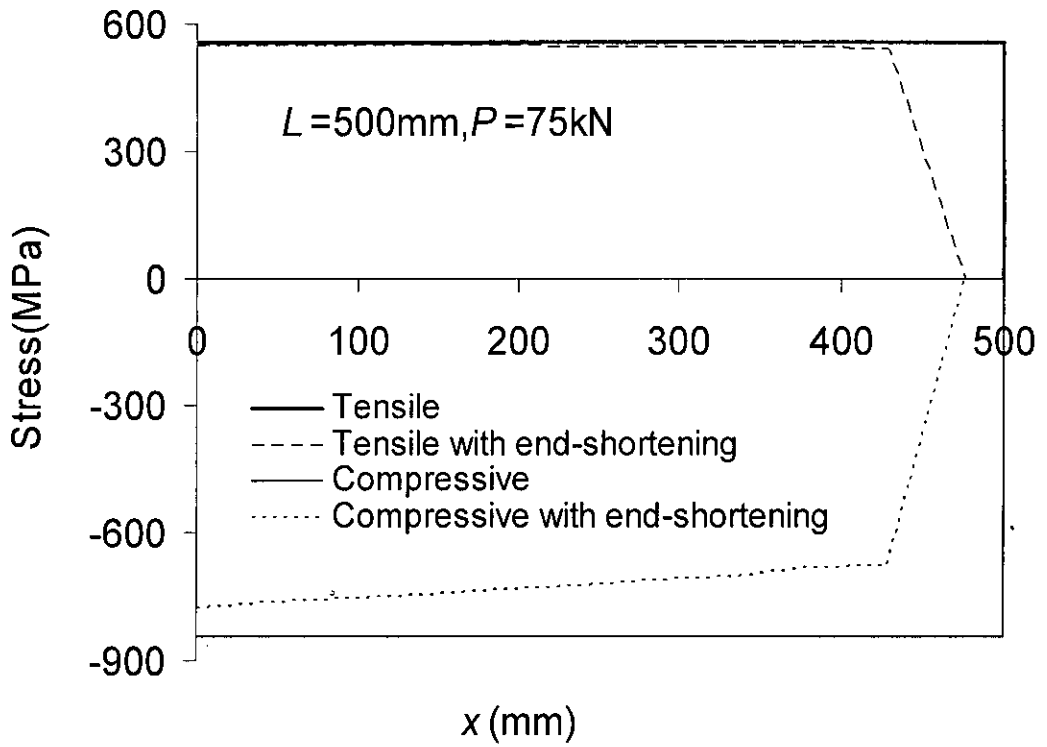


Figure 5.5(b): Stress distribution along the horizontal distance from the fixed end of the SMA beam by nonlinear analysis (Case 2: $L = 500\text{mm}$, $b_0 = 100\text{mm}$, $h = 50\text{mm}$, Maximum design strain = 7.31% by linear theory without end-shortening).

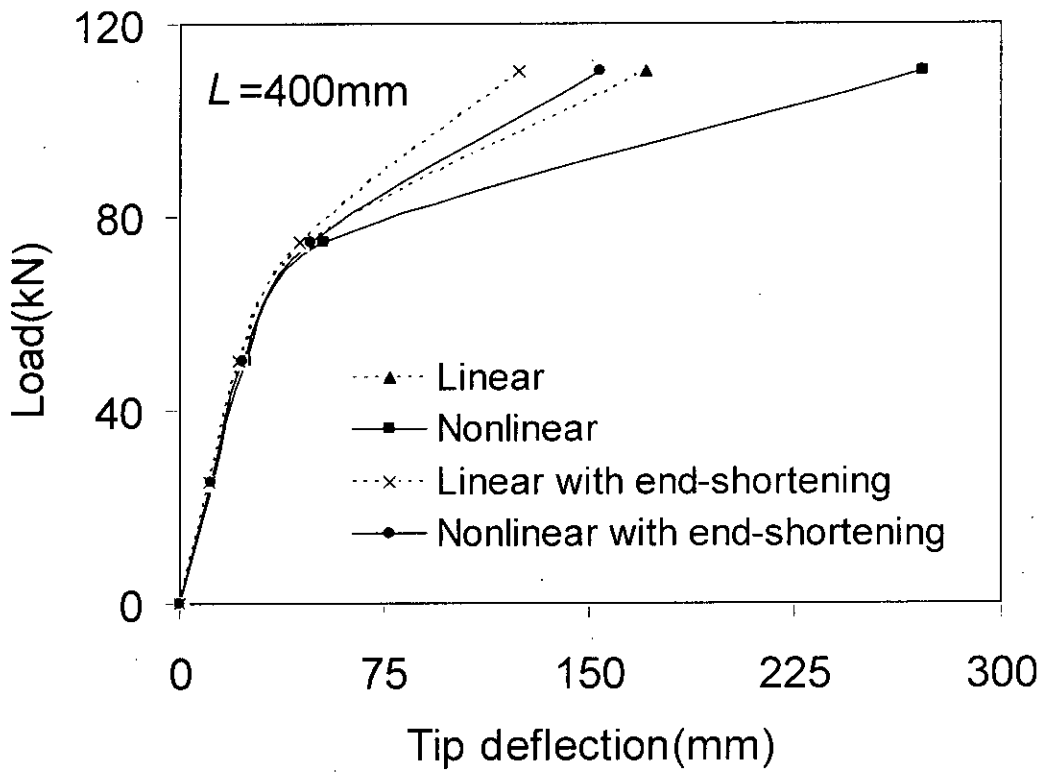


Figure 5.6: Load-deflection curve of SMA cantilever beam (Cases 3, 4: $L = 400\text{mm}$, $b_0 = 100\text{mm}$, $h = 50\text{mm}$, Maximum design strain = 11.62% by linear theory without end-shortening).

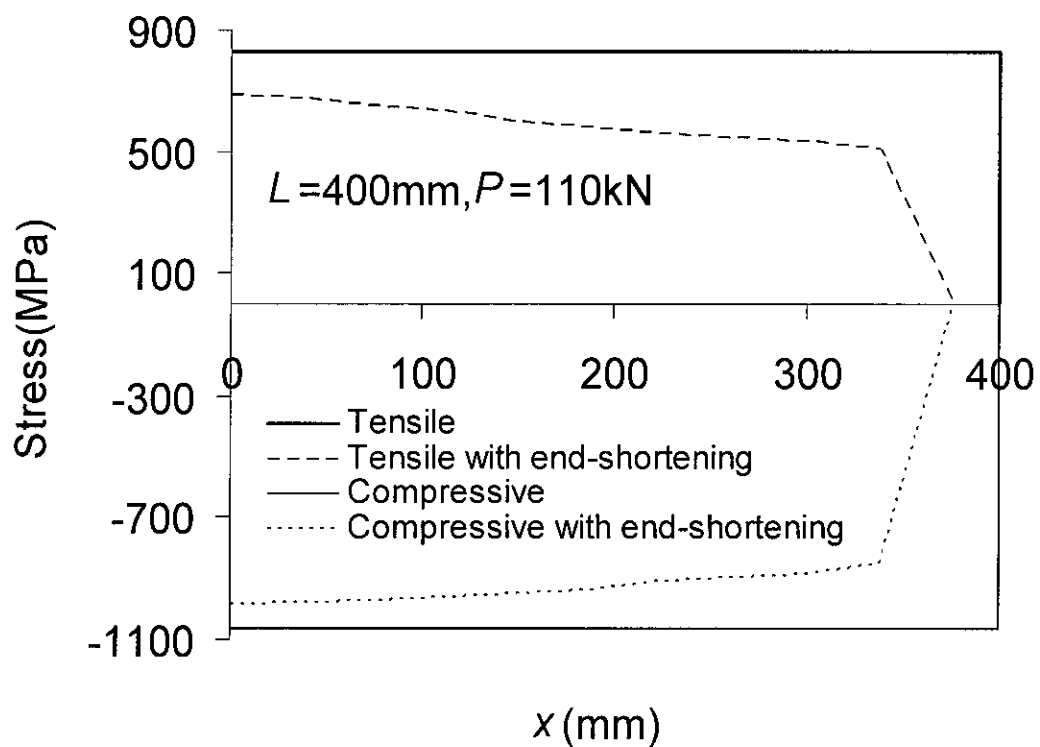


Figure 5.7(a): Stress distribution along the horizontal distance from the fixed end of the SMA beam by linear analysis (Case 3: $L = 400\text{mm}$, $b_0 = 100\text{mm}$, $h = 50\text{mm}$, Maximum design strain = 11.62% by linear theory without end-shortening).

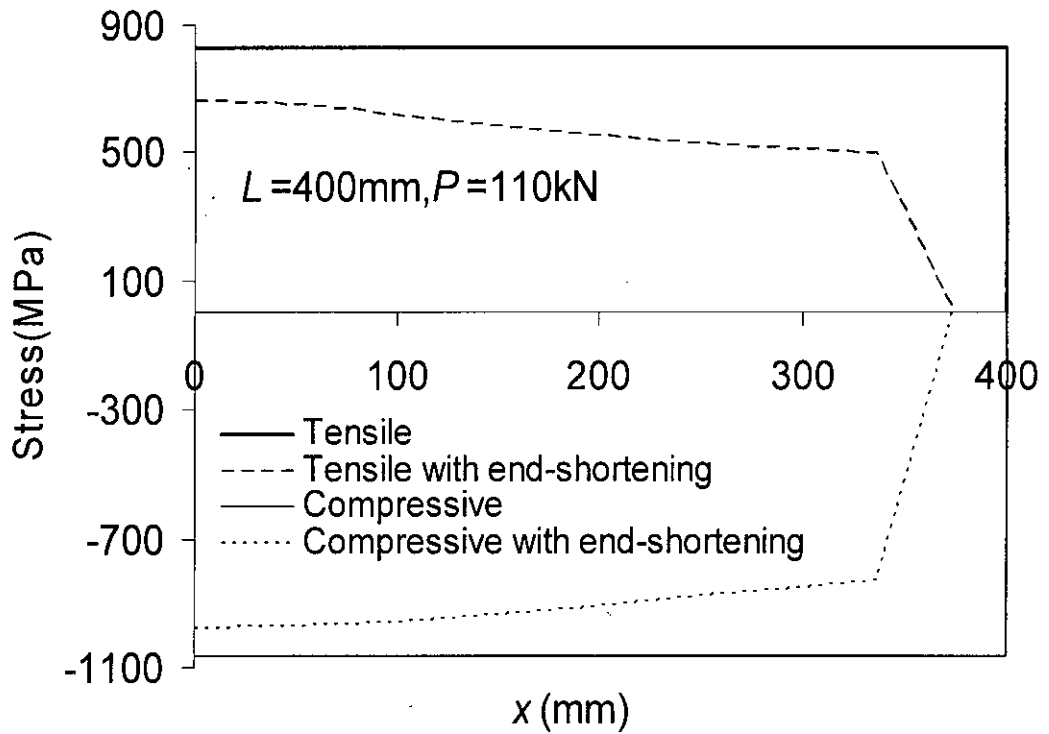


Figure 5.7(b): Stress distribution along the horizontal distance from the fixed end of the SMA beam by nonlinear analysis (Case 3: $L = 400\text{mm}$, $b_0 = 100\text{mm}$, $h = 50\text{mm}$, Maximum design strain = 11.62% by linear theory without end-shortening).

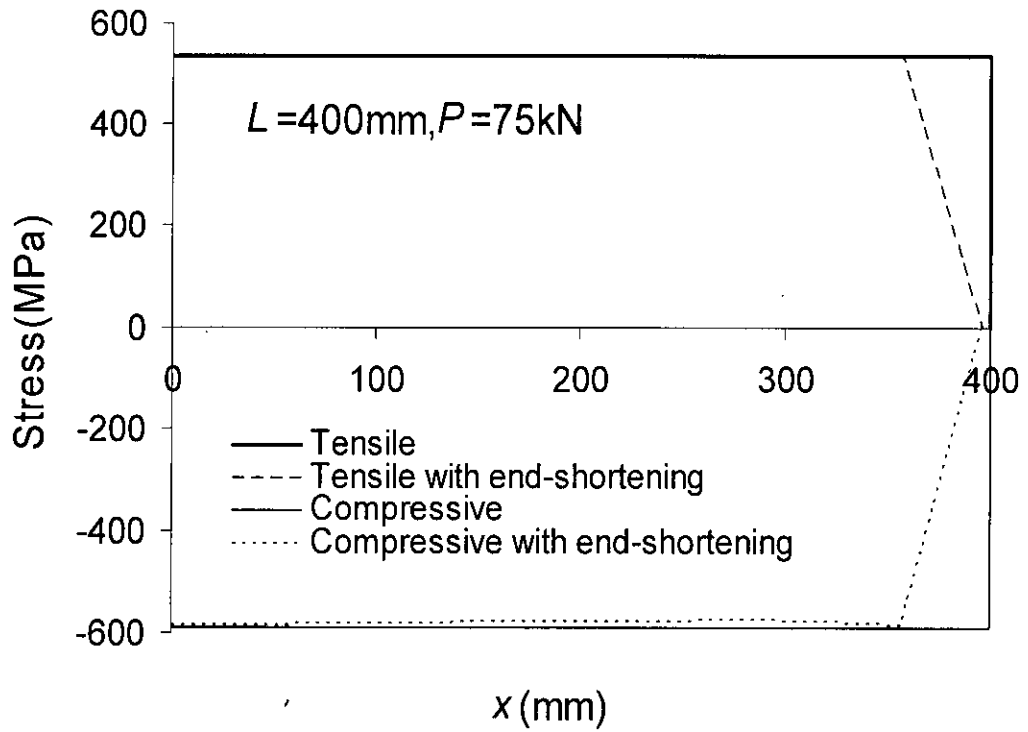


Figure 5.8(a): Stress distribution along the horizontal distance from the fixed end of the SMA beam by linear analysis (Case 4: $L = 400\text{mm}$, $b_0 = 100\text{mm}$, $h = 50\text{mm}$, Maximum design strain = 3.22% by linear theory without end-shortening).

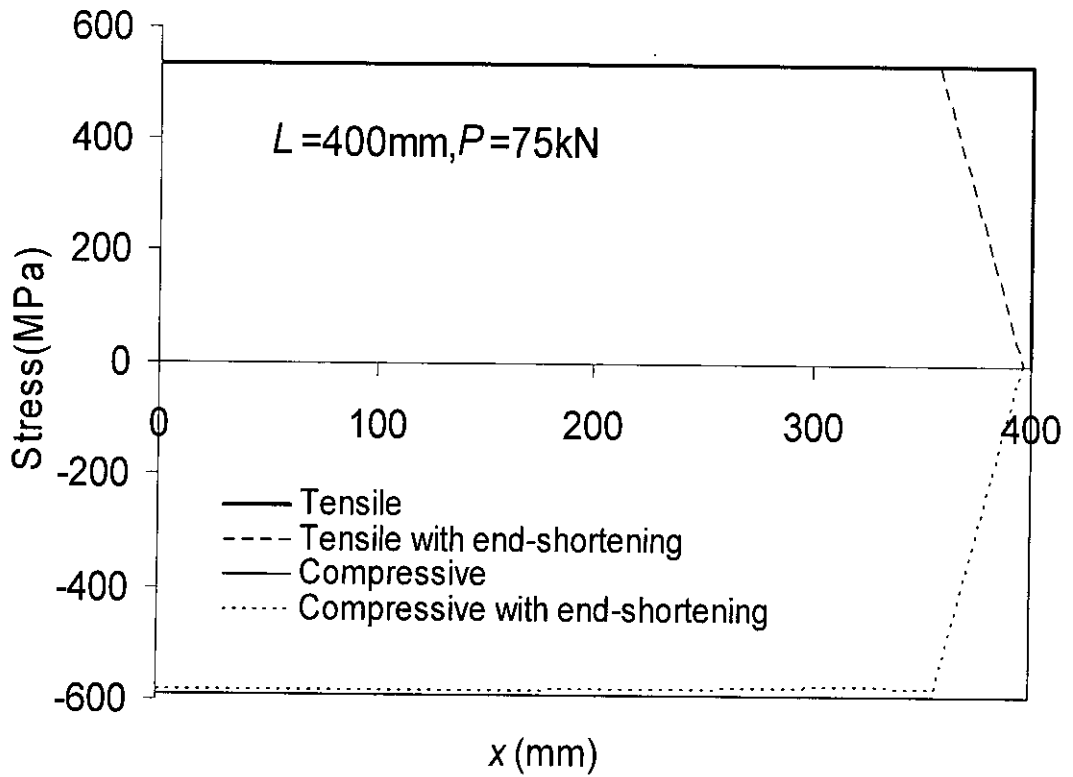


Figure 5.8(b): Stress distribution along the horizontal distance from the fixed end of the SMA beam by nonlinear analysis (Case 4: $L = 400\text{mm}$, $b_0 = 100\text{mm}$, $h = 50\text{mm}$, Maximum design strain = 3.22% by linear theory without end-shortening).

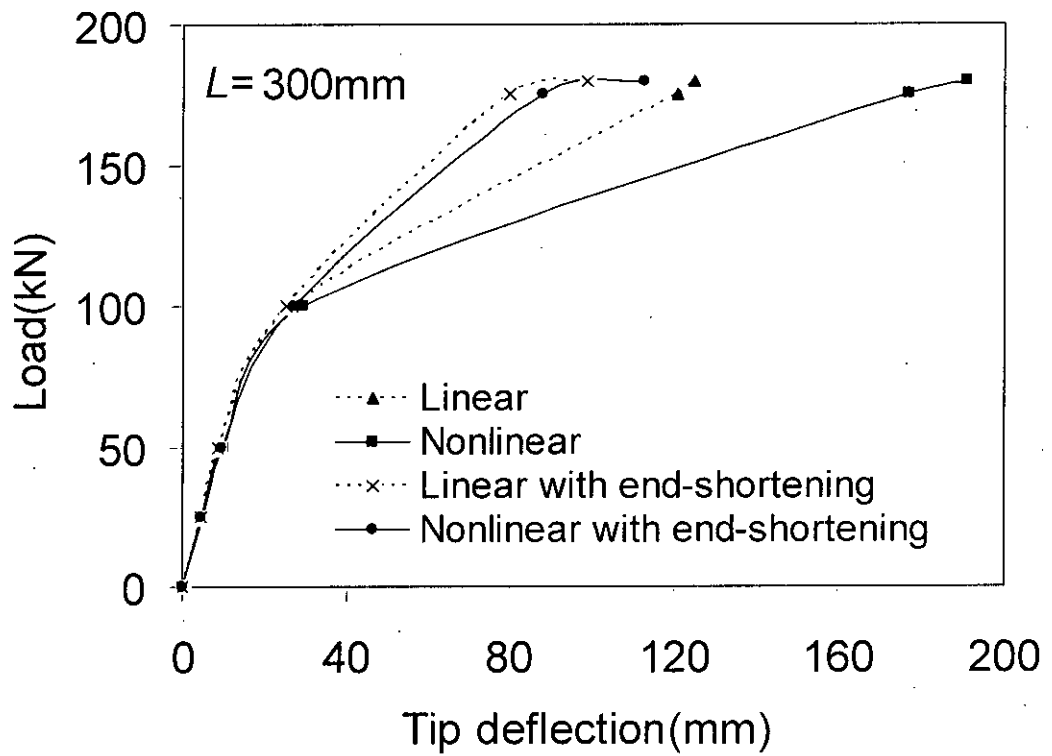


Figure 5.9: Load-deflection curve of SMA cantilever beam (Cases 5,6: $L = 300\text{mm}$, $b_0 = 100\text{mm}$, $h = 50\text{mm}$, Maximum design strain = 15.20% by linear theory without end-shortening)

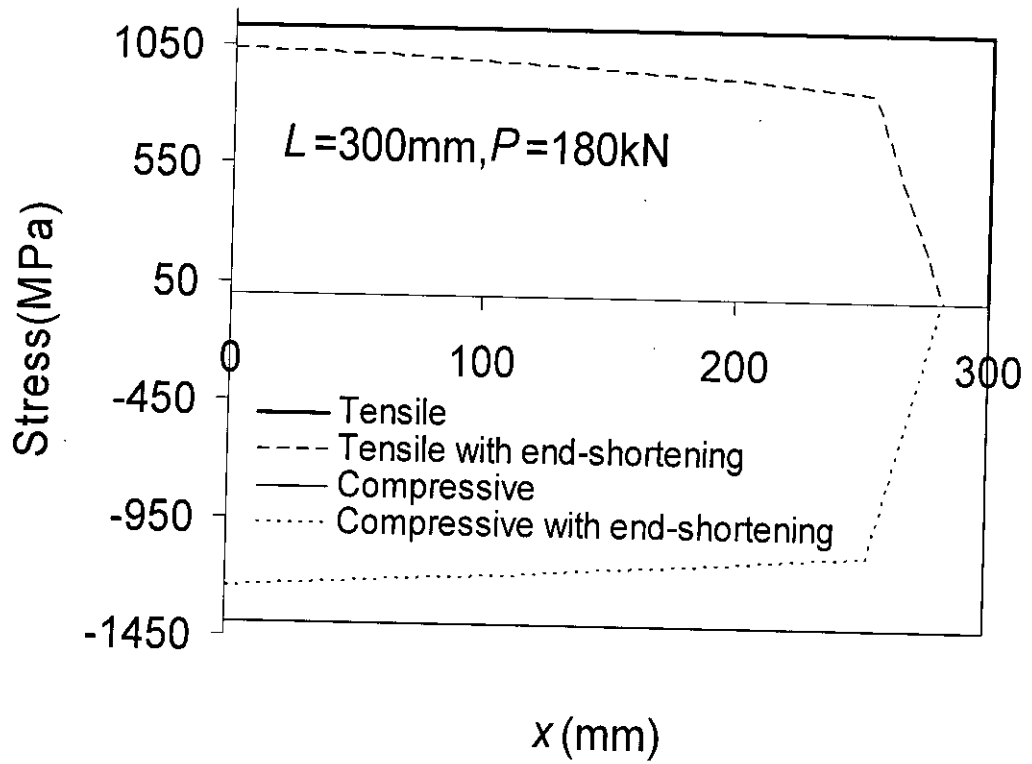


Figure 5.10(a): Stress distribution along the horizontal distance from the fixed end of the SMA beam by linear analysis (Case 5: $L = 300\text{mm}$, $b_0 = 100\text{mm}$, $h = 50\text{mm}$, Maximum design strain = 15.20% by linear theory without end-shortening).

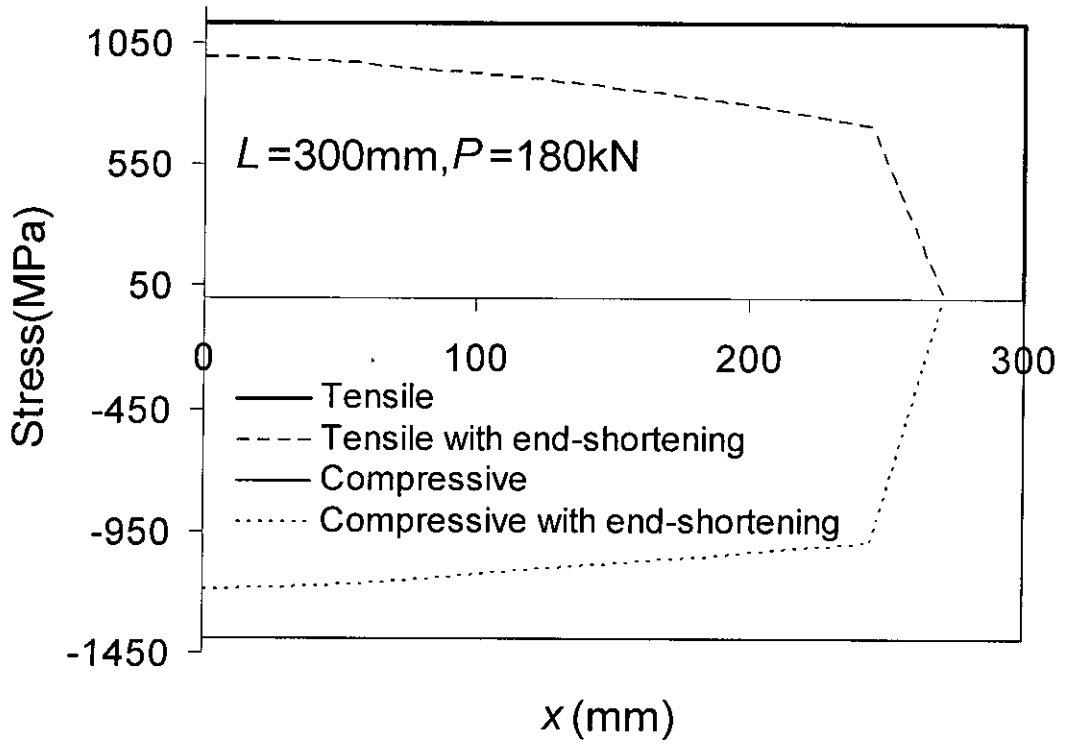


Figure 5.10(b): Stress distribution along the horizontal distance from the fixed end of the SMA beam by nonlinear analysis (Case 5: $L = 300\text{mm}$, $b_0 = 100\text{mm}$, $h = 50\text{mm}$, Maximum design strain = 15.20% by linear theory without end-shortening)

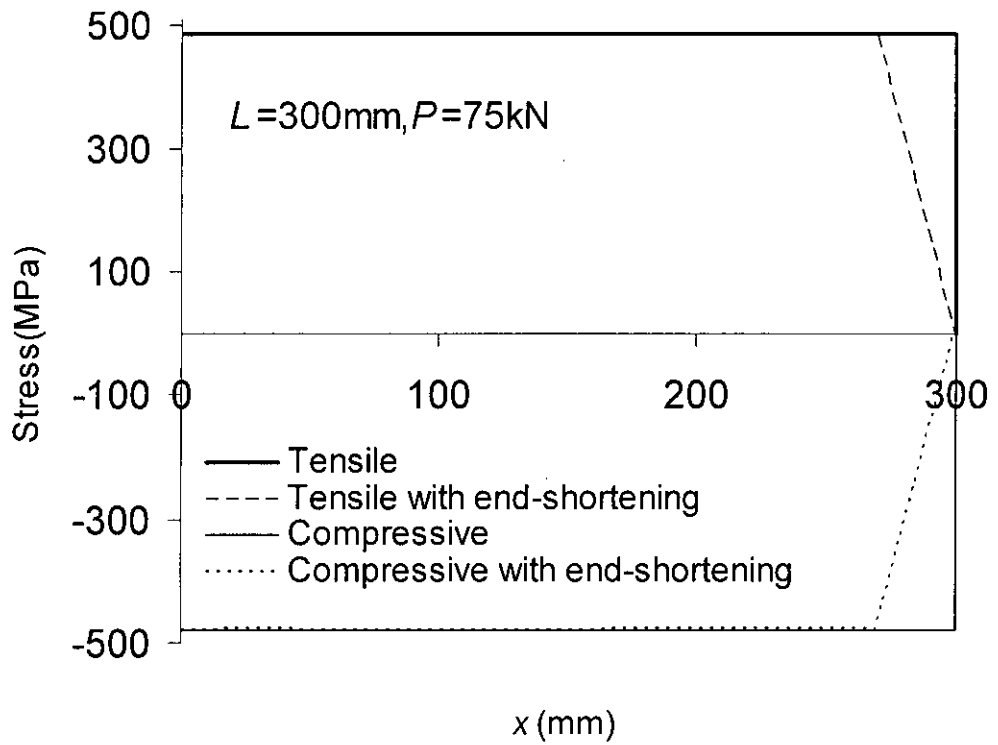


Figure 5.11(a): Stress distribution along the horizontal distance from the fixed end of the SMA beam by linear analysis (Case 6: $L = 300\text{mm}$, $b_0 = 100\text{mm}$, $h = 50\text{mm}$, Maximum design strain = 1.78% by linear theory without end-shortening).

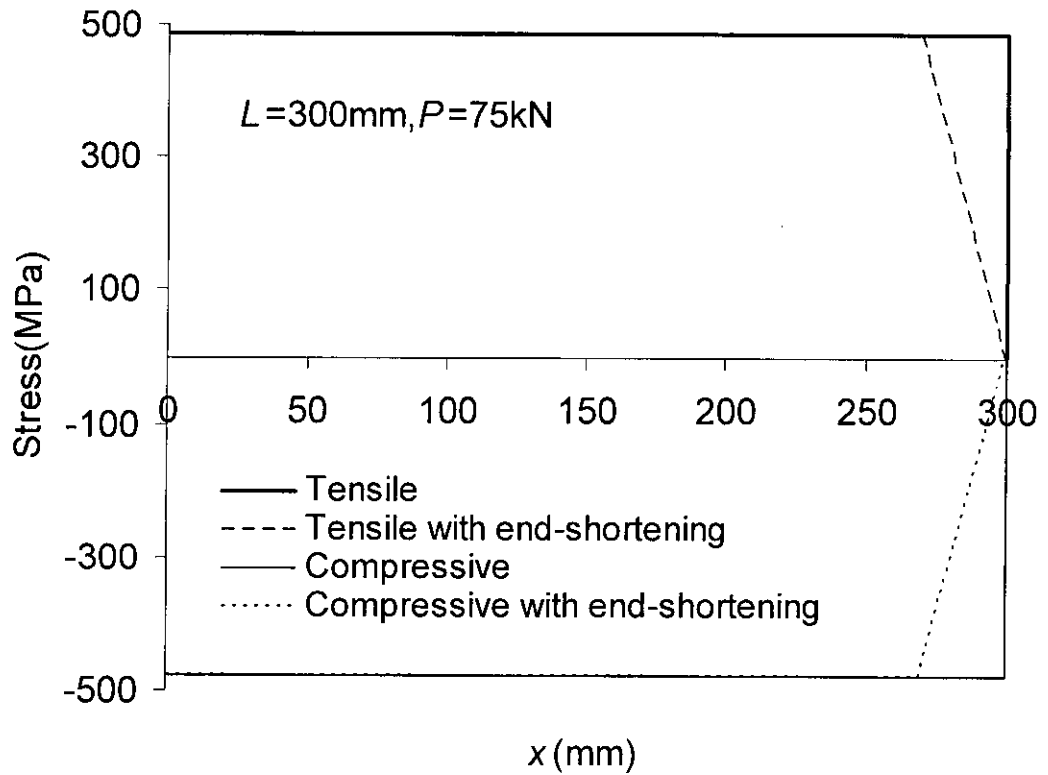


Figure 5.11(b): Stress distribution along the horizontal distance from the fixed end of the SMA beam by nonlinear analysis (Case 6: $L = 300\text{mm}$, $b_0 = 100\text{mm}$, $h = 50\text{mm}$, Maximum design strain = 1.78% by linear theory without end-shortening).

APPENDIX- A

A 1 Numerical Analysis

The Runge-Kutta solution technique is briefly described below, as it is the tool of the present analysis. In this solution technique for any first order differential equation, the unknowns y_1, y_2 etc. are successively evaluated at each grid point starting from the initial boundary as described below.

$$\frac{dy}{dx} = f(x, y)$$

$$y_{a+h} = y_a + \frac{1}{6}(k_1 + 2k_2 + 2k_3 + k_4)h$$

$$\text{where, } k_1 = hf(a, y_a)$$

$$k_2 = hf\left(a + \frac{h}{2}, y_a + \frac{k_1}{2}\right)$$

$$k_3 = hf\left(a + \frac{h}{2}, y_a + \frac{k_2}{2}\right)$$

$$k_4 = hf(a + h, y_a + k_3)$$

For an m^{th} order ordinary differential equation (ODE), it is first reduced to m number of first order ODE. Then the variables are evaluated as described below.

$$\begin{bmatrix} y_1 \\ y_2 \\ \vdots \\ y_m \end{bmatrix}_{a+h} = \begin{bmatrix} y_1 \\ y_2 \\ \vdots \\ y_m \end{bmatrix}_a + \frac{1}{6} \left[\begin{bmatrix} k_{11} \\ k_{12} \\ \vdots \\ k_{1m} \end{bmatrix} + 2 \begin{bmatrix} k_{21} \\ k_{22} \\ \vdots \\ k_{2m} \end{bmatrix} + 2 \begin{bmatrix} k_{31} \\ k_{32} \\ \vdots \\ k_{3m} \end{bmatrix} + \begin{bmatrix} k_{41} \\ k_{42} \\ \vdots \\ k_{4m} \end{bmatrix} \right]$$

$$\text{where, } \left\{ \begin{array}{l} k_{11} \\ k_{12} \\ \vdots \\ k_{1m} \end{array} \right\} = h \left\{ \begin{array}{l} f_1(a, y_{1a}, y_{2a}, \dots, y_{ma}) \\ f_2(a, y_{1a}, y_{2a}, \dots, y_{ma}) \\ \vdots \\ f_m(a, y_{1a}, y_{2a}, \dots, y_{ma}) \end{array} \right\}$$

$$\left\{ \begin{array}{l} k_{21} \\ k_{22} \\ \vdots \\ k_{2m} \end{array} \right\} = h \left\{ \begin{array}{l} f_1 \left[\left(a + \frac{h}{2} \right), \left(y_{1a} + \frac{k_{11}}{2} \right), \left(y_{2a} + \frac{k_{12}}{2} \right), \dots, \left(y_{ma} + \frac{k_{1m}}{2} \right) \right] \\ f_2 \left[\left(a + \frac{h}{2} \right), \left(y_{1a} + \frac{k_{11}}{2} \right), \left(y_{2a} + \frac{k_{12}}{2} \right), \dots, \left(y_{ma} + \frac{k_{1m}}{2} \right) \right] \\ \vdots \\ f_m \left[\left(a + \frac{h}{2} \right), \left(y_{1a} + \frac{k_{11}}{2} \right), \left(y_{2a} + \frac{k_{12}}{2} \right), \dots, \left(y_{ma} + \frac{k_{1m}}{2} \right) \right] \end{array} \right\}$$

$$\left\{ \begin{array}{l} k_{31} \\ k_{32} \\ \vdots \\ k_{3m} \end{array} \right\} = h \left\{ \begin{array}{l} f_1 \left[\left(a + \frac{h}{2} \right), \left(y_{1a} + \frac{k_{21}}{2} \right), \left(y_{2a} + \frac{k_{22}}{2} \right), \dots, \left(y_{ma} + \frac{k_{2m}}{2} \right) \right] \\ f_2 \left[\left(a + \frac{h}{2} \right), \left(y_{1a} + \frac{k_{21}}{2} \right), \left(y_{2a} + \frac{k_{22}}{2} \right), \dots, \left(y_{ma} + \frac{k_{2m}}{2} \right) \right] \\ \vdots \\ f_m \left[\left(a + \frac{h}{2} \right), \left(y_{1a} + \frac{k_{21}}{2} \right), \left(y_{2a} + \frac{k_{22}}{2} \right), \dots, \left(y_{ma} + \frac{k_{2m}}{2} \right) \right] \end{array} \right\}$$

$$\left\{ \begin{array}{l} k_{41} \\ k_{42} \\ \vdots \\ k_{4m} \end{array} \right\} = h \left\{ \begin{array}{l} f_1 [(a+h), (y_{1a} + k_{31}), (y_{2a} + k_{32}), \dots, (y_{ma} + k_{3m})] \\ f_2 [(a+h), (y_{1a} + k_{31}), (y_{2a} + k_{32}), \dots, (y_{ma} + k_{3m})] \\ \vdots \\ f_m [(a+h), (y_{1a} + k_{31}), (y_{2a} + k_{32}), \dots, (y_{ma} + k_{3m})] \end{array} \right\}$$

APPENDIX- B

Programming Features

B.1 Input of the programs

In the sixth program data of experimental σ - ε diagram (figures 1.2, 4.3 (b), 4.4 (b)) are used. The data (e, s, f, t) are given in a file name "2.txt" and the programs take the data itself when run. Upper limit of strain (g) and lower limit of strain (h) of the first two programs. The data of E'' - Δ and M - Δ curves (figure 4.3 and figure 4.4) are used in first and second programs. The value of E'' is obtained from corresponding moment that obtained from equilibrium condition of the beam.

B.2 Output of the programs

The sixth program will give the values of e_2 , delta, E , M , of rectangular cross-section. The fifth program will give the values of b after end-shortening. The first and second programs will give the deflections at different grid points for repeated loading at different E'' and b . From the last program stress can be found at corresponding strain.

B.3 TABLE OF INPUT-OUTPUT VARIABLES

Variable	Definition
e	Strain at upper fiber
s	Stress at upper fiber
f	Strain at lower fiber
t	Stress at lower fiber
sigma_c	Compressive stress
g	Upper limit of strain
h	Lower limit of strain
e_2	compressive strain
delta	Total strain
E	Modulus of Elasticity
M	Bending moment
Y	Deflections at different grid points

APPENDIX- C

Programme Code

```
/******  
/**PROGRAM OF LINEAR EQUATION BY R-K METHOD FOR SMA BEAM**/  
*****  
#include<iostream.h>  
#include<conio.h>  
#include<fstream.h>  
#include<math.h>  
#define f1(y2) y2  
#define f2(x) lam*(x-L)  
  
void main()  
{  
float p=80000, xp, E1[200], E[210], y1[200], lam, L=500;  
float y2[200], b0=100, b[200], h=50, f1, f2;  
int i, j, x=0, N, H=50;  
float y[200], I[200], Z[210], C=25;  
float k11, k12, k21, k22, k31, k32, k41, k42, M[200], sig[200];  
  
ofstream outf ("zeee.xls");  
//ifstream inputf("10.txt");//ofstream outf1("out00053.xls");  
//ifstream infilef1("11.txt");  
  
clrscr();  
  
y1[0]=0;  
y2[0]=0;  
xp=L;  
N=((xp-x)/H);  
  
for(i=0; i<N; i++)  
{  
E[i]=65000;  
//inputf>>E[i];  
//infilef1>>b[i];  
b[i]=b0*(L-x)/L;  
I[i]=b[i]*pow(h,3)/12;  
//I[i]=10416.667*b[i];  
Z[i]=E[i]*I[i];  
lam=p/Z[i];  
k11=H*f1(y2[i]);  
k12=H*f2(x);
```

```

        k21=y2[i]+(k12/2);
        k22=x+0.5*H;
        k21=H*f1(k21);
        k22=H*f2(k22);
        k31=y2[i]+(k22/2);
        k32=x+0.5*H;
        k31=H*f1(k31);
        k32=H*f2(k32);
        k41=y2[i]+(k32);
        k42=x+H;
        k41=H*f1(k41);
        k42=H*f2(k42);
        M[i]=p*(L-x);
        x+=H;
        y1[i+1]=y1[i]+(k11+2.0*k21+2.0*k31+k41)/6.0;
        y2[i+1]=y2[i]+(k12+2.0*k22+2.0*k32+k42)/6.0;
        cout<<y1[i+1]<<" \n";
    }
getch();
}

/*****
/*PROGRAM OF NON LINEAR EUATION BY R-K METHOD FOR SMA BEAM*/
*****/

#include<iostream.h>
#include<conio.h>
#include<fstream.h>
#include<math.h>
#define f1(y2) y2
#define f2(y2) pow((1+y2*y2),1.5)*((-9.6E-7*p*L)/E[i])

void main()
{
double p=80000,xp,E[200],y1[200],lam,L=500,y2[200],f1,f2,b0=100,b[200];
int i,j,x=0,N,H=50;
double y[200],I[200],Z[200],C=25;
double k11,k12,k21,k22,k31,k32,k41,k42,M[200],sig[200];
ofstream outf ("zeee.xls");
ifstream infile("10.txt");
ifstream inputf1("11.txt");

clrscr();
y1[0]=0;

```

```

y2[0]=0;
xp=L;
N=((xp-x)/H);

for(i=0;i<N;i++)
{
E[i]=65000;
//infile>>E[i];
//inputf1>>b[i];
b[i]=(b0*(L-x))/L;
I[i]=10416.667*b[i];
Z[i]=E[i]*I[i];
k11=H*f1(y2[i]);
k12=y2[i];
k12=f2(k12);
k12=H*k12;
k21=y2[i]+(k12/2.0);
k21=f1(k21);
k21=H*k21;
//k22=x+0.5*H;
k22=y2[i]+(k12/2.0);
k22=f2(k22);
k22=H*k22;
k31=y2[i]+(k22/2.0);
k31=f1(k31);
k31=H*k31;
//k32=x+0.5*H;
k32=y2[i]+(k22/2.0);
k32=f2(k32);
k32=H*k32;
k41=y2[i]+(k32);
k41=f1(k41);
k41=H*k41;
//k42=x+H;
k42=y2[i]+k32;
k42=f2(k42);//cout<<k12<<" \n";
k42=H*k42;
M[i]=p*(L-x);
x+=H;
y1[i+1]=y1[i]+(k11+2.0*k21+2.0*k31+k41)/6.0;
y2[i+1]=y2[i]+(k12+2.0*k22+2.0*k32+k42)/6.0;
cout<<y1[i+1]<<" \n";
}
getch();
}

```

```

/*****
/*PROGRAM OF LINEAR EQUATION BY R-K METHOD WITH SELF WEIGHT */
*****/

#include<iostream.h>
#include<conio.h>
#include<fstream.h>
#include<math.h>
#define f1(y2) y2
#define f2(x) lam*(2*p*(L-x)+w*(pow((L-x),2)))

void main()
{
float p=0.,xp,E=200000,y1[420],lam,L=389.8,w=0.000758,y2[420],f1,f2;
int i,j,x=0,N,H=1;
float y[400],I=0.1333333,Z,C,k11,k12,k21,k22,k31,k32,k41,k42;

ofstream outf ("z.xls");

clrscr();
y1[0]=0;
y2[0]=0;
xp=L;
N=((xp-x)/H);
Z=E*I;
lam=-0.5/Z;
for(i=0;i<=N;i++)
{
k11=H*f1(y2[i]);
k12=H*f2(x);
k21=y2[i]+(k12/2);
k22=x+0.5*H;
k21=H*f1(k21);
k22=H*f2(k22);
k31=y2[i]+(k22/2);
k32=x+0.5*H;
k31=H*f1(k31);
k32=H*f2(k32);
k41=y2[i]+(k32);
k42=x+H;
k41=H*f1(k41);
k42=H*f2(k42);
x+=H;
y1[i+1]=y1[i]+(k11+2.0*k21+2.0*k31+k41)/6.0;
y2[i+1]=y2[i]+(k12+2.0*k22+2.0*k32+k42)/6.0;
}
}

```

```

        outf<<y1[i]<<" \n";
    }

cout<<y1[389.8]<<" \n";
getch();
}

/*****
/* PROGRAM OF NONLINEAR EQUATION BY R-K METHOD WITH SELF WEIGHT*/
*****/

#include<iostream.h>
#include<conio.h>
#include<fstream.h>
#include<math.h>
#define f1(y2) y2
#define f2(x,y2) pow((1+y2*y2),1.5)*lam*(2*p*(L-x)+w*(pow((L-x),2)))

void main()
{
double p=0.,xp,E=200000,y1[410],lam,L=400,w=0.000758,y2[410];
double f1,f2,m12,m22,m32,m42,a,b,c;
int i,j,x=0,N,H=1;
double y[410],I=0.1333333,Z,C,k11,k12,k21,k22,k31,k32,k41,k42;

ofstream outf ("z.xls");

clrscr();
y1[0]=0;
y2[0]=0;
xp=L;
N=((xp-x)/H);
Z=E*I;
lam=-0.5/Z;
for(i=0;i<=N;i++)
    {
        k11=H*f1(y2[i]);
        k12=x;
        m12=y2[i];
        k12=f2(k12,m12);
        k12=H*k12;
        k21=y2[i]+(k12/2.0);
        k21=f1(k21);
        k21=H*k21;
    }
}

```



```

k22=x+0.5*H;
m22=y2[i]+(k12/2.0);
k22=f2(k22,m22);
k22=H*k22;
k31=y2[i]+(k22/2.0);
k31=f1(k31);
k31=H*k31;
k32=x+0.5*H;
m32=y2[i]+(k22/2.0);
k32=f2(k32,m32);
k32=H*k32;
k41=y2[i]+(k32);
k41=f1(k41);
k41=H*k41;
k42=x+H;
m42=y2[i]+k32;
k42=f2(k42,m42);
k42=H*k42;
x+=H;
y1[i+1]=y1[i]+(k11+2.0*k21+2.0*k31+k41)/6.0;
y2[i+1]=y2[i]+(k12+2.0*k22+2.0*k32+k42)/6.0;
outf<<y1[i]<<" \n";
}

cout<<y1[400]<<endl;
getch();
}

```

```

/*****
/*PROGRAM FOR CALCULATING"END-SHORTENING" AND CORRESPONDING
WIDTH "b" AT DIFFERENT POSITION OF X*/
*****/

#include<iostream.h>
#include<stdio.h>
#include<conio.h>
#include<math.h>
#include<fstream.h>
#include<dos.h>
#define f(z) sqrt(1+(pow((-0.0058*z+0.0929),2)))
//define f(z) sqrt(1+(pow((-0.0076*z-0.0837),2)))

void main ()
{
clrscr();
double y[4];
float xo[200], b[200];
int b0=0;
cout<<"Enter the value of b at X=0:";
cin>>b0;
ofstream outf ("out0551.xls");
int L=500;
float a;
textcolor(3);
cout<<"\tX after bending\t\tX before bending\t\tCorresponding b"<<endl;
outf<<"\tX after bending\t\tX before bending\t\tCorresponding b"<<endl;
for(float xn=0; xn<480; xn++)
{
a=0.0;
float h=xn/3;
for(int i=0;i<4;i++)
{
y[i]=f(a);
a+=h;
}
xo[xn]=(y[0]+3*y[1]+3*y[2]+y[3])*(3*h)/8;
b[xn]=-b0*(xo[xn]-L)/L;
printf("\t%.0f\t\t%.3f\t\t%.3f\n",xn,xo[xn],b[xn]);//delay(50);
outf<<"\t"<<xn<<"\t"<<xo[xn]<<"\t"<<b[xn]<<endl;
}
getch();
}

```

```

/*****
/*PROGRAM FOR CALCULATING 'DELTA' 'E''' AND 'M' */
/*****
#include<iostream.h>
#include<conio.h>
#include<math.h>
#include<fstream.h>

void main()
{
int j;
long double sigma_c=0,g,a,h,b,area2,e2,area,Ea;
long double delta,sigma,p,L,r;
long double area1,rmoe1,rmoe2,b_h=0.1,h_b=0.05;
long double MO,M,i,e1;
long double e[50],s[50],Em[50],Em1[25],f[25],t[25];
ifstream infile("2.txt");
clrscr();

for( j=1; j<=42; j++)
    infile>> e[j],s[j];

for( j=22; j<=42; j++)
    {
    f[j-21]=e[j];
    t[j-21]=s[j];
    }

for( j=1; j<=20; j++)
    Em[j]=(s[j+1]-s[j])/(pow(10.0,6)*(e[j+1]-e[j]));

for( j=1; j<=20; j++)
    Em1[j]=(t[j+1]-t[j])/(pow(10.0,6)*(f[j+1]-f[j]));
again2:
cout<<"Enter the value of higher limit";
cin>>g;
a=0.0;
rmoe1=0.0;
area1=0.0;
for( e1=0.0; e1<=g; e1+=0.00001)
    {
    if(e1>=e[1]&&e1<=e[2])
        {
        area1=area1+Em[1]*e1*0.00001;
        }
    }
}

```

```

        rmoe1=rmoe1+Em[1]*e1*0.00001*(a+0.00001/2.);
        a=a+0.00001;
    }
else if(e1>e[2]&&e1<=e[3])
    {
        area1=area1+(Em[2]*(e1-e[2])+s[2]/pow(10,6))*0.00001;
        rmoe1=rmoe1+0.00001*(a+0.00001/2.)*(Em[2]*(e1-e[2])+s[2]/pow(10,6));
        a=a+0.00001;
    }
else if(e1>e[3]&&e1<=e[4])
    {
        area1=area1+(Em[3]*(e1-e[3])+s[3]/pow(10,6))*0.00001;
        rmoe1=rmoe1+0.00001*(a+0.00001/2.)*(Em[3]*(e1-e[3])+s[3]/pow(10,6));
        a=a+0.00001;
    }
else if(e1>e[4]&&e1<=e[5])
    {
        area1=area1+(Em[4]*(e1-e[4])+s[4]/pow(10,6))*0.00001;
        rmoe1=rmoe1+0.00001*(a+0.00001/2.)*(Em[4]*(e1-e[4])+s[4]/pow(10,6));
        a=a+0.00001;
    }
else if(e1>e[5]&&e1<=e[6])
    {
        area1=area1+(Em[5]*(e1-e[5])+s[5]/pow(10,6))*0.00001;
        rmoe1=rmoe1+0.00001*(a+0.00001/2.)*(Em[5]*(e1-e[5])+s[5]/pow(10,6));
        a=a+0.00001;
    }
else if(e1>e[6]&&e1<=e[7])
    {
        area1=area1+(Em[6]*(e1-e[6])+s[6]/pow(10,6))*0.00001;
        rmoe1=rmoe1+0.00001*(a+0.00001/2.)*(Em[6]*(e1-e[6])+s[6]/pow(10,6));
        a=a+0.00001;
    }
else if(e1>e[7]&&e1<=e[8])
    {
        area1=area1+(Em[7]*(e1-e[7])+s[7]/pow(10,6))*0.00001;
        rmoe1=rmoe1+0.00001*(a+0.00001/2.)*(Em[7]*(e1-e[7])+s[7]/pow(10,6));
        a=a+0.00001;
    }
else if(e1>e[8]&&e1<=e[9])
    {
        area1=area1+(Em[8]*(e1-e[8])+s[8]/pow(10,6))*0.00001;
        rmoe1=rmoe1+0.00001*(a+0.00001/2.)*(Em[8]*(e1-e[8])+s[8]/pow(10,6));
        a=a+0.00001;
    }
}

```

```

else if(e1>e[9]&&e1<=e[10])
{
    area1=area1+(Em[9]*(e1-e[9])+s[9]/pow(10,6))*0.00001;
    rmoe1=rmoe1+0.00001*(a+0.00001/2.)*(Em[9]*(e1-e[9])+s[9]/pow(10,6));
    a=a+0.00001;
}
else if(e1>e[10]&&e1<=e[11])
{
    area1=area1+(Em[10]*(e1-e[10])+s[10]/pow(10,6))*0.00001;
    rmoe1=rmoe1+0.00001*(a+0.00001/2.)*(Em[10]*(e1-
e[10])+s[10]/pow(10,6));
    a=a+0.00001;
}
else if(e1>e[11]&&e1<=e[12])
{
    area1=area1+(Em[11]*(e1-e[11])+s[11]/pow(10,6))*0.00001;
    rmoe1=rmoe1+0.00001*(a+0.00001/2.)*(Em[11]*(e1-
e[11])+s[11]/pow(10,6));
    a=a+0.00001;
}
else if(e1>e[12]&&e1<=e[13])
{
    area1=area1+(Em[12]*(e1-e[12])+s[12]/pow(10,6))*0.00001;
    rmoe1=rmoe1+0.00001*(a+0.00001/2.)*(Em[12]*(e1-
e[12])+s[12]/pow(10,6));
    a=a+0.00001;
}
else if(e1>e[13]&&e1<=e[14])
{
    area1=area1+(Em[13]*(e1-e[13])+s[13]/pow(10,6))*0.00001;
    rmoe1=rmoe1+0.00001*(a+0.00001/2.)*(Em[13]*(e1-
e[13])+s[13]/pow(10,6));
    a=a+0.00001;
}
else if(e1>e[14]&&e1<=e[15])
{
    area1=area1+(Em[14]*(e1-e[14])+s[14]/pow(10,6))*0.00001;
    rmoe1=rmoe1+0.00001*(a+0.00001/2.)*(Em[14]*(e1-
e[14])+s[14]/pow(10,6));
    a=a+0.00001;
}
else if(e1>e[15]&&e1<=e[16])
{
    area1=area1+(Em[15]*(e1-e[15])+s[15]/pow(10,6))*0.00001;

```

```

        rmoel=rmoel+0.00001*(a+0.00001/2.)*(Em[15]*(e1-
e[15])+s[15]/pow(10,6));
        a=a+0.00001;
    }
    else if(e1>e[16]&&e1<=e[17])
    {
        areal=areal+(Em[16]*(e1-e[16])+s[16]/pow(10,6))*0.00001;
        rmoel=rmoel+0.00001*(a+0.00001/2.)*(Em[16]*(e1-
e[16])+s[16]/pow(10,6));
        a=a+0.00001;
    }
    else if(e1>e[17]&&e1<=e[18])
    {
        areal=areal+(Em[17]*(e1-e[17])+s[17]/pow(10,6))*0.00001;
        rmoel=rmoel+0.00001*(a+0.00001/2.)*(Em[17]*(e1-
e[17])+s[17]/pow(10,6));
        a=a+0.00001;
    }
    else if(e1>e[18]&&e1<=e[19])
    {
        areal=areal+(Em[18]*(e1-e[18])+s[18]/pow(10,6))*0.00001;
        rmoel=rmoel+0.00001*(a+0.00001/2.)*(Em[18]*(e1-
e[18])+s[18]/pow(10,6));
        a=a+0.00001;
    }
    else if(e1>e[19]&&e1<=e[20])
    {
        areal=areal+(Em[19]*(e1-e[19])+s[19]/pow(10,6))*0.00001;
        rmoel=rmoel+0.00001*(a+0.00001/2.)*(Em[19]*(e1-
e[19])+s[19]/pow(10,6));
        a=a+0.00001;
    }
    else if(e1>e[20]&&e1<=e[21])
    {
        areal=areal+(Em[20]*(e1-e[20])+s[20]/pow(10,6))*0.00001;
        rmoel=rmoel+0.00001*(a+0.00001/2.)*(Em[20]*(e1-
e[20])+s[20]/pow(10,6));
        a=a+0.00001;
    }
    else if(e1>e[21]&&e1<=e[22])
    {
        areal=areal+(Em[21]*(e1-e[21])+s[21]/pow(10,6))*0.00001;
        rmoel=rmoel+0.00001*(a+0.00001/2.)*(Em[21]*(e1-
e[21])+s[21]/pow(10,6));
        a=a+0.00001;
    }

```

```

    }
    else if(e1>e[22]&&e1<=e[23])
    {
        area1=area1+(Em[22]*(e1-e[22])+s[22]/pow(10,6))*0.00001;
        rmoe1=rmoe1+0.00001*(a+0.00001/2.)*(Em[22]*(e1-
e[22])+s[22]/pow(10,6));
        a=a+0.00001;
    }
    else if(e1>e[23]&&e1<=e[24])
    {
        area1=area1+(Em[23]*(e1-e[23])+s[23]/pow(10,6))*0.00001;
        rmoe1=rmoe1+0.00001*(a+0.00001/2.)*(Em[23]*(e1-
e[23])+s[23]/pow(10,6));
        a=a+0.00001;
    }
    else if(e1>e[24]&&e1<=e[25])
    {
        area1=area1+(Em[24]*(e1-e[24])+s[24]/pow(10,6))*0.00001;
        rmoe1=rmoe1+0.00001*(a+0.00001/2.)*(Em[24]*(e1-
e[24])+s[24]/pow(10,6));
        a=a+0.00001;
    }
    else if(e1>e[25]&&e1<=e[26])
    {
        area1=area1+(Em[25]*(e1-e[25])+s[25]/pow(10,6))*0.00001;
        rmoe1=rmoe1+0.00001*(a+0.00001/2.)*(Em[25]*(e1-
e[25])+s[25]/pow(10,6));
        a=a+0.00001;
    }
    else if(e1>e[26]&&e1<=e[27])
    {
        area1=area1+(Em[26]*(e1-e[26])+s[26]/pow(10,6))*0.00001;
        rmoe1=rmoe1+0.00001*(a+0.00001/2.)*(Em[26]*(e1-
e[26])+s[26]/pow(10,6));
        a=a+0.00001;
    }
    else if(e1>e[27]&&e1<=e[28])
    {
        area1=area1+(Em[27]*(e1-e[27])+s[27]/pow(10,6))*0.00001;
        rmoe1=rmoe1+0.00001*(a+0.00001/2.)*(Em[27]*(e1-
e[27])+s[27]/pow(10,6));
        a=a+0.00001;
    }
    else if(e1>e[28]&&e1<=e[29])
    {

```

```

        area1=area1+(Em[28]*(e1-e[28])+s[28]/pow(10,6))*0.00001;
        rmoe1=rmoe1+0.00001*(a+0.00001/2.)*(Em[28]*(e1-
e[28])+s[28]/pow(10,6));
        a=a+0.00001;
    }
    else if(e1>e[29]&&e1<=e[30])
    {
        area1=area1+(Em[29]*(e1-e[29])+s[29]/pow(10,6))*0.00001;
        rmoe1=rmoe1+0.00001*(a+0.00001/2.)*(Em[29]*(e1-
e[29])+s[29]/pow(10,6));
        a=a+0.00001;
    }
    else
    {
        area1=area1+(Em[30]*(e1-e[30])+s[30]/pow(10,6))*0.00001;
        rmoe1=rmoe1+0.00001*(a+0.00001/2.)*(Em[30]*(e1-
e[30])+s[30]/pow(10,6));
        a=a+0.00001;
    }
}
again:
cout<<"Input the lower limit";
cin>>h;
b=0.0;
area2=0.0;
rmoe2=0.0;
for( e2=0.0; e2<=h; e2+=0.00001)
{
    if (e2>=f[1]&&e2<=f[2])
    {
        area2=area2-Em1[1]*e2*0.00001;
        rmoe2=rmoe2-Em1[1]*e2*0.00001*(b-0.00001/2.);
        b=b-0.00001;
    }
    else if(e2>f[2]&&e2<=f[3])
    {
        area2=area2-(Em1[2]*(e2-f[2])+t[2]/pow(10,6))*0.00001;
        rmoe2=rmoe2-0.00001*(b-0.00001/2.)*(Em1[2]*(e2-f[2])+t[2]/pow(10,6));
        b=b-0.00001;
    }
    else if(e2>f[3]&&e2<=f[4])
    {
        area2=area2-(Em1[3]*(e2-f[3])+t[3]/pow(10,6))*0.00001;
        rmoe2=rmoe2-0.00001*(b-0.00001/2.)*(Em1[3]*(e2-f[3])+t[3]/pow(10,6));
        b=b-0.00001;
    }
}

```



```

    }
else if(e2>f[4]&&e2<=f[5])
    {
    area2=area2-(Em1[4]*(e2-f[4])+t[4]/pow(10,6))*0.00001;
    rmoe2=rmoe2-0.00001*(b-0.00001/2.)*(Em1[4]*(e2-f[4])+t[4]/pow(10,6));
    b=b-0.00001;
    }
else if(e2>f[5]&&e2<=f[6])
    {
    area2=area2-(Em1[5]*(e2-f[5])+t[5]/pow(10,6))*0.00001;
    rmoe2=rmoe2-0.00001*(b-0.00001/2.)*(Em1[5]*(e2-f[5])+t[5]/pow(10,6));
    b=b-0.00001;
    }
else if(e2>f[6]&&e2<=f[7])
    {
    area2=area2-(Em1[6]*(e2-f[6])+t[6]/pow(10,6))*0.00001;
    rmoe2=rmoe2-0.00001*(b-0.00001/2.)*(Em1[6]*(e2-f[6])+t[6]/pow(10,6));
    b=b-0.00001;
    }
else if(e2>f[7]&&e2<=f[8])
    {
    area2=area2-(Em1[7]*(e2-f[7])+t[7]/pow(10,6))*0.00001;
    rmoe2=rmoe2-0.00001*(b-0.00001/2.)*(Em1[7]*(e2-f[7])+t[7]/pow(10,6));
    b=b-0.00001;
    }
else if(e2>f[8]&&e2<=f[9])
    {
    area2=area2-(Em1[8]*(e2-f[8])+t[8]/pow(10,6))*0.00001;
    rmoe2=rmoe2-0.00001*(b-0.00001/2.)*(Em1[8]*(e2-f[8])+t[8]/pow(10,6));
    b=b-0.00001;
    }
else if(e2>f[9]&&e2<=f[10])
    {
    area2=area2-(Em1[9]*(e2-f[9])+t[9]/pow(10,6))*0.00001;
    rmoe2=rmoe2-0.00001*(b-0.00001/2.)*(Em1[9]*(e2-f[9])+t[9]/pow(10,6));
    b=b-0.00001;
    }
else if(e2>f[10]&&e2<=f[11])
    {
    area2=area2-(Em1[10]*(e2-f[10])+t[10]/pow(10,6))*0.00001;
    rmoe2=rmoe2-0.00001*(b-0.00001/2.)*(Em1[10]*(e2-
f[10])+t[10]/pow(10,6));
    b=b-0.00001;
    }
else if(e2>f[11]&&e2<=f[12])

```

```

        {
            area2=area2-(Em1[11]*(e2-f[11])+t[11]/pow(10,6))*0.00001;
            rmoe2=rmoe2-0.00001*(b-0.00001/2)*(Em1[11]*(e2-
f[11])+t[11]/pow(10,6));
            b=b-0.00001;
        }
    else if(e2>f[12]&&e2<=f[13])
        {
            area2=area2-(Em1[12]*(e2-f[12])+t[12]/pow(10,6))*0.00001;
            rmoe2=rmoe2-0.0001*(b-0.00001/2)*(Em1[12]*(e2-
f[12])+t[12]/pow(10,6));
            b=b-0.00001;
        }
    else if(e2>f[13]&&e2<=f[14])
        {
            area2=area2-(Em1[13]*(e2-f[13])+t[13]/ pow(10,6))*0.00001;
            rmoe2=rmoe2-0.00001*(b-0.00001/2)*(Em1[13]*(e2-f[13])+t[13]/
pow(10,6));
            b=b-0.00001;
        }
    else if(e2>f[14]&&e2<=f[15])
        {
            area2=area2-(Em1[14]*(e2-f[14])+t[14]/pow(10,6))*0.00001;
            rmoe2=rmoe2-0.00001*(b-0.00001/2)*(Em1[14]*(e2-f[14])+t[14]/
pow(10,6));
            b=b-0.00001;
        }
    else if(e2>f[15]&&e2<=f[16])
        {
            area2=area2-(Em1[15]*(e2-f[15])+t[15]/ pow(10,6))*0.00001;
            rmoe2=rmoe2-0.00001*(b-0.00001/2)*(Em1[15]*(e2-f[15])+t[15]/
pow(10,6));
            b=b-0.00001;
        }
    else if(e2>f[16]&&e2<=f[17])
        {
            area2=area2-(Em1[16]*(e2-f[16])+t[16]/ pow(10,6))*0.00001;
            rmoe2=rmoe2-0.00001*(b-0.00001/2)*(Em1[16]*(e2-
f[16])+t[16]/pow(10,6));
            b=b-0.00001;
        }
    else if(e2>f[17]&&e2<=f[18])
        {
            area2=area2-(Em1[17]*(e2-f[17])+t[17]/ pow(10,6))*0.00001;

```

```

        rmoe2=rmoe2-0.00001*(b-0.00001/2)*(Em1[17]*(e2-
f[17])+t[17]/pow(10,6));
        b=b-0.00001;
    }
    else if(e2>f[18]&&e2<=f[19])
    {
        area2=area2-(Em1[18]*(e2-f[18])+t[18]/ pow(10,6))*0.00001;
        rmoe2=rmoe2-0.00001*(b-0.00001/2)*(Em1[18]*(e2-
f[18])+t[18]/pow(10,6));
        b=b-0.00001;
    }
    else
    {
        area2=area2-(Em1[19]*(e2-f[19])+t[19]/pow(10,6))*0.00001;
        rmoe2=rmoe2-0.00001*(b-0.00001/2)*(Em1[19]*(e2-
f[19])+t[19]/pow(10,6));
        b=b-0.00001;
    }
}

area=area1+area2;
MO=rmoe1+rmoe2;
delta=a-b;
sigma=-(1.0/delta)*area;
cout<< " Lower limit="<<b;

if(abs(sigma_c-sigma)>1.0)
{
    cout<< "There is no solution";
    goto again;
}
else
{
    i=1.0/12.0*(b_h*pow(h_b,3));
    p=h_b/delta;
    M=12*i*MO/(p*pow(delta,3))*pow(10,6);
    Ea=M*p/(i*pow(10,9));
    cout<<"e2="<<b<<" delta="<<delta<<" E="<<Ea<<" M="<<M;
}
goto again2;
}

```

```

/*****
/*PROGRAM FOR CALCULATING 'STRAIN' AND 'E' */
/*****
#include<iostream.h>
#include<conio.h>
#include<fstream.h>
#include<math.h>

void main(){
int i,j,m,n,p,k,kk;
m=2;
n=11;
k=10;
ifstream inf ("f.txt");
ifstream inf1 ("f1.txt");
ofstream outf ("10.txt");
double xp[20],delta[50],sum,pi,x[50][50],f[50],a[50],d[50][50];
clrscr();
for(i=1;i<=m;i++)
{
for (j=1;j<=n;j++)
inf>>x[i][j];
f[i]=x[i][11]; }
for (kk=1;kk<=10;kk++)
inf1>>xp[kk];
//cout<<f[16];
for (k=1;k<=10;k++)
{
for(i=1;i<=m;i++)
d[i][1]=f[i];
for(j=2;j<=m;j++)
for(i=1;i<=m-j+1;i++)
d[i][j]=(d[i+1][j-1]-d[i][j-1])/(x[i+j-1][k]-x[i][k]);
for(j=1;j<=m;j++)
a[j]=d[1][j];
sum=a[1];
for(i=2;i<=m;i++)
{
pi=1.0;
for(j=1;j<=i-1;j++)
pi=pi*(xp[k]-x[j][k]);
sum=sum+a[i]*pi;
}
delta[k]=sum;
outf<<delta[k]<<"\n";
}
}

```

```

        cout<<delta[k]<<"\n";
    }
getch();
}

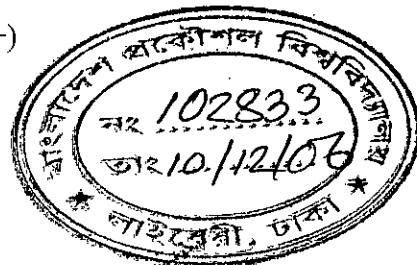
/*****
**PROGRAM FOR CALCULATING STRESS FROM TOTAL STRAIN**
*****/
#include<iostream.h>
#include<conio.h>
#include<fstream.h>
#include<math.h>
void main(){
int i,j,n,p,k,m;
n=3;
m=10;
ifstream inf ("input1.txt");
ifstream inf1("input2.txt");
ofstream outf ("input.txt");
double eps[50],sigma,sum,pi,x[50],f[50],a[50],d[50][50];

clrscr();

for(i=1;i<=n;i++)
{
inf>>x[i]>>f[i];}
for(i=1;i<=n;i++)
d[i][1]=f[i];
for(j=2;j<=n;j++)
for(i=1;i<=n-j+1;i++)
d[i][j]=(d[i+1][j-1]-d[i][j-1])/(x[i+j-1]-x[i]);

for(j=1;j<=n;j++)
a[j]=d[1][j];
for (k=1;k<=m;k++)
{
inf1>>eps[k];
sum=a[1];for(i=2;i<=n;i++)
{
pi=1.0;
for(j=1;j<=i-1;j++)
pi=pi*(eps[k]-x[j]);
sum=sum+a[i]*pi;
}
sigma=sum;

```



```
    cout<<eps[k]<<"\t"<<sigma<<"\n";  
    outf<<sigma<<"\n";  
}  
getch();  
}
```